STUDY OF GENERALIZED SPIN AND CHARGE STIFFNESS CONSTANTS OF DOPED QUANTUM ANTI-FERROMAGNETS ON LOW-DIMENSIONAL LATTICES BASED ON t-J LIKE MODELS

THESIS SUBMITTED FOR THE DEGREE OF

DOCTOR OF PHILOSOPHY (SCIENCE)

IN PHYSICS (THEORETICAL)

by

SURAKA BHATTACHARJEE

Department of Physics

University of Calcutta

2020

Dedicated to

My mother

Acknowledgement

I am extremely grateful to my supervisor Professor Ranjan Chaudhury for his guidance and continuous encouragement during my Ph.D tenure. The discussions with him, together with his dedicated supervision, not only enriched my knowledge, but also improved my writing skill and vocabulary. I would like to express my sincere gratitude towards INSPIRE for the financial support and the SN Bose Centre for providing me with this opportunity to carry out Doctoral research in the centre.

I am thankful to my officiating supervisor Dr.Manoranjan Kumar for his valuable suggestions and inspiration for pursuing my research work. I also got highly benefited from the group discussions in Manoranjan sir's group. The different ideas discussed in the group meetings have given me a vast exposure to the interesting problems in the related areas. The individual discussions with Subhajit da, Aslam da, Rakesh da, Debasmita, Monalisa, Sudip, Saniur, Monalisa(junior), Jyotirmoy, Somasree and Monodeep have motivated me towards optimism. My bay mates Shreya and Tuhin always kept me joyous with their jovial gestures and my friends Anita di, Arpan da, Hrishit da, Sumanti, Jayeeta, Somonnita, Sucheta, Anuvab and Prantik have turned my entire strenuous journey into a cheerful one. Above all, I would like to convey my heartiest gratitude towards my senior Soumi di and my group mate Koushik. For these years of Ph.D, Soumi di was my friend as well as elder sister. I am really thankful to Koushik for the wonderful times we spent in discussing our research problems and motivating me with enduring patience in the depressing moments.

I have learnt the basic Physics from my teachers Dr.Muktish Acharyya, Chapal Kumar Chatterjee, Taniya Basu, Amritendu da, Bivas da. They have driven me

towards my journey with Physics. I am also thankful to my teachers Sukanya Chatterjee and Bhabani Nath Sanyal for inspiring and motivating me from my school life. I would specially thank my friend Moumita di for being with me from my college days.

My grand parents have always supported and guided me throughout my career. My grandfather had been my friend, philosopher and guide, who persuaded me in getting all my dreams fulfilled. At last, the entire thesis would remain incomplete leaving out the contribution of my mother, without whom I would have been nothing. It is for her, I could come to the SN Bose Centre and continue my research work. I am really indebted to her for always being with me at all the moments I needed her the most.

Publications

(1) **Calculation of generalized spin stiffness constant of strongly correlated doped quantum antiferromagnet on two-dimensional lattice and it's application to effective exchange constant for semi-itinerant systems**, Suraka Bhattacharjee, Ranjan Chaudhury, Physica B **500**, 133 (2016)

(2) **Effective Interaction in a Non-Fermi Liquid Conductor and Spin Correlations in Under-Doped Cuprates**, Suraka Bhattacharjee, Ranjan Chaudhury, J.Low Temp. Phys. **193**, 21 (2018)

(3) **Investigation of the magnetic behaviour of doped quantum antiferromagnets on low-dimensional lattices**, Suraka Bhattacharjee, e-poster abstract, "2nd International Conference and Exhibition on Mesoscopic and Condensed Matter Physics", J.Mat.Sc.Eng.,doi:10.4172/2169- 0022.C1.053 (2016)

(4) **Effective Charge Coupling in Low Dimensional Doped Quantum Antiferromagnets**,
S.Bhattacharjee, R.Chaudhury, Int. J.Phys. and Math. Sc. **14**, 23 (2020)

(5) **Study of effective coupling between charge degrees of freedom in low-dimensional hole-doped quantum antiferromagnets**,
Suraka Bhattacharjee, Ranjan Chaudhury, arXiv:Cond-mat/1904.09319 v3 (2020) [communicated]

Contents

List of Figures

List of Symbols and Abbreviations

BCS Theory - Bardeen, Cooper, Schrieffer Theory

SBB Theory - Schafroth, Blatt, Butler Theory

FL - Fermi Liquid

NFL - Non-fermi Liquid

$\mathbf{T}_c$ - Critical temperature

HTSC - High T_c superconductor

BT - Band Theory

M-H - Mott-Hubbard

C-T - Charge-Transfer

DOS - Density of States

ZSA - Zaanen-Sawatzky-Allen

W - anion band-width

w - cation band-width

Δ - superconducting gap

$\mathbf{D}_s$ - Spin stiffness constant

$\mathbf{D}_c$ - Charge stiffness constant

$|\,\boldsymbol{\psi}\rangle_{\boldsymbol{G}}$ - Gutzwiller state

$\boldsymbol{\alpha}$ - variational parameter in Gutzwiller state

$|\,\boldsymbol{FS}\rangle$ - Fermi sea ground state

$|\,\boldsymbol{vac}\rangle$ - vacuum state

U - onsite Coulomb repulsion

J - exchange constant

$\boldsymbol{\delta}$ - doping concentration

Chapter 1

Introduction

The field of strongly correlated systems is gradually flourishing and has become one of the most important areas of Condensed Matter Physics for almost three decades. This field first came into the limelight after the discovery of heavy-quasiparticle excitations and superconductivity in materials like $CeAl_3$ and $CeCu_2Si_2$, in a Fermi liquid-like scenario [1,2]. Although, the idea of strong electron correlations that suppress the metallic character of materials prevailed long before their discovery. The electron correlations are responsible for the metal to insulator transition and these insulators were named as 'Mott-Hubbard insulators' according to the names of the scientists N.F.Mott and J.Hubbard, who first pointed out this phenomenon [3, 4]. Another type of insulators known as charge transfer insulators were also discussed based on the relative magnitudes of the Mott Hubbard and charge transfer gaps (the details are discussed in the subsequent subsection). Moreover, the materials discussed above, generally show antiferromagnetic ordering, the initial explanation of which was given by Louis Néel, as early as in 1936 [5]. It was found that the ordering is lost above a critical temperature, henceforth named as the 'Neel temperature' for the corresponding antiferromagnets. The reason behind this antiferromagnetic

alignment is the kinetic exchange, originating as a consequence of strong Coulomb repulsion between the electrons. However, in those times, the primary focus was on the transition metal oxides and the phase transition, as for example, the Verwey transition in Fe_3O_4 [6]. Furthermore, the strong correlation leading to formation of Wigner crystal and Heitler and London Theory for chemical bonding also came into being [7].

Later on the real thrust for the growth of this field was provided by the discovery of high temperature superconductivity in the cuprate materials like hole-doped $La_{2-x}Ba_xCuO_4$ and $La_{2-x}Sr_xCuO_4$. Since its discovery, high temperature superconductivity has drawn the interest of many scientists. Until now many high temperature superconductors have been found, yet the aim of reaching room temperature superconductivity still works as a driving force for finding new materials with exceptionally high critical temperatures [8, 9]. Besides these experimental progresses, the quest to know the bewildering mechanism behind pair formation in these superconductors has also led to many theoretical researches; however, many of these findings deepened the mystery further.

For a long time, superconductivity itself remained as a challenging problem in the field of Condensed Matter Physics and the efforts to understand this phenomena have eluded many scientists working on it. The breakthrough came in 1957 when three researchers viz. J.Bardeen, L.Cooper, J.R.Schrieffer came up with a microscopic theory (very well known as the BCS Theory) that could successfully explain various properties of conventional superconductors [10]. Around the same time, another microscopic theory was proposed by M.R.Schafroth, J.M.Blatt and S.T.Butler (SBB), involving the evaluation of partition function using the quasi-chemical equilibrium approach [11,13]. Motivated by the works of N.N.Bogoliubov and collaborators, they suggested that the superconducting pairs are the Bosons and that the superconduct-

ing state originates from the Bose Einstein condensation of the electron pairs [11,12]. This theory predicts the size of the localized pairs to be very small compared to the separation between the pairs and the pairs could translate leading to a gap-less Bose-Einstein excitations above the ground state, which is in contrast to the BCS pairing theory. However, due to the complexity of their formulation, they could not carry out the complete calculations and did not obtain the simplified BCS energy gap equation and quasi-particle spectrum [14, 15]. Again, the destruction of the superconductivity was proved to be due the breaking of the electron pairs and not as an effect of evaporation of pairs as a whole from the condensate, as was predicted by the SBB Theory [16]. Furthermore, according to this theory, the specific heat was supposed to exhibit a lambda-peak at the critical transition temperature, as seen at the point of transition from normal to superfluid Helium [17, 18]. But experimental results on conventional superconductors could not show this type of feature at the point of transition from normal to superconducting phase [19].

Although the BCS Theory was immensely successful in deriving the superconducting gap equation and a relation between the superconducting gap and critical temperature for certain materials, later on a few experimental results highlighted that the material independent value of the ratio of superconducting gap and critical temperature was not always true [20]. The discrepancy with the experimental results was primarily due to some inadequacies of the BCS Theory including the effect of not incorporating the change in effective mass of the electrons in presence of very strong electron-phonon coupling [21]. The renormalization of the electron mass in presence of electron-phonon coupling as well as the retardation in electron-electron effective interaction were was taken into consideration by G.M.Éliashberg in 1961 [22]. Moreover, the BCS Theory, initially developed for the conventional s-wave superconductors was later extended to take into account d-wave and p-wave

superconductivity [23]. However, the pure electron-phonon interaction based mechanism was proved to be insufficient for properly describing the origin of pairing in these systems [24–26]. In this scenario, different theories came into being for understanding the actual origin of pairing in various exotic superconductors, including the high T_c cuprate superconductors. Among the high temperature superconductors, the most well known ones are the cuprates, the superconductivity of which are mainly governed by the Cu-O chains and planes. In this chapter, the Mott Hubbard and Charge Transfer insulators, the BCS Theory for the conventional superconductors, the detailed structure of the perovskite materials and the models used for describing the strongly correlated materials, exhibiting high temperature superconductivity in the optimal doping region, are discussed in some details.

1.1 Mott-Hubbard and Charge Transfer Insulators

The strongly correlated solids can be classified into Mott Hubbard or charge transfer conductors or insulators based on the relative magnitudes of Mott Hubbard gap 'U' and charge transfer gap 'Δ'. This classification can be very well understood from the plot of Zaanen, Sawatzky and Allen (ZSA) [27]. The Fig.(1.1) shows the ZSA plot:

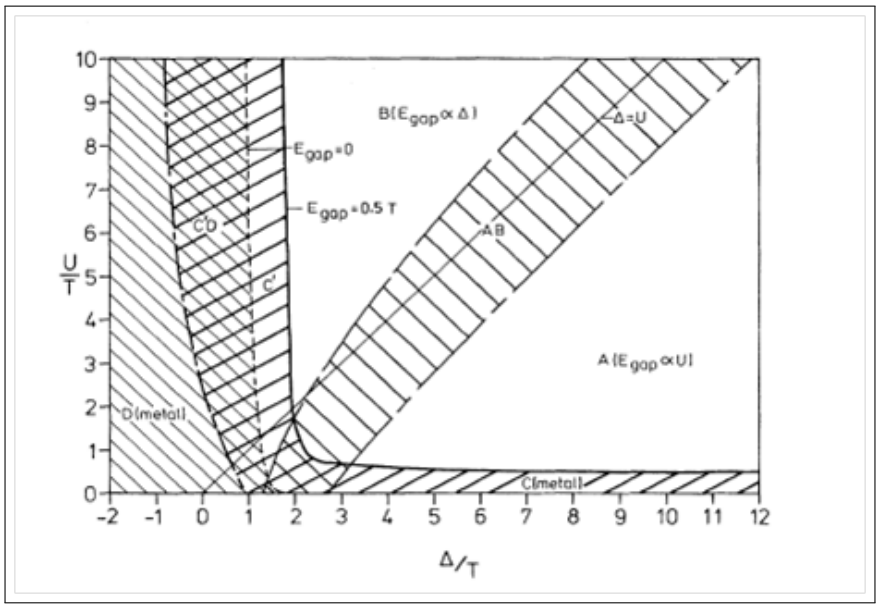

Figure 1.1: The phase diagram exhibiting of ZSA. The regions shown are :(A) Mott-Hubbard insulators; (B) Charge-transfer semiconductors; (AB) Intermediate region between A and B; (C) d-band metals;(D) p-type metals; (CD+C'D) Intermediate Regions between C and D [27]

According to the Band Theory (BT), a solid is guaranteed to be a metal if the valence and conduction bands overlap. However, BT neglects the inter-electronic Coulomb repulsion U, which is the principal cause behind the insulating behaviour in many compounds.

When the orbitals of the electrons in the valence band of solids overlap, the electrons try to delocalize over the entire volume of the solids to minimize their kinetic energy. In this case, there is a possibility for two delocalized electrons to come to the same orbital and if the on-site Coulomb repulsion >> the band width (U>>w), then the energy becomes very high and it exceeds the gain in kinetic energy. As a result, the electrons get localized in a particular unit cell. Now, at half filling of the band, exactly one electron sits on all the sites. In this situation, a gap opens up, equal in magnitude to U and this gap separates the band into an upper and a lower Hubbard sub-band. This type of insulators are known as the Mott Hubbard insulators [28].

The other branch of solids, called the charge transfer solids are also important in the context of transition metal oxides. This type of materials are characterized by the transfer of electrons from closed shell anion to the cation, if U>> Δ. For U> Δ, the gap is of a charge transfer (CT) type and even for U$\rightarrow \infty$, we can get a metallic ground state ie., a CT or a p-band metal (since the charge transfer takes place between the anion p-band and the cation d-band) if Δ <(W+w)/2 and when Δ >(W+w)/2 the system behaves as a CT insulator. On the other hand, when U<< Δ, one gets back into the Mott Hubbard regime, which can be further classified into Mott Hubbard (MH) insulator for U>w and d-band metal (as the electron transfer takes place only between the cation d-bands) for U<w [27]. Here 'w' and 'W' represents the band width of the cations and the anions respectively.
The energy for charge fluctuations are defined as [29]:

$$U_{eff}^{dd} = E_0(d^{n-1}) - E_0(d^n) + E_0(d^{n+1}) - E_0(d^n) \tag{1.1}$$

is the energy required to move a d electron from one transition metal ion to another, and

$$\Delta_{eff} = E_0(d^{n+1}\underline{L}) - E_0(d^n) \tag{1.2}$$

which represents the energy needed to move an anion p ligand electron, resulting in a ligand hole ($\underline{L}$), to a transition metal d state. Here E_0 in each case is the lowest energy state according to Hund's rule.
Fig.(1.2) and (1.3) show the Energy vs. Density of states (DOS) plots for the CT and MH solids respectively.

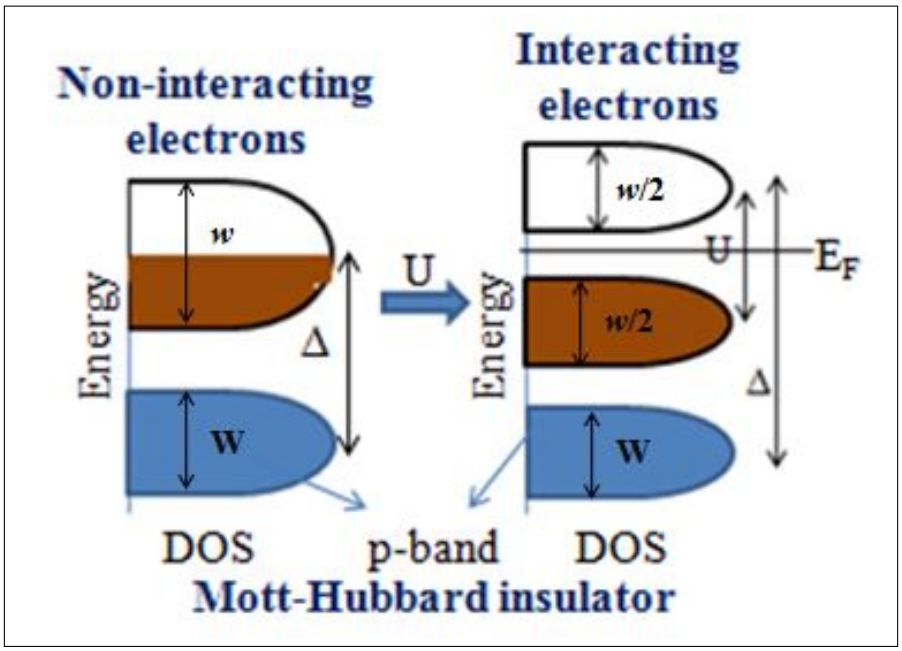

Figure 1.2: Energy vs. DOS plot showing the d-band metals and MH insulators; (i) The diagram in the left is for non-interacting electrons. The anion p-band is separated from the transition metal d-band by the charge transfer gap Δ. The half-filled d-band represents a d-band metal, (ii) In the right, the bands for interacting electrons are shown. The interaction 'U' opens up a gap between the upper and lower sub-bands and the system behaves as an insulator as U>w. As U< Δ, so it a Mott Hubbard insulator ['E_F' represents the position of the Fermi energy, 'w' represents band width of cation d-band and 'W' represents the band width of the anion p-band].

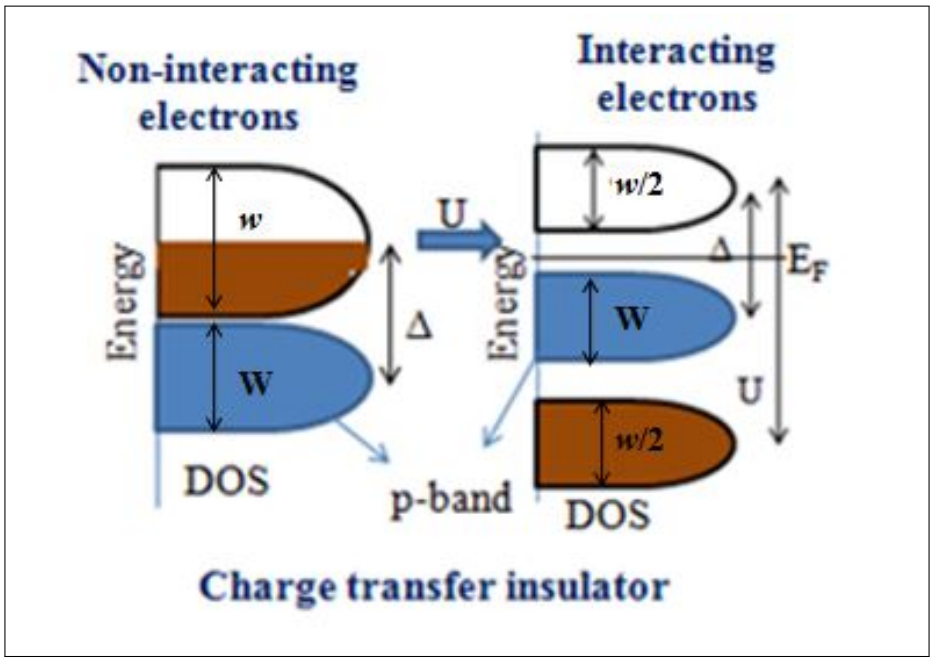

Figure 1.3: Energy vs. DOS plot showing the d-band metals and MH insulators; (i) The diagram in the left is for non-interacting electrons. The anion p-band and the transition metal d-band overlaps representing a p-band metal Δ. The half-filled d-band represents a band metal, (ii) In the right, the bands for interacting electrons are shown. The interaction 'U' opens up a gap between the p and the d bands and the system behaves as an insulator as Δ >(W+w)/2. As Δ <U, so it a Charge Transfer insulator ['E_F' represents the position of the Fermi energy, 'w' represents band width of cation d-band and 'W' represents the band width of the anion p-band].

1.2 BCS Theory

The theory put forward by Bardeen, Cooper and Schrieffer was the well acceptable microscopic theory for conventional superconductors. The main challenge was the formation of attractive pairing between two electrons in presence of a background of positively charged ions. Though this theory was greatly successful in handling the challenge for conventional superconductors, it could not satisfactorily describe the mechanism of pair formation in the strongly correlated high T_c superconductors. However, in this context, the discussions on the BCS Theory are necessary to get an idea about the notion of pair formation in the superconductors, at least in the

conventional cases.

Cooper showed that the Fermi sea is unstable with respect to the formation of at least one quasi-bound pair, as long as the interaction is attractive, regardless of how weak it is [13, 30]. The attraction is usually mediated by the electron-phonon interaction and the formation of macroscopic number of Cooper pairs gives rise to an energy gap. The principal aspects and the formulation of the theory are briefly discussed below:

Let us consider the interaction between two electrons in k and k′ state as shown in Fig(1.4):

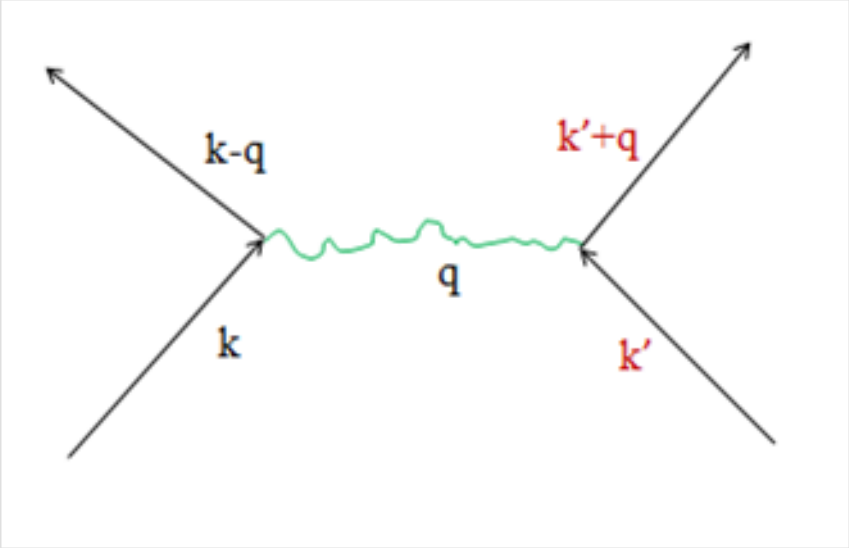

Figure 1.4: Feynman diagram showing the phonon mediated interaction between two electrons in k and k′ states scattering to (k-q) and (k′+q) states

The electrons in k and k′ states scatter to (k-q) and (k′+q) states respectively due to an interaction mediated by an exchange of a phonon of momentum q. When this interaction is attractive, one expects the pairs to condense in a real macroscopic system until and unless an equilibrium point is reached [30].

For simplicity, one can first consider the zero momentum pairing case, where interaction takes place between two electrons in l and $-l$ states.

Then the matrix element of the potential V_{kl} is given as [13]:

$$V_{kl} = \langle k, -k|V|l, -l\rangle \tag{1.3}$$

where the electrons in l and $-l$ states scatter to k and -k states respectively.
As already mentioned, this attractive interaction owes its origin to the electron-phonon interaction, which was first accounted for in the framework of the 'jellium model' [31–33]. A schematic diagram of the electron-phonon interaction is given in Fig.(1.5).

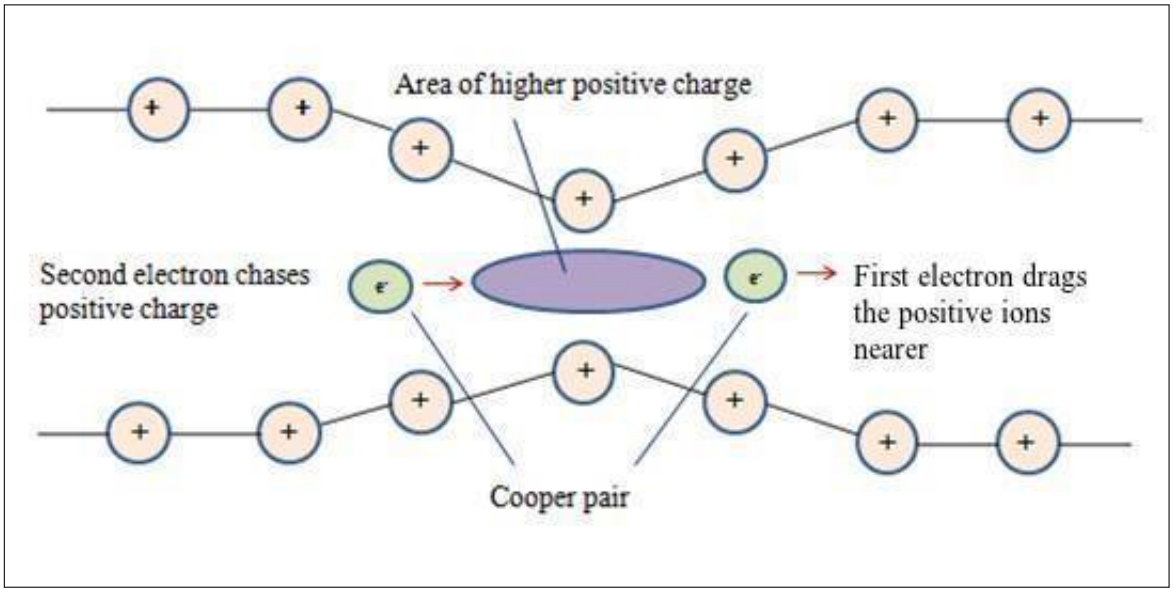

Figure 1.5: Electron-phonon coupling, giving rise to the pair forming attractive interaction between two electrons

According to the Jellium model, the solid is approximated as continuous fluid of electrons and ions and the Brillouin Zone effects and finite ion-core size effects are completely neglected. The interaction comes out to be [34]:

$$V(q,\omega) = \frac{4\pi e^2}{q^2 + k_s^2} + \frac{4\pi e^2}{q^2 + k_s^2}\frac{\omega_q^2}{\omega^2 - \omega_q^2} \tag{1.4}$$

The second term in eq.(1.2) originates from the phonon-mediated interaction and is negative for $\omega <$ the phonon frequency ω(q). Although this model can not capture the entire physics of realistic electronic solids, it gives an idea regarding the origin of the attractive pairing interaction to start with.

The BCS pairing Hamiltonian is:

$$\mathscr{H} = \sum_{k\sigma} \varepsilon_k n_{k\sigma} + \sum_{kl} V_{kl} C^{+}_{k\uparrow} C^{+}_{-k\downarrow} C_{-l\downarrow} C_{l\uparrow} \tag{1.5}$$

In the original BCS formalism, V_{kl} is considered to be an attractive square potential originating from the electron-phonon interaction as described above. The range of the potential is in a shell of width ω_c (cut-off frequency $\sim \omega_D$) centred at the Fermi surface [13]. Therefore, the range of the potential is taken as:

$$V_{kl} = -V \quad for \quad |\epsilon_k - E_F| \leqslant \hbar\omega_c \tag{1.6}$$

$$V_{kl} = 0 \qquad\qquad otherwise \tag{1.7}$$

Now, in the presence of this kind of attractive interaction, BCS proposed the ground state wave function [13, 30]:

$$|\psi\rangle_{BCS} = \prod_{k=k_1,\ldots k_M} (u_k + v_k C^{+}_{k\uparrow} C^{+}_{-k\downarrow})|\phi_0\rangle \tag{1.8}$$

where 'u_k' and 'v_k' are the probability amplitudes of the state k being unoccupied and occupied respectively. The quantities 'u_k' and 'v_k' can be determined variationally

and the calculation brings out these probability amplitudes as [13]:

$$u_k = \sqrt{\frac{1}{2}(1 - \frac{\xi_k}{E_k})} \tag{1.9}$$

$$v_k = \sqrt{\frac{1}{2}(1 + \frac{\xi_k}{E_k})} \tag{1.10}$$

where ξ_k is the kinetic energy of a quasi-particle with respect to the Fermi energy ($\xi_k = \varepsilon_k - E_F$) and E_k is the excitation energy of the quasi-particle given by [13]:

$$E_k = (\Delta_k^2 + \xi_k^2)^{\frac{1}{2}} \tag{1.11}$$

The Δ_k in eq.(1.11) is the BCS energy gap for the k^{th} state satisfying the condition [13]:

$$\Delta_k = \Delta \quad for \quad |\xi_k| \leqslant \hbar\omega_D \tag{1.12}$$

$$\Delta_k = 0 \qquad\qquad otherwise \tag{1.13}$$

where ω_D is the Debye frequency. Using the above conditions and the expressions for u_k and v_k, the expression for the BCS gap at T=0 can be derived as [13]:

$$\Delta(T = 0) = \frac{\hbar\omega_D}{sinh(\frac{1}{N(0)V})} \tag{1.14}$$

where N(0) is the single spin electronic density of states at the Fermi level.
In the weak coupling limit i.e, N(0)V<<1, eq.(1.14) reduces to:

$$\Delta(T = 0) = 2\hbar\omega_D \ exp(-\frac{1}{N(0)V}) \tag{1.15}$$

whereas in the strongly coupling limit i.e., N(0)V>>1,

$$\Delta(T=0) = \hbar\omega_D N(0) V \tag{1.16}$$

However, in reality, in the very strong coupling case, the electronic states on the Fermi surface get modified due to the strong electron-phonon interaction and *É*liashberg's formalism is required to describe superconductivity [22].

At low temperatures, the weak coupling Δ(T) obeys the relation [13, 30]:

$$\frac{\Delta(T)}{\Delta(0)} \approx 1.74(1 - T/T_c)^{\frac{1}{2}} \tag{1.17}$$

where T_c is the critical temperature of the superconductor.

It can be seen from eq.(1.16) that Δ is non-vanishing for T<T_c. Thus, the conduction electrons form genuine quasi-bound paired states below the critical temperature, which is conventionally known as Cooper pairs.

1.3 High temperature superconductors

Superconductivity above 30K was discovered in 1986 by Bednorz and Muller in a copper based material, $La_{2-x}Ba_xCuO_4$ [35]. $YBa_2Cu_3O_{7-x}$ was found within a year, which exhibited a critical temperature of 93K, well above the boiling point of nitrogen. The superconductivity in these materials is mainly contributed by the Cu-O planes and chains and the complexities in their structure are responsible for their characteristic behaviour [35, 36]. The charge density in these compounds can be externally tuned by changes in their chemical composition. The Band Theory predicts the undoped parental phase of the compounds(eg.La_2CuO_4 or $YBa_2Cu_3O_6$) to be metallic. However, for the very strong Coulomb repulsion, the electrons are localized

and the compounds behave as insulators [35, 36]. The additional charges introduced as doping are mobile. The charges destroy the antiferromagnetic property of the parental state and are responsible for the superconductivity. The phase diagram of the high T_c superconductors is shown in Fig.(1.6).

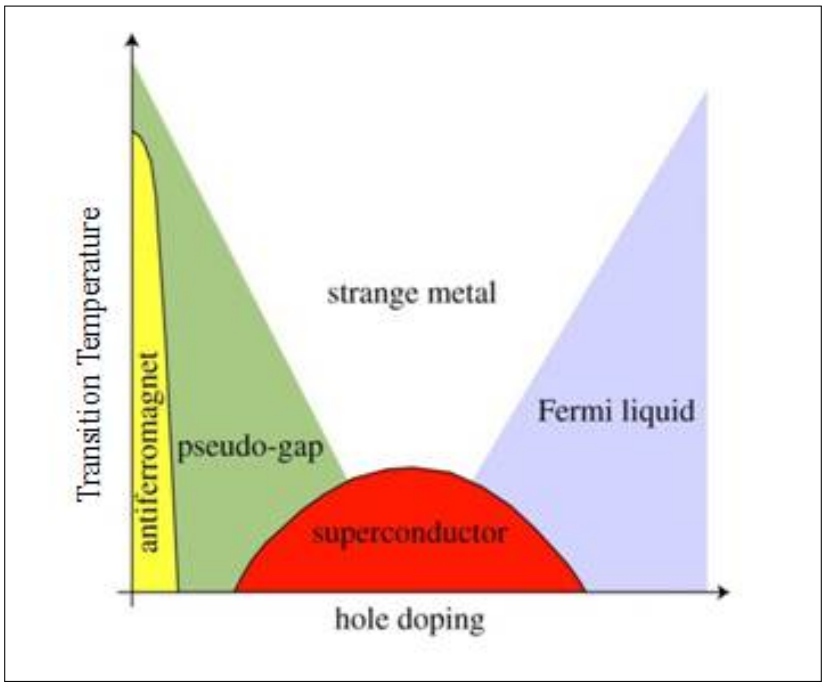

Figure 1.6: Phase Diagram of hole-doped high T_c superconductors [37]

1.4 Structure of Cuprate Superconductors (Perovskites)

The cuprate superconductors mainly belong to the crystallographic family of the perovskites [38].

Perovskite are the ceramic materials having metallic elements combined with non-metals (usually oxygen) in a particular atomic arrangement. The formula for the perovskite is ABX_3, where A,B are metallic cations (positive) and X is non-metallic anion (negative) present in the ratio 1:1:3 [39]. The perovskites normally consists of

cubes, in which the largest cation A lies in the centre, B cations occupy the eight corner sites and the anions remain at the centre of all the twelve edges. Here, in this section we would discuss the structure of two most important cuprate superconductors - doped La_2CuO_4 and $YBa_2Cu_3O_6$. In the next three chapters we will also show the comparison between the experimental results on these compounds with our theoretical outcomes.

1.4.1 Structure of La_2CuO_4 (LCO)

The structure of La_2CuO_4 is primarily determined by X-Ray powder diffraction method [40–42]. The experimental results reveal that LCO has square co-ordinate CuO_2 layers, which is the common characteristics of most of the cuprate superconductors. The CuO_2 layers lie at the top, bottom and the middle of an unit cell. The La-atoms are the largest cation 'A', Cu-atoms represent the 'B' cations and O atoms are present at the centre of the edges [39]. In LCO, double layers of LaO sit between two CuO_2 layers. The structure also shows that the Cu ions are situated in the centre of elongated oxygen octahedron, but the conductivity of LCO along the c-axis is negligibly small. Overall La_2CuO_4 is insulating in the parental state, however, replacement of La ions by Sr introduces conducting holes in the system. These introduced holes are responsible for making doped $La_{2-x}Sr_xCuO_4$ (LSCO) an important member in the family of high T_c superconductors. The structure of LSCO is shown in Fig.(1.7):

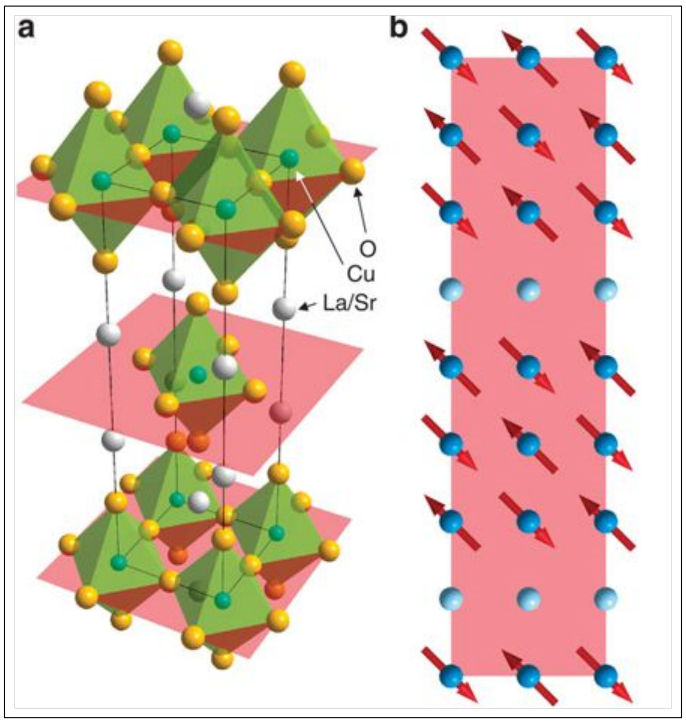

Figure 1.7: (a) Structure of $La_{2-x}Sr_xCuO_4$ showing the position of the Cu, O, La/Sr atoms; (b) antiferromagnetic arrangement of the Cu-atoms in the planes [43]

1.4.2 Structure of $YBa_2Cu_3O_6$ (YBCO)

The undoped YBCO is insulating and has tetragonal unit cell, whereas the unit cell of $YBa_2Cu_3O_{6+x}$ is orthorhombic [40]. One of the characteristic feature of $YBa_2Cu_3O_{6+x}$ is the presence of Cu-O chains formed by the Cu1 and O4 atoms along the b-axis (as shown in Fig.(5)). CuO_2 planes are also present, similar to the other cuprates. The O atoms in the Cu-chains are surrounded by four O atoms and that in planes are at the centre of a pyramid formed by five O atoms [44–47]. The Cu and O atoms in the CuO_2 planes are slightly buckled up and the O atoms occupy the edge sites. Two CuO_2 planes are separated by Y atoms, which together forms a block separated by Ba-O layers. The structure of a typical $YBa_2Cu_3O_{6+x}$ unit cell is shown in Fig.(1.8) [48]:

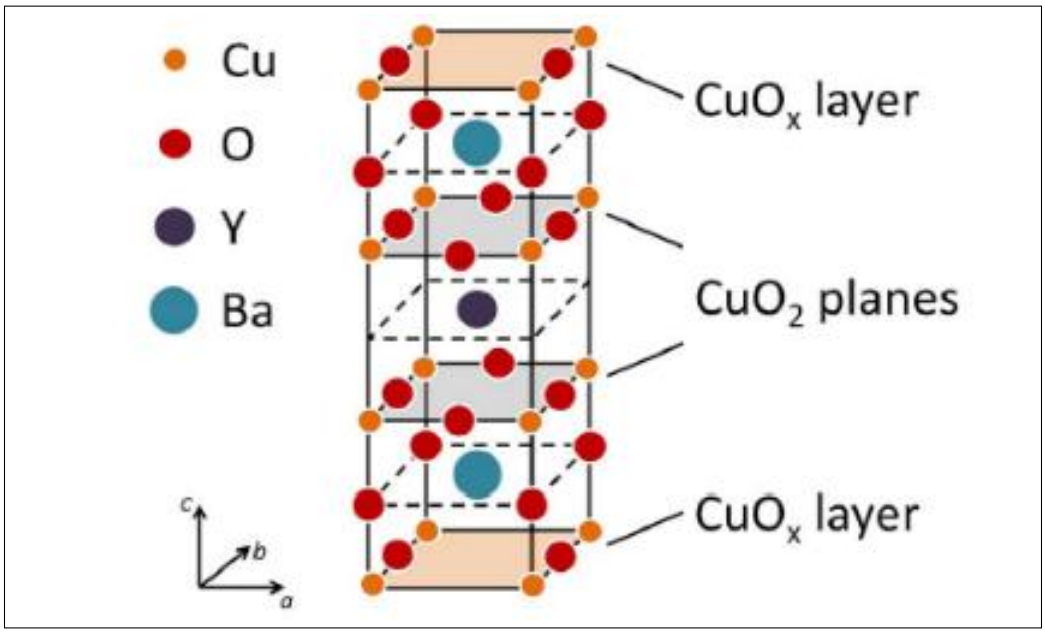

Figure 1.8: (a) Structure of $YBa_2Cu_3O_{6+x}$ highlighting the CuO_2 planes and CuO_x chain layers [48]

1.5 The Hubbard Model for Strongly Correlated Systems

The electronic correlation is the most important effect, that gives rise to many interesting phenomena encompassing the many body Physics. According to the Band Theory, a material is predicted to be a metal if the density of states at the Fermi level is non-zero i.e, $\rho(\epsilon_F) \neq 0$ and it is predicted to be an insulator if $\rho(\epsilon_F) = 0$ [49]. The condition of metallicity is easily satisfied in the alkali metals as well as alkali earth metals i.e., Gr - I and Gr - II metals. However, the transition metal oxides like CoO, CuO etc. are insulators which violates this rule by defying the prediction of Band Theory for independent electrons. This violation in rule is attributed to the very strong correlation effect between the electrons. For a long time, after the discovery of the insulating property of transition metal oxides, there have been

several attempts to develop a model including the large-U interaction between the electrons. In this context, the Anderson's superexchange mechanism was explained, which is based on a Hubbard like Hamiltonian in the large-U half filled limit [50]. Finally the Hubbard Model was given the shape in 1963. This is believed to be the simplest model for strongly correlated electron systems, which basically comprises of the kinetic energy term and the electron-electron interaction term [4].
The one-band Hubbard Model is of the form [4]:

$$\mathscr{H} = -t \sum_{<j,l>} \sum_{\sigma} (C^{\dagger}_{j\sigma} C_{l\sigma} + C^{\dagger}_{l\sigma} C_{j\sigma}) + U \sum_{j} \widehat{n}_{j\uparrow} \widehat{n}_{j\downarrow} \tag{1.18}$$

The first term corresponds to the kinetic energy, with 't' as the hopping amplitude parameter and 'U' represents the onsite Coulomb repulsion. The Coulomb repulsion between two electrons sharing the same orbital is defined as [49]:

$$U = \int \overrightarrow{dr}_1 \int \overrightarrow{dr}_2 |\phi(\overrightarrow{r}_1 - \overrightarrow{R}_j)|^2 \frac{e^2}{|\overrightarrow{r}_1 - \overrightarrow{r}_2|} |\phi(\overrightarrow{r}_2 - \overrightarrow{R}_j)|^2 \tag{1.19}$$

where $\phi(\overrightarrow{r} - \overrightarrow{R}_j)$ is the Wannier State and $(\overrightarrow{r}_1 - \overrightarrow{R}_j)$ and $(\overrightarrow{r}_2 - \overrightarrow{R}_j)$ are the respective position co-ordinates of the electrons with respect to the ionic location for the j^{th} ion.

Normally from definition U is positive, which is the case for most of the solids that are known. The Hubbard model is integrable only in 1D and the physical properties can be determined exactly [51]. The first attempt to solve the one dimensional Hubbard model was made by Lieb and Wu, using the Bethe Ansatz [52]. The ground state energy was calculated solving the Lieb Wu equations and the solution showed that the ground state is metallic for U=0 in the half-filled limit, whereas, the Mott insulator phase exists for U>0 at this filling [52]. Later the complicated Lieb Wu equations were replaced by the simpler thermodynamic Bethe Ansatz (TBA) equa-

tions and the entire thermodynamics of the one dimensional Hubbard model was obtained [53–55].

The 2D Hubbard model is studied numerically using several techniques [56–61]. The model, in the weak coupling limit, is analyzed in the mean field approach [56]. The Renormalization Group Analysis of the of the model in the strong coupling limit, using the first and second near neighbour hoppings identifies the antiferromagnetic and d-wave superconducting instabilities as the leading instabilities [57]. Again, the Monte Carlo simulations predict the system to be antiferromagnetically ordered in the half filled limit at all values of coupling at T=0 [58, 59]. However, in the slightly less than half-filled case the long range order is seen to completely destroy much earlier than that of the mean field approach [58]. The phase diagrams are also drawn showing the spin density wave and the d-wave superconducting phases [57, 59, 61].

1.6 Extended Hubbard Model

The model which I have discussed in the preceding section is the conventional Hubbard model introduced individually by Hubbard, Gutzwiller and Kanamori [4,62,63]. This model takes into account only interactions between electrons on a particular site. It was done with a view that the entire physics, including the major magnetic orderings would be same as from the complete forms of the Coulomb interaction i.e., considering the interaction between electrons on other sites. But, it was later understood that the description of charge orderings in the less than half- filled bands requires the inter-site interactions [49]. The search for the mechanisms behind ferromagnetism and superconductivity in the model has necessitated the inclusion of the neglected terms in the Hubbard model, which were already mentioned by Hubbard himself in his several papers [4, 64].

The general form of the model with on-site interactions and the interactions between the neighbouring sites is given as: [65]:

$$\mathscr{H} = -t \sum_{<j,l>} \sum_{\sigma} (C^{\dagger}_{j\sigma} C_{l\sigma} + C^{\dagger}_{l\sigma} C_{j\sigma}) + U \sum_{j} \widehat{n}_{j\uparrow} \widehat{n}_{j\downarrow} + V \sum_{j} n_j n_{j+1} \tag{1.20}$$

where 'U' is strength of the Coulomb interaction between electrons in the same site as mentioned above and 'V' denotes the strength of the inter-site Coulomb interaction.

Initially extended Hubbard Model was studied only at the mean field level [66, 67]. However, the spin density to charge density wave transition in this model were studied using Monte Carlo Simulation as early as in 1984 [68]. A few years later, the complete thermodynamics was investigated using perturbative expansion technique [69]. The phase diagrams of the model in one dimension at half-filled and quarter-filled limits have also been presented in numerous papers [70–74]. Moreover, the phase diagram for both attractive and repulsive Coulomb interaction has been drawn using exact diagonalization and variational techniques, which clearly analyzes the different properties of the ground state [75]. Afterwards, the quantum entanglement in the extended Hubbard model was investigated to predict quantum phase transition in fermionic systems [76].

1.7 t-J-like Models

1.7.1 t-J Model

The t-J model is the most important model for describing the strongly correlated electrons in the high T_c superconductors. It is a progeny model derived from the Hubbard model using a second order perturbation in the U>>W limit [77, 78]. A schematic diagram of the origin of exchange interaction in t-J model is given below:

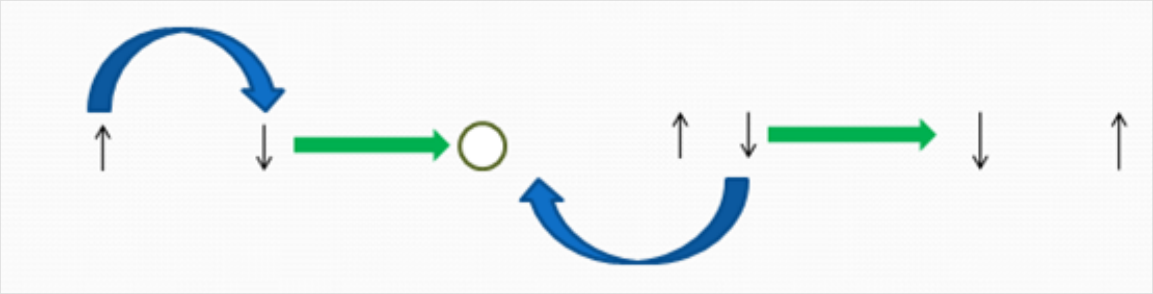

Figure 1.9: Schematic diagram showing the origin of exchange interaction in the strongly correlated systems

One of the characteristic features of this model is that it prevents the double occupancy at a particular site due to very large Coulomb repulsion [4]. The effective Hamiltonian is of the form [79–82]:

$$H^{t-J} = -t \sum_{<i,j>,\sigma} (X_i^{\sigma,0} X_j^{0,\sigma} + X_j^{\sigma,0} X_i^{0,\sigma}) + J \sum_{<i,j>} (S_i.S_j - \frac{1}{4} n_i n_j) \tag{1.21}$$

where 't' is the nearest-neighbour hopping amplitude connecting j^{th} and i^{th} site and J=$\frac{t^2}{U}$ is the exchange constant between the carriers on nearest neighbours; X_i and X_j are the Hubbard operators which prevents the double occupancy on a particular site. The Hubbard operators satisfy the commutation relation [83]:

$$[X_i^{\alpha\beta}, X_j^{\gamma\delta}] = \delta_{ij}(\delta^{\beta\gamma} X_i^{\alpha\delta} - \delta^{\alpha\delta} X_i^{\gamma\beta}) \tag{1.22}$$

The Hubbard operators are related to the Fermion operators [78]:

$$X_i^{\sigma 0} = C_{i\sigma}^{\dagger}(1 - n_{\overline{\sigma}}), \qquad X_i^{2\sigma} = \sigma C_{i\overline{\sigma}}^{\dagger} n_{i\overline{\sigma}}, \tag{1.23}$$

$$X_i^{\sigma\overline{\sigma}} = C_{i\sigma}^{\dagger} C_{i\overline{\sigma}}, \qquad X_i^{20} = \sigma C_{i\overline{\sigma}}^{\dagger} C_{i\sigma}^{\dagger}, \tag{1.24}$$

$$X_i^{00} = (1 - n_{i\uparrow})(1 - n_{i\downarrow}), \tag{1.25}$$

$$X_i^{\sigma\sigma} = n_{i\sigma}(1 - n_{\overline{\sigma}}), \qquad X_i^{22} = n_{i\uparrow} n_{i\downarrow} \tag{1.26}$$

The t-J model Hamiltonian can be written in terms of the Fermion creation and annihilation operators, using the relations given in eqs.(1.21-1.24). The t-J model Hamiltonian takes the form:

$$H^{t-J} = -t \sum_{<i,j>,\sigma} C^{\dagger}_{i\sigma}(1 - n_{i\sigma})C_{j\sigma}(1 - n_{j\sigma}) + J \sum_{<i,j>} (S_i.S_j - \frac{1}{4}n_i n_j) \qquad (1.27)$$

(1-$n_{i\sigma}$) and (1-$n_{j\sigma}$) prevents double occupancies on the i^{th} and j^{th} sites respectively. The high T_c superconductors can be well explained by the Hubbard model, provided the very strong interaction limit U>> W is applied. Hence the t-J model Hamiltonian can be applied for these systems.

The parent compounds like La_2CuO_4 or $YBa_2Cu_3O_6$ are Mott insulators in the half-filled limit. Upon doping La_2CuO_4 with Sr or $YBa_2Cu_3O_6$ with excess O, the hole type charge carriers are introduced on both Cu and O-atoms [78]. The holes form the Zhang-Rice singlet that are referred to in the t-J model Hamiltonian and are created and destroyed by the Fermion creation and annihilation operators respectively [84]. The t-J model in 1D is exactly solvable using Bethe Ansatz at specific values of J/t, but no ground state solution can be obtained for general values of J/t [79]. However, the most important applicability of the t-J model lies in correctly determining the characteristic behaviour of the 2D layered cuprates. Some machine learning methods like artificial neural networks and numerical techniques like exact diagonalization of small clusters and Quantum Monte Carlo (QMC) have been used, although the latter exhibited the well known Fermionic sign problem [85–87]. In spite of having several problems and difficulties, these techniques have paved the way for considerable progress in understanding the physics of the materials described by the t-J model [78].

Now, this t-J model is valid only in the less than half filled-band limit. In the exactly

half-filled case, when no holes are present, all the orbitals are filled with one electron. In this situation, the hopping part in the Hamiltonian (eq.(1.10)) vanishes and one can get back the well known antiferromagnetic **Heisenberg Model** [49]:

$$H^J = J \sum_{<i,j>} (S_i.S_j - \frac{1}{4} n_i n_j) \tag{1.28}$$

where antiferromagnetic exchange constant J>0 and 'S_i', 'S_j' have the usual meaning as mentioned before.

1.7.2 t_1-t_2-t_3-J Model

The t_1-t_2-t_3-J model is the extension of the well known t-J model, taking into account the second and third nearest neighbour hopping [88]:

$$H = -t_1 \sum_{<i,j>,\sigma} C^{\dagger}_{i\sigma} C_{j\sigma} - t_2 \sum_{<<i,j>>,\sigma} C^{\dagger}_{i\sigma} C_{j\sigma} - t_3 \sum_{<<<i,j>>>,\sigma} C^{\dagger}_{i\sigma} C_{j\sigma} + J \sum_{<i,j>,\sigma} S_i.S_j \tag{1.29}$$

where 't_1', 't_2' and 't_3' are the first, second and third neighbour hopping amplitudes respectively.

There are many reasons for considering the higher neighbour hoppings, the most important of which is the changes in the topology of the Fermi surface near half-filling [89–91]. In these cases the shape of the Fermi surface depends on the sign of t_2, whereas no sign dependence is seen when only the nearest neighbour 't' is considered [78]. The shape of true Fermi surface have been studied in the strong correlation limit i.e., U>>W [90]. At half-filling, the nesting of the Fermi surface is complete when t_2=t_3=0, confirming the existence of antiferromagnetic order in the

system. However, in the over-doped regimes, the nesting is disrupted representing the destruction of the antiferromagnetic order [90]. This necessitates the inclusion of higher neighbour hopping terms in the higher doping regions. The experimental studies using angle resolved photo emission spectroscopy (ARPES) also suggests the inclusion of higher neighbour hopping terms in the high T_c superconductors [92, 93]. The sign of t_2 depends on the type of carrier doped in the system i.e, t_2 is negative for hole type carriers and positive for electron carriers [94]. Moreover, the hopping between the second nearest neighbour site takes place between the same sub-lattice of a Neel antiferromagnet, so that the magnetic order is not violated [95].

The t_1-t_2-t_3-J model studied numerically using exact diagonalization technique shows that a gap opens up for 10% doping of holes around k=(π,0), however, for electron doping, the gap opens around k=($\pi/2$,$\pi/2$) and persists upto 20% doping concentration [88]. Among the other numerical techniques, Slave boson approach is important, the result of which get very good support from the ARPES results on electron-doped cuprates [96]. Furthermore, QMC simulations for U$\sim$W have shown that the antiferromagnetic order for the systems with $t_2 < 0$ decay faster than that of the systems with only nearest neighbour 't' [97]. This is due to the fact that the hopping to the nearest neighbour induces an exchange interaction J$\sim t^2/U$ between the sites, whereas the hopping to the next nearest neighbour induces an interaction J$'$ (depending on the model parameters) between the next nearest neighbour sites. In the moderate correlation limit U$\sim$W, the antiferromagnetic exchange between the next nearest neighbour sites thus leads to the frustration in the model that destroys the Neel order [97]. In contrast to this, for the strong correlation limit, the mean field approximation for the effective Hamiltonian emerging in the slave-boson representation proves that the antiferromagnetic Neel state in the t-J model is unstable with respect to the formation of incommensurate spiral phases [98]. However, if the higher

neighbour hopping terms are included, the Neel state becomes stable in the very low doping concentration [98]. In spite of having several views and results about the nature of spin correlations in the strong as well as in the weakly correlated phases, the actual magnetic behaviour in these phases and the location of the phase boundaries require further investigation and study.

1.8 Gutzwiller state for strongly correlated electrons

M.C.Gutzwiller formulated a wave function for handling the ground state of the correlated electrons in the Hubbard model [62]. He started from a filled Fermi sea state with non-interacting electrons |FS> and then introduced the correlation factor for taking into account the electron interactions [62].

$$|\psi_G\rangle = \prod_l (1 - \alpha \widehat{n}_{l\uparrow} \widehat{n}_{l\downarrow}) |FS\rangle \tag{1.30}$$

where |FS> is the Fermi sea ground state and 'α' is the variational parameter which decides the amplitude for the on-site fermionic double occupancies in the system. Now writing the Fermi sea ground state in terms of fermion creation operators:

$$|\psi_G\rangle = \prod_l (1 - \alpha \widehat{n}_{l\uparrow} \widehat{n}_{l\downarrow}) \prod_{k\sigma}^{k_F} \sum_{ij} C^{\dagger}_{i\sigma} C^{\dagger}_{j-\sigma} e^{i(\overrightarrow{r_i} - \overrightarrow{r_j}).\overrightarrow{k}} |vac\rangle \tag{1.31}$$

$|\text{vac}\rangle$ being the vacuum state (having fermionic occupation number equal to zero at all sites). The symbols i, j and l denote the lattice sites and k represents the wave vector for the fermion (existing hole), bounded by k_F (Fermi wave vector) from above. The variational parameter α is determined by minimizing the expression for

energy E; where E is the energy expectation value in the Gutzwiller state itself. The parameter α=1 represents very strong correlation i.e., when all the doubly occupied states in the system are projected out. In the absence of correlation or in the very weakly correlated case (α=0), one can get back the Fermi sea ground state (see eq.(1.30)) [62]; α assumes the values from 0 to 1 in the intermediate correlation regions.

Using this Gutzwiller state $|\psi_G\rangle$ the energy expectation value can be calculated as:

$$E = \langle\psi_G|H|\psi_G\rangle/\langle\psi_G|\psi_G\rangle \tag{1.32}$$

where $\langle\psi_G|\psi_G\rangle$ is the normalization for the Gutzwiller state.

Fot t-J model, the expectation values of the kinetic energy and exchange energy part are derived separately as:

$$T = \langle\psi_G|H_t|\psi_G\rangle/\langle\psi_G|\psi_G\rangle \tag{1.33}$$

$$and \quad E_J = \langle\psi_G|H_J|\psi_G\rangle/\langle\psi_G|\psi_G\rangle \tag{1.34}$$

where 'T' and 'E_J' are the expectation values of the kinetic energy part H_t and exchange energy part H_J of the t-J Hamiltonian respectively (see eq.(19))

This idea was previously put forward by Himeda and Ogata in a different way [99]. They renormalized the expectation values by comparing the statistical weighting factors in the wave functions with and without projection [100, 101]. As a result, the parameters t and J are renormalized to g_tt and g_sJ [102]. This result is compared with the variational Monte Carlo (VMC) results and it gives a proper estimate of the variational energy of the pure d-wave superconducting state [100, 102]. However it

was shown that there is no region in the phase diagram where the antiferromagnetic state is stabilized [100]. This contradicts with the VMC results. To solve this puzzle, they investigated the Variational Monte Carlo data and found that the Gutzwiller approximation has to be modified in the presence of long range antiferromagnetic correlations in the system [99]. Based on these observations, they extended the Gutzwiller approximation and derived an analytic formalism for the renormalization factors which reproduces the variational Monte Carlo results. They showed that it is important to take into account the longer range correlations for the weighting factors, in contrast to the previous approximation where only the site-diagonal expectation are considered. They introduced the effect of strong correlation only in the renormalization factors of hopping and effective exchange constant. The effective values are given by [103]:

$$t_{eff} = g_t t \qquad\qquad J_{eff} = g_s J \tag{1.35}$$

where g_t and g_s are the Gutzwiller factors calculated from variational energy calculation by Ogawa et al. [103].

The Gutzwiller constants g_t and g_s have been derived [99]:

$$g_t = \frac{2\delta(1-\delta)}{(1-\delta^2+4m^2)} \qquad\qquad g_s = \frac{4(1-\delta)^2}{(1-\delta^2+4m^2)^2} \tag{1.36}$$

where 'm' is the expectation value of antiferromagnetic order parameter denoting the staggered magnetization in antiferromagnetic state and 'δ' is the doping concentration. The vanishing of g_s and hence J_{eff} at δ=1 is evident from the above expression for g_s. m is a doping dependent quantity (m=m(δ)) upto δ=0.1 and m$\rightarrow$0 approximately after 10% doping concentration.

Himeda and Ogata also calculated the Gutzwiller factors using variational Monte

Carlo results. The dependence of g_s on the staggered magnetization m for different values of Δ (variational parameter) is given as (Fig.(1.10)) [99]:

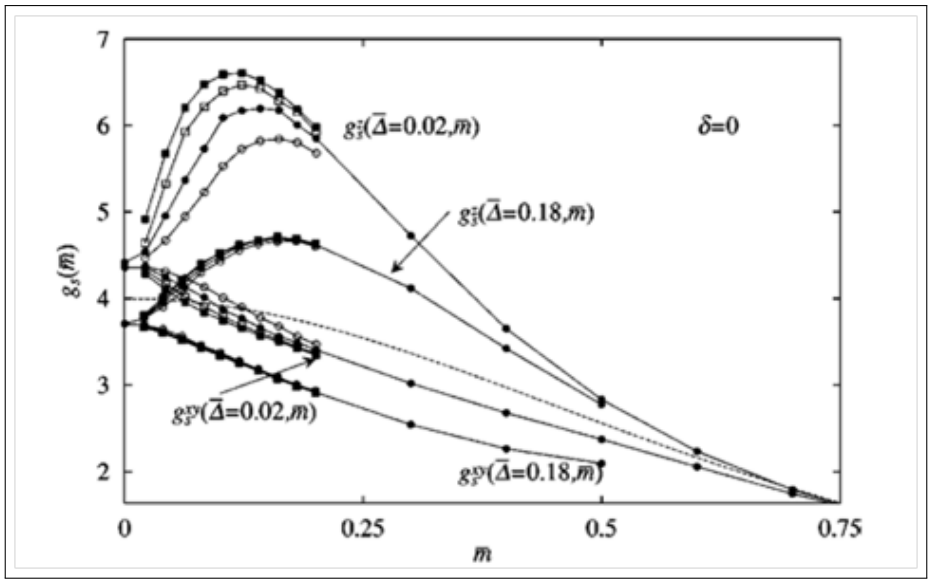

Figure 1.10: m dependence of g_s with fixing Δ=0.02,0.18.Sizes are 8x8(open circles), 10x10 (filled circles), 12x12 (open squares) and 14x14 (filled squares) [99].

The important feature seen in the plot is that the z component of the enhancement factor g_s^z has a maxima at m $\sim$0.15. On the other hand, the XY component does not have this feature and decreases monotonically as m increases. The size dependence of the maxima are found but the qualitative features do not change for almost all the values of Δ. This enhancement of g_s^z near m$\sim$0.15 is not expected in simple Gutzwiller approximation. This enhancement stabilizes the antiferromagnetic order, though the error of introducing the effect of no double occupancy only within the Gutzwiller factors, is included in it. The maximum exists for all values of doping concentrations, however the enhancement becomes weaker as the number of holes is increased [99].

1.9 Outline of the thesis

The thesis is arranged in the following way:

In Chapter 2, I have formulated a non-perturbative approach for deriving the effective exchange interaction between the itinerant spin degrees of freedom in doped two dimensional antiferromagnets. The approach is based on the calculation of generalized spin stiffness constant (spin asymmetric quantity) for the nearest neighbour t-J model. The results are compared with experimental results on layers of $La_{2-x}Sr_xCuO_4$ and the different characteristic features and magnetic behaviours of the strongly correlated antiferromagnetic systems have been studied as a function of doping concentration.

In chapter 3, the generalized spin stiffness constant for 1D doped antiferromagnets are derived. The results are compared with experimentally extracted results from the chains of $YBa_2Cu_3O_{6+x}$. A novel prediction is given regarding the emergence of a ferromagnetic-like coupling between the itinerant spins, after the decay of the original antiferromagnetic ordering in the undoped phase at zero temperature.

In the next chapter, I have given a detailed derivation of the generalized charge stiffness constant (spin symmetric quantity) for 2D and 1D antiferromagnets. The strongly correlated under-doped and the weakly correlated over-doped regimes are separately studied using the nearest neighbour t-J model and t_1-t_2-t_3-J model respectively. The comparison with other theoretical results established the equivalence of charge stiffness constant and the effective Drude weight. The relation between charge stiffness and effective Coulomb interaction at different doping concentrations is also established, based on the comparison with experimental results on $La_{2-x}Sr_xCuO_4$. Moreover, the possibility of charge density wave formation is analyzed in quite detail. In the last and the concluding chapter, I have given a brief summary of all the chapters in a nutshell and given the necessary concluding remarks regarding the chapters.

Chapter 2

Study of interactions between spin degrees of freedom in two-dimensional doped quantum antiferromagnets

2.1 Introduction

In the preceding chapter, I have discussed about the cuprate superconductors like La_2CuO_4 or $YBa_2Cu_3O_6$, which are antiferromagnetic insulators in the parental undoped phase [104, 105]. Now, these relevant antiferromagnetic parental compounds like La_2CuO_4 or $YBa_2Cu_3O_6$ can be explained with the help of nearest neighbour quantum Heisenberg Hamiltonian. However, this long range Neel ordering is lost in cuprates at temperature above the corresponding Neel temperatures and these materials can be treated as purely two dimensional systems in this regime. In view of this, the doped compounds (like $La_{2-x}Sr_xCuO_4$ or $YBa_2Cu_3O_{6+x}$) are well understood with the help of two dimensional t-J model derived from strongly correlated Hubbard model, as has been detailed in the previous chapter.

The effect of the inclusion of higher neighbour interaction in the t-J has considerable importance in describing the pair formation in d-wave superconducting state [106]. Recently renormalized mean field (RMF) t-J model has been used to

study the possibility of d-wave pairing in high temperature superconductors, which is able to produce results comparable to the variational Monte Carlo results [107]. In addition to it, two dimensional t-J model on square lattice based on infinite projected-entangled pair states, has been used to study the occurrences of stripes and the competition of uniform d-wave states versus striped states [108, 109]. Another issue that has been much talked about till today is the frustration in the quantum antiferromagnets where the most studied example is the J_1-J_2 Heisenberg model for spin 1/2 systems (where J_1 and J_2 are the nearest and next-nearest-neighbour exchange constants respectively). Sometimes even the third nearest-neighbour exchange interaction J_3 is taken into account and phase diagram of J_1-J_2-J_3 Heisenberg model, bearing the signature of possible quantum phase transitions, has been studied [110, 111]. The spin fluctuations in doped quantum antiferromagnets is studied based on the extended t-J model taking into account the next-nerarest-neighbour hopping term (t′) [89]. Moreover, the t-J_1-J_2 model is formulated for investigating the orbital-selective superconducting pairing, gap anisotropy and detailed magnetic behavior of the iron based superconductors like iron pnictides having co-existing localized and itinerant character [112, 113].

Here, the magnetic properties of two dimensional doped strongly correlated quantum antiferromagnets are investigated using the nearest-neighbour t-J model. This model involves mobile holes, which has a vast applicability in the layered cuprate systems [105,114]. The presence of the mobile holes in cuprates have also been established by many experiments on the cuprate layers. The results are consistent with the Monte Carlo results, that showed the exponential decay of correlation length and then a power law decay with the increase in doping concentration [115]. Vajk et al. studied the magnetometry of Zn or Mg doped La_2CuO_4 and noted the low-temperature tetragonal (LTT) structural phase transition above 10% doping concen-

tration. Above 25% doping the Neel ordering occurs in the LTT phase and persists upto 40.7% site dilution [115].

Some of the theoretical techniques based on t-J and t_1-t_2-t_3-J model have been already discussed in the last chapter. Besides these, some other important approaches related to the different aspects of the t-J models are mentioned here. Mori's projection is a powerful technique that establishes a connection between susceptibility and self-energy using the Green's function in relaxation-function theory. The study of two dimensional t-J model using the Mori's projection technique was done in the doping range $0 \leqslant \delta \leqslant 0.16$ and the obtained homogeneous solution negates the possibility of stripes formation or phase separation in this doping region [116]. Again, the Mori's projection technique is used to investigate the hole and spin excitation spectrum in the background of t-J model [117]. More complicated systems like oppositely doped layers of Bismuth are insulators of Mott-Hubbard type [118]. These kind of systems form inter-layer excitons and hence it is difficult to find any single layer analogue of these systems. The memory function method has also been used to find the charge dynamics and optical and d.c. conductivity in the t-J model [119–121]. Later on, the electron spectrum and superconductive pairing in the t-J model in a paramagnetic state is studied using the projection technique of the two-time Green's function, consistent with the Eliashberg equations [122]. Among the other methods extensively used are the variational Monte Carlo and the Gutzwiller wave function approach minimizing the effective single particle Hamiltonian and structure of gap function [123, 124]. The diagrammatic expansion of Gutzwiller wave function has shown the possibility of superconducting pairing for $U/t \geqslant 3$ and for $\delta \leqslant 0.32$ [123]. But all the above variational calculations involve only the lowest order contribution in the couplings 't' and 'J'. The calculation of dynamical spin susceptibility for the study of spin dynamics in the t-J model was also done considering only

the lowest-order approximation, which has been later proved to be insufficient in correctly determining the dynamical spin susceptibility [120, 125]. The self-energy calculation for the strongly correlated t-J model involving the Mori-type technique in two-time thermodynamic Green's function takes into account the spin excitation which is proportional to the square of hopping amplitude (t^2) and the imaginary part of self-energy $\Sigma'' \propto t^4$ [126–128]. The consideration of the higher order terms can correctly predict the disappearance of long-range ordering with increase in doping which is in general agreement with the results presented in this chapter . In [127], the critical value of doping concentration (δ_c), above which the long range order vanishes, is also derived for different values of J/t ratio and δ_c is found to be proportional to J/t. However, none of the above results were sufficiently conclusive in predicting the detailed magnetic behaviour of strongly correlated itinerant antiferromagnets. Here comes the importance of a different kind approach for rigorously determining the magnetic behaviour of correlated itinerant systems. In this note a first principle quantum mechnical method is developed for deriving generalized spin stiffness constant corresponding to the 2D t-J model. Although the relevance and usefulness of the t-J model for describing the itinerant doped antiferromagnets have been proved long ago, but the model is applicable only in the low doping region. The heavily doped region in reality shows substantial weakening of the correlation between the charge carriers and may not be governed by the t-J model in real systems [129].

The formalism used here for deriving the generalized spin stiffness constant of strongly correlated t-J model is based on an idea originally proposed by Kohn and Thouless [130]. In this calculation, the variational parameter in the Gutzwiller state 'α' is taken to be unity for projecting out all the doubly occupied sites (NDOC condition applied). The plot of stiffness constant as a function of doping concentration shows substantial weakening of the spin-spin couplings, thus predicting the quantum

melting of the long range antiferromagnetic order. This result also gets good support from earlier theoretical and experimental results [99, 132, 133].

The temperature dependence of the spin-spin correlation length in two dimensions has been derived analytically by Chakravarty, Halperin and Nelson (CHN) for pure two-dimensional nearest neighbor Quantum Heisenberg Antiferromagnet corresponding to undoped parent compound (La_2CuO_4). The calculations have been done using Renormalization Group technique, starting from a field theoretic action [134]. The calculation predicts the decrease of correlation length as temperature increases. This result has been modified later to take into account the large excess of charge carriers in real materials like laboratory-grown La_2CuO_4 [135]. Although the formulation of CHN was originally developed for pure (undoped) cuprates, similar results were obtained even in the case of very lightly doped cuprates [136]. This was demonstrated by Manousakis for 'static holes', which is a crude assumption in the sense that completely static holes are impossible in the present scenario. In the very low doping region however, the holes with heavier masses are rather constrained within a small spatial region around the dopant atoms [136, 137]. This situation may be regarded as that of nearly static holes. Moreover, in such a low doping region the hopping amplitude is negligibly small.

The neutron scattering experimental results of Thurston et al. show the fall of 2-dimensional correlation length (ξ_{2D}) with increase in doping concentration (x) of $La_{2-x}Sr_xCuO_4$ [105]. On the other hand, the numerical results for spin stiffness constant qualitatively and even quantitatively describe the nature of its decrease with increase in doping starting from the half-filled band limit and interestingly is quite similar to the behaviour of the result obtained from the above experimental work. This carries a strong hint that spin stiffness constant may very well play the role of an effective exchange constant in doped antiferromagnets. In addition, the analyti-

cal calculations and nature of the calculated spin stiffness constant are in qualitative agreement with the Quantum Monte Carlo results, which also predicts the reduction of antiferromagnetic ordering with the increase in doping [105, 136].

As discussed in the previous chapter, a slightly different type of concept and estimate for effective exchange constant in an effective ideal Fermi-sea like background was introduced by Himeda and Ogata [99]. Here a detailed comparison between their results and the results obtained using the approach mentioned above are presented. The vanishing of spin stiffness constant as $\delta \rightarrow 1$ agrees with the results of Himeda and Ogata; however their calculations did not produce any plausible signature of phase transition which comes as a possible outcome of the present analytical and numerical calculations.

Here, once again it should be made clear that the most important feature of the doped magnetic systems is the presence of the strongly correlated itinerant non Fermi liquid-like conducting phase around the optimal doping region. The previous researches for determining the magnetic interactions done using the density-functional theory, were for completely localized spins [138–140]. There were a few other attempts to study the properties of conventional itinerant magnetic systems using coherent-potential, where local exchange-correlation approximation was used in the band calculations [141]. Later Antropov calculated the effective exchange coupling of the itinerant systems using a combination of 'inverse susceptibility' approach and multiple-scattering theory [142, 143]. However, these calculations are valid in the weak correlation limit. Henceforth, the rigorous analytical and numerical calculations presented here provide a simple and comprehensive way for determination of effective exchange coupling and description of the magnetic correlations of strongly correlated semi-itinerant systems both qualitatively and quantitatively.

Thus, one of the major aims to be accomplished in this chapter would be to

theoretically determine and establish a more quantitative relation between generalized spin stiffness constant and effective exchange constant corresponding to a doped strongly correlated quantum antiferromagnet in 2-dimension, described by the nearest-neighbour t-J model. In the subsequent sections, the problem is formulated and solved analytically. The results of generalized spin stiffness constant are plotted as a function of doping concentration and then compared with previous experimental and theoretical results.

2.2 Formulation and Calculation

2.2.1 nearest neighbour t-J model

The Hamiltonian of the strongly correlated nearest neighbour t-J model is given by [146]:

$$H_{t-J} = H_t + H_J \tag{2.1}$$

where

$$H_t = \sum_{<i,j>,\sigma} t_{ij} X_i^{\sigma 0} X_j^{0\sigma} \tag{2.2}$$

and

$$H_J = \sum_{<i,j>} \{J_{ij}(S_i.S_j - (\frac{1}{4})n_i n_j)\} \tag{2.3}$$

(with $J_{ij} > 0$) where t_{ij} is the nearest-neighbour hopping amplitude connecting j^{th} and i^{th} site and J_{ij} is the exchange constant between the carriers on nearest neighbours; X's are the Hubbard operators, satisfying the appropriate commutation

relations and the usual Hubbard algebra [132]. For nearest neighbour hopping and exchange interaction, t_{ij}=t and J_{ij}=J are taken. It may be recalled that the quantities 't' and 'J' are considered independent.

The generalized spin stiffness constant $\tilde{D}_{spin}$ is defined as [132],

$$\tilde{D}_{spin} = lim_{\phi \to 0}(\frac{1}{2})\frac{\delta^2 E}{\delta \phi^2} \tag{2.4}$$

where E(ϕ) is the total ground state energy in the presence of staggered Peierl's phase (resembling a magnetic flux) ϕ_σ with $\sigma = \uparrow$ or $\downarrow$, arising from an applied vector potential A(r), such that

$$\phi_\downarrow = \phi_\uparrow = \phi \tag{2.5}$$

The hopping amplitude t_{ij} for a fermion with spin σ is modified to $t_{ij}e^{i\phi_\sigma}$, only if the vector potential has a component along the direction of hopping. The factor of $(\frac{e}{\hbar c})$ in the phase ϕ is included in the final expression of $\tilde{D}_{spin}$ with proper scaling. The total spin stiffness constant $\tilde{D}_{spin}$, abbreviated as '$\tilde{D}_s$', may be written as,

$$\tilde{D}_s = \tilde{D}_s^t + \tilde{D}_s^J \tag{2.6}$$

where $\tilde{D}_s^t$ and $\tilde{D}_s^J$ are the contributions from the 't' term and the 'J' term respectively. They are defined as

$$\tilde{D}_s^t = lim_{\phi \to 0}(\frac{1}{2})\frac{\delta^2 T}{\delta \phi^2} \tag{2.7}$$

and

$$\tilde{D}_s^J = lim_{\phi\to 0}(\frac{1}{2})\frac{\delta^2 E_J}{\delta\phi^2} = lim_{\phi\to 0}(\frac{1}{2})\frac{\delta^2 E_J^{sf}}{\delta\phi^2} \tag{2.8}$$

where T is the kinetic energy contribution, E_J is the total exchange energy and E_J^{sf} is the spin flip part of the exchange energy, which again are the ground state expectation values of the corresponding parts of the Hamiltonian. It may be pointed out that the direct part of the exchange energy term does not contribute to $\tilde{D}_s^J$ [132]. Furthermore, it may be noted that $\tilde{D}_s^t$ and $\tilde{D}_s^J$ both have the dimension of energy since ϕ is a dimensionless quantity.

In calculating E, avoiding the rather complicated Hubbard algebra, the Gutzwiller state is used with strictly NDOC imposed upon it [62]. The very general form of the Gutzwiller state is given by [62]:

$$|\psi_G\rangle = \prod_l (1 - \alpha\widehat{n}_{l\uparrow}\widehat{n}_{l\downarrow})|FS\rangle \tag{2.9}$$

where |FS> is the Fermi sea ground state and α is the variational parameter determined by minimizing the expression for E in the general case. In the case of NDOC however, α is taken as 1 without going into any variational scheme to determine 'α'. As stated earlier, this is in the spirit of the very strong correlation situation assumed to persist even in the doped phase, with effective on-site Coulomb repulsion much larger than the band-width, leading to strict avoidance of double occupancy on each site.

Now expressing the Fermi sea ground state |FS> in terms of fermion creation

operators, Eq.(2.9) takes the following form : -

$$|\psi_G\rangle = \prod_l (1 - \widehat{n}_{l\uparrow}\widehat{n}_{l\downarrow}) \prod_{k\sigma}^{k_F} \sum_{ij} C^{\dagger}_{i\sigma} C^{\dagger}_{j-\sigma} e^{i(\overrightarrow{r_i} - \overrightarrow{r_j}).\overrightarrow{k}} |vac\rangle \tag{2.10}$$

where $|vac>$ is the vacuum state (having fermionic occupation number equal to zero at all sites) and the normalization constant is omitted for the time being which will be included later in the calculation for the energy eigen values. The symbols i, j and l all denote the lattice sites and k represents the wave vector for the fermion, bounded by k_F (Fermi wave vector) from above [132]. Here k_F is defined corresponding to the sea of holes which are considered as the existing carriers in the presence of doping(vacancies). It may be recalled that the insulating phase corresponds to one hole per site with the holes being immobile. The Fermi wave vector for the two dimensional systems,

$$k_F = \sqrt{2\pi n/a} \tag{2.11}$$

where 'n' is the concentration of existing fermionic carriers (holes) present in the doped system and 'a' is the lattice spacing. 'n' is related to the doping (vacancy) concentration 'δ' (doping introduces vacancies in the system by removing carriers) as, n=1-δ. Thus, k_F gets related to δ as

$$k_F = \sqrt{2\pi(1 - \delta)/a} \tag{2.12}$$

The Eq. (2.3) can now be rewritten as:

$$H_J = \sum_{\langle i,j \rangle} J_{ij} H'_J \tag{2.13}$$

where,

$$H'_J = \overrightarrow{S_i}.\overrightarrow{S_j} - \frac{1}{4}n_i n_j \tag{2.14}$$

Again,

$$E_J^{sf} = (\frac{4t_{eff}^2 cos(2\phi)}{V_{eff}}) \frac{{}_{NDOC}\langle\psi_G|H'_J|\psi_G\rangle_{NDOC}}{{}_{NDOC}\langle\psi_G|\psi_G\rangle_{NDOC}} \tag{2.15}$$

where ${}_{NDOC}\langle\psi_G|\psi_G\rangle_{NDOC}$ is the normalization for the Gutzwiller state; t_{eff} is the effective nearest neighbour hopping amplitude and V_{eff} is the effective on-site Coulomb barrier potential in the doped phase for infinitesimal doping ie., $\delta \to 0$ within the effective one band scenario [132]. Thus one can model the initial J (J_{bare} or $J(\delta)$ with $\delta \to 0$) as $4t_{eff}^2/Veff$ as considered in the t-J model and estimate the initial t/J ratio (in the limit $\delta \to 0$) as $V_{eff}/4t_{eff}$ [132].

Carrying out detailed and more rigorous calculation after normalizing the Gutzwiller state and considering only the contribution from the nearest neighbour interaction, the exchange energy contribution comes as (the major steps of the calculation are shown in Appendix A):

$$\frac{{}_{NDOC}\langle\psi_G|H'_J|\psi_G\rangle_{NDOC}}{{}_{NDOC}\langle\psi_G|\psi_G\rangle_{NDOC}} = \prod_k^{k_F} 2(1-\delta)^2 \tag{2.16}$$

The square on (1-δ) is the consequence of the exchange interaction operating only between the occupied sites. Making use of equation (2.8) and by taking derivative of equation (2.15) twice the exchange part of the spin stiffness constant can be obtained as,

$$\tilde{D_s^J} = -4J \prod_k^{k_F} 2(1-\delta)^2 \tag{2.17}$$

From the earlier calculation described in [132], the kinetic energy contribution of the Fermionic system at zero temperature can be found from the following equation,

$$T = \frac{{}_{NDOC}\langle\psi_G|H_t|\psi_G\rangle_{NDOC}}{{}_{NDOC}\langle\psi_G|\psi_G\rangle_{NDOC}} \tag{2.18}$$

The above quantity is evaluated in the presence of staggered phase $\phi(\sigma)$ (staggered phase corresponding to up or down spins) making use of the orthogonality of the independent states and the result comes out to be (the major steps of the calculation are shown in Appendix(B)):

$$T(\phi \neq 0) = (t)[\prod_{k,\sigma}^{k_F}\sum_{\sigma} 4cos(ka)(1-\delta)^2 cos(\phi_\sigma) - N_l \prod_{k,\sigma}^{k_F}\sum_{\sigma} 4cos(ka)cos(\phi_\sigma)/N^2] \tag{2.19}$$

Here equation (2.5) is used for ϕ_σ corresponding to up and down spin respectively; 'N_l' is the expectation value of the number operator corresponding to the total number of lattice sites singly occupied by spins corresponding to the holes and 'N' is the total number of sites.

Thus,

$$N_l = N(1-\delta) \tag{2.20}$$

For 2D lattice, the vector potential $A(\mathbf{r})$ is assumed to be applied along the x direction and making use of equations (2.7) and (2.19), one can get the expression for the kinetic part of the spin stiffness constant as:

$$\tilde{D_s^t} = (-t)[\prod_{k,\sigma}^{k_F} 4cos(k_x a)(1-\delta)^2 - N_l \prod_{k,\sigma}^{k_F} 4cos(k_x a)/N^2] \tag{2.21}$$

The second term in equation (2.21) is physically important since it signifies the complete projecting out of double occupancy in the occupied sites N_l. The increase in doping concentration 'δ' decreases the number of occupied sites, thus decreasing the probability of double occupancy.

The vanishing of the total spin stiffness constant $\tilde{D}_s$ implies the loss of rigidity (rigidity arising from the antiferromagnetic coupling) of the spins of the carriers (holes) in the doped phase.

Again the vanishing of $\tilde{D}_s^t$ can arise from the vanishing of $\cos(k_x a)$ at $k_x=\pi/2$ and for the whole set of values of k_x ($0 \leq | k_x | \leq k_F$), at least one value should satisfy the above relation. Hence the boundary condition for the vanishing of $\tilde{D}_s^t$ should be determined by $k_F=\pi/2$. Thus from equation (2.11) and (2.12),

$$k_F = \sqrt{2\pi(1-\delta)}/a = \sqrt{2\pi n}/a = \pi/2 \tag{2.22}$$

This condition leads to,

$$n \geq 0.39 \tag{2.23}$$

$$i.e., \delta = (1-n) \leq 0.61 \tag{2.24}$$

The above inequality is the same as was obtained earlier [132]. So for doping concentration less than 0.61, $\tilde{D}_s^t$ goes to zero. Therefore the region below 61% doping is entirely governed by spin stiffness from the exchange part $\tilde{D}_s^J$. Again $\tilde{D}_s^J$ vanishes only when $\delta \to 1$ ie, for 100% doping and for $\delta \to 1$, the concentration of hole carriers (n) vanishes resulting in the vanishing of k_F and $\tilde{D}_s^t$ as well. Hence the total spin stiffness constant falls with increasing doping concentration and exactly goes to zero for $\delta=1$. The detailed numerical results elaborated later show that the stiffness constant practically vanishes at a much lower value of doping concentration, but a

negligibly small value prevails and it theoretically tends to zero as $\delta \rightarrow 1$. This result is in quantitative agreement with that of Himeda and Ogata that antiferromagnetic correlation prevails upto 100% doping [99].

Let me now come back to the conjecture involving the relation between the spin stiffness constant and the effective antiferromagnetic exchange coupling between mobile holes in the doped phase, as stated earlier. In order to test this conjecture, total spin stiffness constant is first of all scaled down by the effective number of pair of holes, ${}^{N_l}\mathrm{C}_2$, where N_l has been defined earlier. This makes the comparison between the spin stiffness constant and the antiferromagnetic exchange constant more meaningful and transparent in the background of a semi itinerant magnetic system produced by doping. Moreover, $\tilde{D}_s$ shows a very drastic fall with very small increase of δ and in contrast to it, the scaled stiffness constant shows a comparatively moderate fall with the increase of δ, which is much more alike to the plot obtained from the combined results of experiments and Monte Carlo calculations. This result is verified for all the lattice sizes including the 200x200 lattice, the largest lattice size that could be handle here. Thus the total spin stiffness constant corresponding to a single pair of mobile holes to be denoted as '$\tilde{D}_s$' is given as:

$$D_s = (\tilde{D}_s^J + \tilde{D}_s^t)/{}^{N_l}C_2 \tag{2.25}$$

This new quantity D_s is then calculated from the earlier obtained results for $\tilde{D}_s$ with parameters appropriate to $\mathrm{La}_{2-x}\mathrm{Sr}_x\mathrm{CuO}_4$ for different lattice sizes for enumeration and is plotted against doping concentration (δ). The theoretical graph is then compared with the experimental results in combination with those from other theoretical and computational techniques, as will be discussed in the next section.

2.3 Calculational Results and Comparison with Phenomenology and other Theoretical Approaches

Let us first of all review the relevant experimental and other theoretical and computational results for this problem. Neutron scattering studies have been carried out on $La_{2-x}Sr_xCuO_4$ samples at different doping concentrations. The results reveal the presence of finite intraplane magnetic correlation in 2-dimension above it's Neel temperature (T_N=190K) [105].

Above T_N, the long range interplane correlation is lost and 2-dimensional correlation length in pure La_2CuO_4 is $\sim 200\mathring{A}$ at 300 K. But in this temperature range the planes are still at low temperature since T<< intraplanar J.

The 2D antiferromagnetic correlation length, ξ_{2D} , has been measured in double-axis (energy integrating) experiments on a number of doped samples. It was found that ξ_{2D} is approximately independent of temperature, but it strongly depends on doping concentration [105] (see Fig.(2.1)).

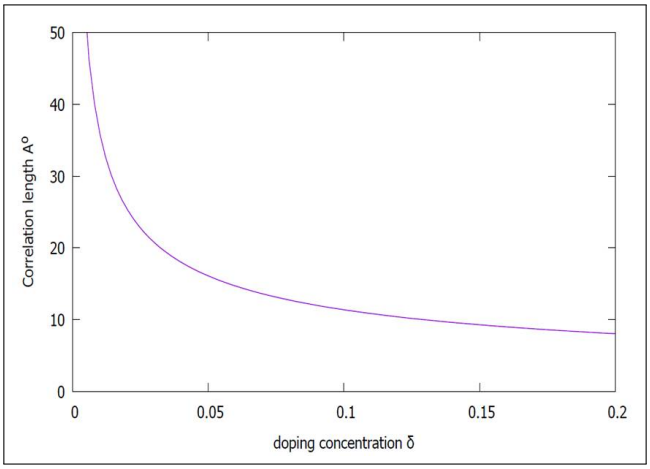

Figure 2.1: Magnetic correlation length vs. doping concentration 'δ' of $La_{2-x}Sr_xCuO_4$

This purely experimental plot gives the relation between 2-dimensional correlation length and doping concentration. However to extract the dependence of effective exchange constant on doping concentration, the Monte Carlo results for 2-dimensional Quantum Heisenberg Antiferromagnetic Model (2D QHAFM) is used, as will be discussed below. It must however be stressed that this combined semi-phenomenological scheme is only to provide a link between the results from rigorous theoretical approach and the experimental situation.

CHN calculated the temperature dependence of the magnetic correlation length of the spin 1/2 Heisenberg antiferromagnet corresponding to pure La_2CuO_4 using renormalization group analysis of quantum non-linear σ model (QNLσM).
They obtained for T$\rightarrow$0 [134]:

$$\xi_{2D} = C_\xi \, exp[\frac{2\pi\rho_s}{k_B T}] \tag{2.26}$$

where ξ_{2D} is the 2-dimensional antiferromagnetic correlation length and $2\pi\rho$s (=1.25J for undoped state corresponding to half-filled band) is the well known spin wave stiffness constant which is proportional to the bare nearest neighbour antiferromagnetic exchange constant 'J'. But, the significance of the derived generalized spin stiffness constant for the doped Heisenberg antiferromagnet is quite different from the spin wave stiffness constant defined above. Hence it is apprehended that the spin wave stiffness constant, which is also proportional to J_{bare}, should be different in magnitude from the doping dependent generalized spin stiffness constant derived by us. Moreover, the applicability of the t-J model is restricted to slightly less than half-filled band limit in the low doping side. So calculations are not possible at exactly δ=0 and thus, in this formalism all the calculations are restricted to $\delta \rightarrow 0$ limit.

Again Quantum Monte Carlo (QMC) studies have been performed on 2-dimensional Heisenberg antiferromagnets by Manousakis for very low doping at T$\rightarrow$0. The holes

in such a low doping limit are considered to be almost localized and the increase in doping enhances the itinerancy in the system. This character of doping is also experimentally observed in the layers of Sr doped La_2CuO_4 [147]. The numerical results of Manousakis in this 'nearly static hole regime' are fitted quite well with a function of exponential form, as in equation (2.26). The best fit is given by [136]:

$$\xi_{2D} = (\frac{0.276a}{\sqrt{(1-\delta)}})exp[\frac{1.25J}{T}] \tag{2.27}$$

where a=3.77A^o is the lattice constant for La_2CuO_4 and 0.276a is the prefactor for pure 2-dimensional Heisenberg antiferromagnet with 'J' appearing in the above equation to be regarded as '$J_{eff}(\delta)$' [148].

On the other hand the best fit of the experimental result from neutron scattering, neglecting the weak temperature dependence, is found to be [105],

$$\xi_{2D} = \frac{3.8}{\sqrt{\delta}} \tag{2.28}$$

Combining Eqs. (2.27) and (2.28), one arrives at the following semi-phenomenological relation between the effective anti-ferromagnetic exchange constant J_{eff} (>0) and δ in the very low doping regime (neglecting the temperature dependent prefactor),

$$J_{eff} = -ln[0.075(\frac{\delta}{1-\delta})] \tag{2.29}$$

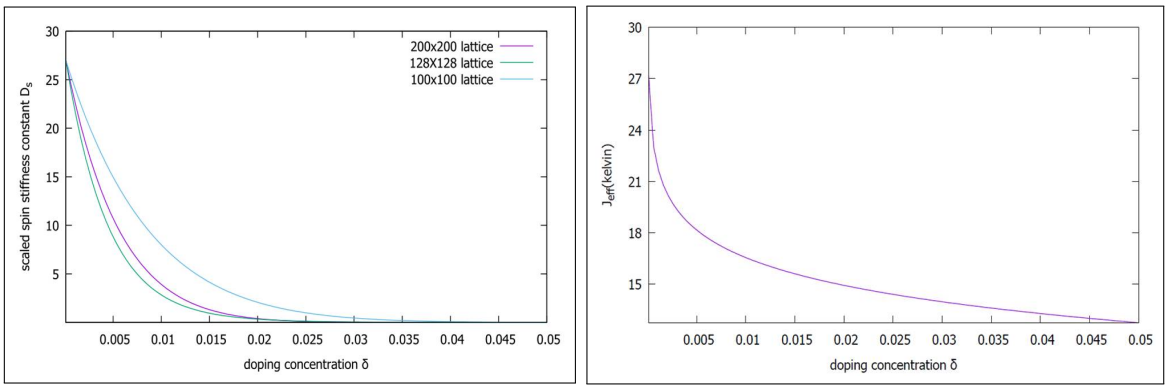

Figure 2.3: (a) Scaled spin stiffness constant 'D_s' vs. doping concentration 'δ' plot obtained from analytical calculation using t-J model with t$\sim$8J for three different lattice sizes [100x100(upper-most), 128x128(lower-most), 200x200(middle)]; (b) J_{eff} vs. doping concentration 'δ' plot using Eq. (2.32).

It is very clear from the strong similarities between the nature of the graphs seen in the two plots in Figs. (2.2) and (2.3), that the pair spin stiffness constant (D_s), calculated from the t-J model with strict NDOC at zero temperature and multiplied with proper proportionality constant, can very well represent the real physical effective antiferromagnetic exchange coupling constant 'J_{eff}' in the presence of doping at least qualitatively. Hence, the pair spin stiffness constant can truly be considered as equivalent to the effective exchange coupling at least in the very low doping region.

Here it may be noted that the plots show the effective exchange constant starting from $\delta \rightarrow 0$ limit (slightly less than half-filling) as the t-J model is not valid at exactly δ=0. The similarity is also prevalent for other samples with different band widths (2t) and Coulomb repulsion barrier V_{eff} ie., corresponding to different initial t/J ratios.

Having established the equivalence of this calculated 'D_s' and the physical 'J_{eff}', the variation of 'D_s' with doping concentration δ in the entire doping regime is studied (see Figs. 3(a)–3(c)). However, it must again be emphasized that the t-J model provides a genuine description of the real doped quantum antiferromagnet only in the low doping regime.

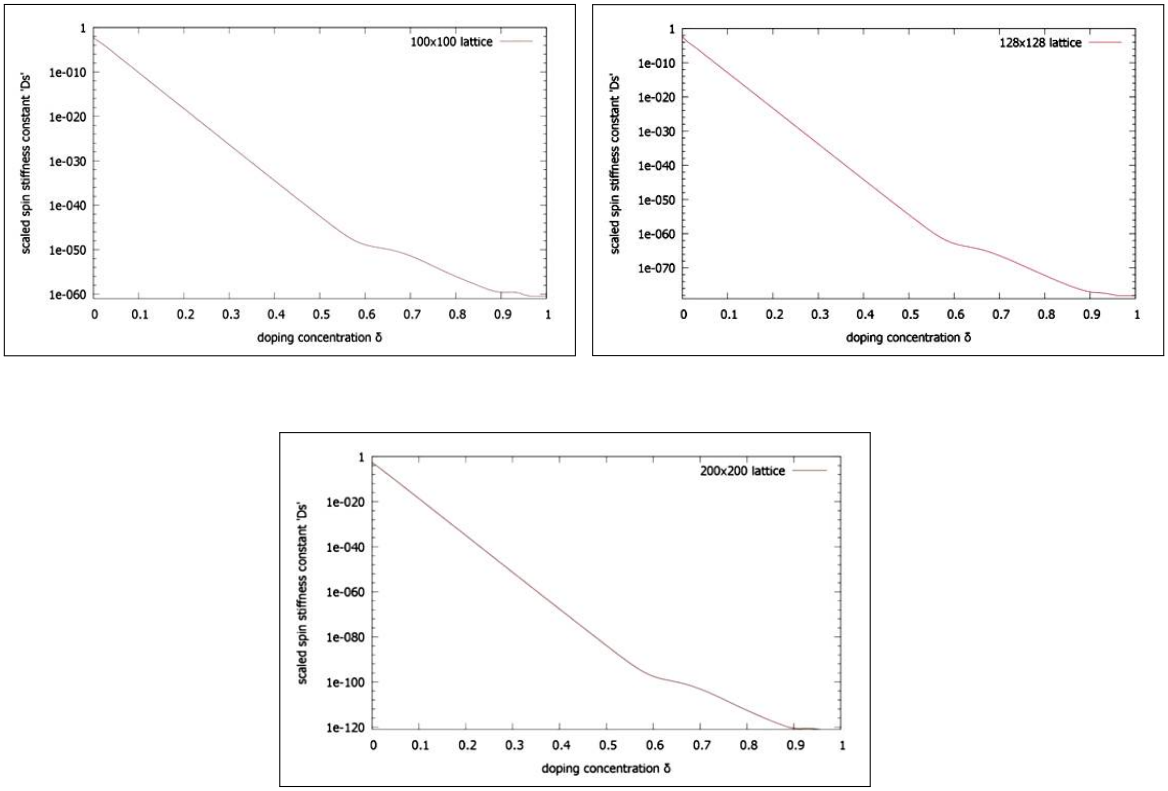

Figure 2.4: Scaled spin stiffness constant 'D_s' vs. doping concentration 'δ' upto 100% doping in logscale; (a) for 100x100 lattice, (b) for 128x128 lattice, (c) for 200x200 lattice.

From the plots displayed in Figs. (3(a)-3(c)), it can be noticed that there is a huge decrease in the magnitude of spin stiffness constant 'D_s' with increase in doping concentration and it practically becomes vanishingly small above 20% doping, which is again supported by the experimental results of Thurston et al. [105].

Moreover, one can find a shoulder-like structure or a point of inflection in all the above plots Figs. (3(a)-3(c)) near δ=0.61. This may very well indicate a point of cross-over or phase transition at zero temperature. Emery et al. have shown

the existence of phase separation in t-J model by both analytical calculation and exact numerical diagonalization in small in finite lattice [149]. The antiferromagnetic phase gets separated into a hole-rich phase and a hole-deficient phase for all J/t ratios below a minimum value of vacancy concentration given by $\delta < \delta_m$. For strong correlation (small J/t), phase separation occurs due to kinetic energy frustration in two dimension and the holes are put in a separate region to reduce kinetic energy [149]. The existence of the point of inflection near δ=0.61 in the derived analytical and numerical results, which is the artefact of the vanishing of $\tilde{D}_s^t$ below δ=0.61, can quite logically represent the occurrence of the phenomenon of phase separation below δ=0.61 as proposed by [149] and absence of it above this doping concentration. The vanishing of the contribution from the kinetic energy part is a plausible signature for the phase separation in this regime where the contribution to the spin stiffness constant arises solely from the exchange interaction term.

Furthermore, the exact vanishing of D_s only at $\delta \rightarrow 1$ in the calculational results, is the signature of the persistence of exchange coupling in the form of short range antiferromagnetic ordering almost upto 100% doping. This is quantitatively in agreement with results of Himeda and Ogata obtained from simplified variational calculations as discussed previously [99].

Himeda and Ogata attempted to implement the effect of NDOC through the projection operator of Gutzwiller state by renormalizing the magnitudes of hopping amplitude and exchange constant with doping dependent multiplicative factors g_t and g_s respectively in the background of an ideal Fermi sea. These renormalized parameters corresponding to hopping and exchange are related to the un-renormalized ones by the equations,

$$\tilde{t}_{eff} = g_t t, \qquad \tilde{J}_{eff} = g_s J \tag{2.30}$$

where g_t and g_s are the Gutzwiller factors calculated from variational energy calculation by Ogawa et al. [103]. The Gutzwiller factor acts as the enhancement factor on J that introduces the effects of the projection operator in the Gutzwiller state and the z-component of g_s stabilizes the antiferromagnetic order, as shown using the variational Monte Carlo results [99]. The Gutzwiller factor g_J has been derived as [99]:

$$g_s = \frac{4(1-\delta)^2}{(1-\delta^2+4m^2)^2} \tag{2.31}$$

where m is the expectation value of antiferromagnetic order parameter denoting the staggered magnetization in the long range antiferromagnetically ordered state. The vanishing of g_s and hence that of $\tilde{J}_{eff}$ at δ=1 is clear from the above expression for g_J . The quantity m is non-zero at $\delta \rightarrow$0 and is doping dependent ie., (m=m(δ)). Further m decreases with increasing doping δ and takes a very small value beyond δ=0.1 [99].

Thus from Eq. (2.31), it follows that g_s decreases with increasing δ and approaches zero value as $\delta \rightarrow$1. This is qualitatively very similar to the fall observed in D_s vs. δ plot and to the acquiring of vanishingly small values of D_s as δ approaches 1. Very importantly however, Himeda and Ogata could not identify any point of possible phase separation which is present in the plot of D_s vs. δ.

2.4 Discussion

The magnetic behaviour of the doped quantum antiferromagnets in 2D is studied in terms of generalized spin stiffness constant (D_s) corresponding to t-J model. The analytical calculations described above show that the calculated D_s theoretically goes to zero at 100% doping concentration. The part of D_s due to kinetic energy part

remains zero upto δ=0.61 for 2-dimensional lattices, then increases and again goes to zero at δ=1; however contribution to D_s from the exchange part monotonically decreases from very low δ and vanishes at δ=1. Total D_s is plotted against δ and it bears a striking similarity with the J_{eff} versus δ plot obtained by a combination of QMC results and experimental data in the low doping regime viz. $\delta \leq$0.05 (see Figs. (2.2),(2.3)) [136]. The results from Monte Carlo calculation with it's error limitations and experimental results are used to extract the dependence of physical J_{eff} on δ . Hence these errors and limita- tions are embedded in the J_{eff} vs. δ plot in (Fig. 2.3). It should be emphasized here however that even in this region of very small doping, the holes are not absolutely static as discussed above, but the kinetic energy contribution itself is very small which allows one to consider the holes as almost static in this region for the QMC based treatment [136, 137]. Regarding the results displayed in (Fig. (2.2)), the calculations could be performed on maximum lattice size only upto 200x200, which is much below the thermodynamic limit. Moreover, the validity of the t-J model is restricted to $\delta \rightarrow$0 limit, which restrained us from calculating the spin stiffness constant at δ =0. Despite all these limitations and crudeness, the similarity of the two plots under (Figs. (2.2),(2.3)) is highly significant.

The calculational results for D_s agree qualitatively with those of Himeda and Ogata at very high δ , as discussed previously. The notable absence of any point of inflexion in the mid-high δ regime in the work of latter, in disagreement with the results discussed above (see Figs. (2.3a)–(c)), is probably due to inadequate handling of correlation [99, 103]. On the other hand, in the very high δ regime the system effectively goes over to a weakly correlated phase even with a given repulsive potential [129]. Therefore, it is not surprising that the results agree with those of Himeda and Ogata in this regime.

The detailed band structure effects and interlayer processes are completely neglected

in my calculation, although it can help determining the magnetic phase boundaries in some of the real cuprate systems. The transition from long range to short range ordered phase has been studied previously using spin diffusion coefficient calculations [132]. This calculation based on time-dependent Hartree-Fock treatment for dynamical spin susceptibility, showed the survival of the long range ordered phase upto a critical doping concentration of 14%. This implied the existence of a finite value of T_N in the regime $0 \leq \delta \leq 0.14$, if the system is made quasi-two dimensional [132]. Later more accurate calculations were performed with the higher orders terms in the hopping amplitude 't' viz. (t^2 and t^4) taken into account in the self energy calculation [127,128]. The fall of correlation length and decay of long range ordered phase with increasing δ for different J/t ratios were studied [127]. According to the above results, the disappearance of long range order at T=0 is predicted from the vanishing of staggered magnetization 'm' at a critical doping concentration $\delta_c \approx 0.025$ for very small J/t ratio (J/t=0.2) [127]. This is in agreement with the present numerical results too (Fig. 1) [128]. In the present work based on non-perturbative method, the calculationally obtained sharp decay of D_s for $\delta \leq 0.03$ corresponding to J/t = 0.125 does also represent the rapid fall of both T_N and long range order with doping in this regime. This is very well supported by the above result [127]. Besides, one also confirms the existence of "novel paramagnetic phase" from present calculations, if bare 'J' is taken to be vanishingly small in the t-J model [132].

The highly doped regions in the plots (see Figs. (3.3a)–(c)) represent in a way the weakly correlated regimes for the system [99,119,129]. The system in this regime appears reasonable to be described by the FL Theory. However, the stringent NDOC at each site ensures the manifestation of the non-Fermi Liquid character of this phase. A detailed calculation here has been done taking into account only the nearest-neighbour exchange constant 'J' and hopping parameter 't' which automatically leads

to the renormalized effective exchange constant 'J_{eff}' (equivalent to D_s). This is in contrast to the various heuristic phenomenological models like, t-t'-t"-J or t-J_1-J_2 model which also try to understand the doped phase [89, 112]. Nevertheless, this first principle approach can very well capture the physics of doped quantum antiferromagnets.

In conclusion, the generalized stiffness constant calculation for the strongly correlated t-J model is quite powerful and does bring out the concept of effective antiferromagnetic exchange constant appropriate to a semi-itinerant system, quite neatly. Furthermore, the theoretical approach and results illustrated above are in excellent agreement with those from various other theoretical approaches and also brings out limitations of some of them. As stated earlier, the effective exchange constants of some itinerant magnets like Fe, Ni, Gd have been determined using the techniques based on 'inverse susceptibility'. Moreover, the exchange correlation in itinerant magnets can be expressed in terms of the elements of scattering path matrix in the framework of density functional approach [139, 142, 143]. Band structure calculation based on multiple-scattering theory and spin-spiral techniques has also been done for estimating the exchange interaction in these itinerant magnets [143]. The effective exchange constant involving the nearest neighbour spins is related to the second order derivative of the magnetic energy with respect to the spin fields. Making use of this formalism the effective exchange constant turns out to be the inverse dynamic magnetic susceptibility (DMS), with some assumptions for the weakly interacting systems [142]. All these approaches described above, show that there has been ongoing theoretical research to determine the exchange constant and study the short range correlations even in weakly correlated itinerant magnetic systems, which is still a challenging problem in the field of condensed matter physics. In this context, the scheme based on generalized spin stiffness calculation provides a novel formalism for

calculating the effective exchange constant of itinerant magnets, both weakly and strongly correlated.

Chapter 3

Determination of effective magnetic behaviour of doped itinerant antiferromagnets on one dimensional lattice

3.1 Introduction

The idea and concept of strong correlation and insulating antiferromagnetic properties in the materials existed from the times of Mott, Hubbard and Neel [3–5], as already mentioned in the first chapter. These materials show several interesting properties, the most important of which is the high temperature superconductivity in the materials at optimal doping region [104]. The interest about this unusual propery and it's theoretical understanding has not faded out even in the era of growing interest in nano and mesoscopic physics. The essential physics of these itinerant magnetic systems can be well captured by the single band t-J model at least in the low to medium doping regime. However, in the case of real materials like $YBa_2Cu_3O_{6+x}$, both Cu and O bands play decisive roles in determining the characteristic behaviour of the systems. The spins residing on the Cu ions situated on the Cu-O layers are almost localized and the introduced holes mainly stay on the O sites keeping the valences of the Cu ions unchanged, which is further supported by

some experimental results [147,150]. The Emery model is commonly used that takes into account these two kinds of atoms within a similar framework of the extended Hubbard model [151]. According to this model, the holes on the O ions are considered as the charge carriers and the pairing is mediated by strong coupling between the localized spins on the Cu sites, sitting between two O atoms [151]. Zhang and Rice derived a single band Hamiltonian starting from the two band model following the idea of single-band effective Hamiltonian originally proposed by Anderson [152]. Later on the two-band p-d model was reduced to the asymmetric Hubbard model, where the lower Hubbard band (LHB) is occupied by one hole Cu-d like states and the upper Hubbard band (UHB) is occupied by two-hole p-d singlet states [119,153]. In the strong coupling limit, this asymmetric Hubbard model can be reduced to the t-J model for the LHB [119,153].

The magnetic properties of the two dimensional layered systems have been studied for a long time based on the 2D t-J model, some of which have been already discussed in the preceding chapters. Although, here the main focus would be on the one-dimensional systems, but before that I would refer a few of the approaches based on 2D t-J model. For example, the Mori's projection technique based on two-time thermodynamic Green's function and Variational Monte Carlo simulations used to determine the magnetic correlations in the doped layered systems [120,123,128,128]. The phase separation in the 2D t-J model was also studied by minimizing the total energy with respect to the number of holes in the hole rich and hole deficient phase [149].

In case of 1D, the attempts are lesser in number, still there has been some progress. In one of those attempts, the holes in the system were only considered as the "missing spins" on a particular site, however, their actual spin configurations were neglected [149]. Moreover, the 1D t-J model has been exactly solved using the Bethe

Ansatz and various other numerical techniques at specific values of J/t [154, 155]. But for general J/t ratio these techniques could not be used. In this context, the Density Matrix Renormalization Group (DMRG) and Transfer Matrix Renormalization Group (TMRG) came up as attempts to study the spin correlations away from the super-symmetric points of the t-J model [156, 157]. The above numerical calculations were performed at certain chemical potentials, which accounts for the dependence of spin correlation on electron densities; whereas, no estimation of the exact values doping concentrations and doping dependence of exchange coupling could be given [157]. Thus there is a genuine need for an alternative approach to be attempted. In such a scenario, a more rigorous quantum mechanical approach was proposed to study the effective interaction between the spin and charge degrees of freedom of the carriers separately in the conducting phase of a strongly correlated system in 2D. This would help in identifying the magnetic correlations as well as fermionic pairing possibilities. For 1D strongly correlated conducting phase, this is even more relevant indeed and very important as there are exotic possibilities like 'spin-charge decoupling' [158].

In the previous chapter, the effective magnetic couplings were determined and various possible magnetic phases were predicted for the doped quantum antiferromagnets on a two-dimensional (2D) lattice. In the calculations the strict 'no double occupancy condition'(NDOC) on each site was imposed in the ground state wave function, characterizing a non-Fermi liquid (NFL) state. The interactions between the itinerant spin degrees of freedom has been studied in details, in the under-doped phase, in particular with the calculation of generalized spin stiffness constant ($\tilde{D}_s$) for this model. Moreover, a point of possible quantum phase transition was predicted in the over-doped regime, with the strongly correlated model extended to that region. The calculational results for the generalized spin stiffness constant corresponding to

a single pair of mobile holes (D_s) were compared with the experimental observations on layers of $La_{2-x}Sr_xCuO_4$ [105, 123, 136]. The comparison established the role of D_s as an effective intra-layer exchange constant between a pair of holes in the quasi-2D doped antiferromagnetic materials, at least in the regime of low doping concentration (δ).

Inspired by the successful application of the formalism in 2D doped quantum antiferromagnetic models, in the present chapter, a similar type of prescription has been has been applied for the theoretical investigation of the doping dependence of effective spin-spin coupling for the strongly correlated t-J model on the 1D lattice. The aim of this study is to explore the spin dynamics of this model as well and find possible application to chained cuprates in the underdoped phases. The results for 1D model are found to be in sharp contrast to the results for that of 2D, implying once again the strong lattice-dimensional dependence of low-dimensional magnetism.

In 2D, calculated exchange energy contribution to spin stiffness constant (D_s^J) shows a drastic fall with increase in δ in the low doping region, whereas, the kinetic energy contribution (D_s^t) remains zero throughout the low doping regime. This is in very good agreement with the previous experimental and theoretical (Monte Carlo) results [105, 136]. On the other hand, the calculated D_s^J in 1D falls even more rapidly initially with δ, and then in striking contrast to the 2D case, the D_s^t in 1D shows an increase with δ in the very low δ region, followed by a drastic fall again throughout the rest of the doping regime. This behaviour results in the appearance of a new peak in the very low δ region of the D_s^t vs. δ plot in 1D.

This approach and the formalism are further enriched by the possible comparison of the derived results in 1D model with the available experimental results from the Cu-O chains of $YBa_2Cu_3O_{6+x}$ (x being the doping concentration), which behaves as an itinerant paramagnet, believed to be describable by the strongly correlated t-J

model.

The role of Cu1-O1 planes in high temperature superconductivity has been a debated issue for a long time, but the necessity of the chains too have been established by many researchers and resonant elastic x-ray scattering has identified distinct ordering in chains and planes of $YBa_2Cu_3O_{6+x}$ [159–164]. Initially the oxygen holes enter the chains of $YBa_2Cu_3O_{6+x}$ followed by entry onto the Cu2-O2 planes beyond a critical value of x (x_c) [153, 160–162]. This indicates that the bulk susceptibility measurements on the sample in lower doping regimes corresponds mostly to the response from the chains of the compound [165].

Static spin susceptibility of exchange coupled paramagnetic systems is generally calculated from zero frequency limit of experimentally extracted imaginary part of dynamic spin susceptibility (DSS), using the Kramers Kronig relations [167]. Again the static limit of the well known Fluctuation Dissipation Theorem relates the real part of DSS to the static correlation function between the spin degrees of freedom in the system [167].

The effective intra-chain wave-vector dependent magnetic exchange constants ($J_{eff}(q)$) can be expressed as the inverse of the wave-vector dependent static spin susceptibility ($\chi(q)$) by using a standard theoretical approach developed for the itinerant magnets [142]. Following this, $J_{eff}(0)$ is calculated, i.e. the effective ferromagnetic exchange constant is extracted from the experimentally observed uniform dc magnetic susceptibility ($\chi(0)$) of $YBa_2Cu_3O_{6+x}$ [165,166]. Again, the scans corresponding to $q=Q\equiv \pi/a$ obtained from the inelastic neutron scattering experimental results for the above material are used to extract the effective exchange constant at the antiferromagnetic wave vector $Q=\pi/a$ [168].

Finally, following the approach, one can handle the short-ranged ordered paramagnetic phases of the strongly correlated doped antiferromagnetic systems in a more

comprehensive way, which has been a major challenge for the theoreticians so far. The earlier attempts to study the exchange interactions between the spins could determine the correlations between the localized spins or the itinerant spins only in the weakly correlated regime [139, 143, 169]. However, the detailed behaviour of exchange interactions between the spins in the strongly correlated itinerant regime remains unexplored till today . In this background, quantum mechanical approach described here, provides an efficient formalism for determining the exchange constant of strongly correlated semi-itinerant systems, without using the Density Functional approach and Multiple Scattering Theory [167, 168, 170, 171].

3.2 Mathematical Formulation and Calculation

As already discussed in the previous chapter, the t-J model Hamiltonian for strongly correlated electronic systems is given by [132]:

$$H_{t-J} = H_t + H_J \tag{3.1}$$

where H_t and H_J are the kinetic (due to doping) and exchange Hamiltonians respectively for the nearest-neighbour processes. Here it may be recalled that this kinetic energy part arises from the hopping of holes in the doped phase and the exchange part represents the exchange interactions between the itinerant spin degrees of freedom. Moreover, the t-J model gets reduced to the well known localized Heisenberg model corresponding to the completely half-filled band (undoped phase).

$$H_J = \sum_{<ij>} J_{ij}(\overrightarrow{S_i}.\overrightarrow{S_j} - \frac{1}{4}n_i n_j) \tag{3.2}$$

where S_i and S_j now represent the localized spin operators corresponding to the i^{th} and j^{th} sites respectively; J_{ij} is the exchange constant involving the i^{th} and the j^{th} site and for nearest neighbour pair $\langle ij \rangle$, J_{ij}=J; n_i and n_j are the occupation number operators for the i^{th} and j^{th} site respectively.

$$H_t = \sum_{<i,j>,\sigma} t_{ij} X_i^{\sigma 0} X_j^{0\sigma} \tag{3.3}$$

Here t_{ij} represents the hopping amplitude from j^{th} to i^{th} site and for nearest neighbour t_{ij}=t. The X's are the Hubbard operators that satisfy the Hubbard algebra and the commutation relation:

$$[X_i^{\alpha\beta}, X_j^{\gamma\delta}] = \delta_{ij}(\delta^{\beta\gamma} X_i^{\alpha\delta} - \delta^{\alpha\delta} X_i^{\gamma\beta}) \tag{3.4}$$

To avoid the rather complicated algebra of the Hubbard operators, for simplicity in the calculation, the Fermion operators satisfying the usual anti-commutation relation have been used. The relations between the spin and the Hubbard operators are also used [132]:

$$S_+ = X^{+-} \qquad S_- = X^{-+} \qquad S_z = \frac{1}{2}(X^{++} - X^{--}) \tag{3.5}$$

where the symbols used for all the spin operators have their usual meanings and they represent the itinerant spin operators.

The generalized spin stiffness constant ($\tilde{D}_s$) can be expressed as [132]:

$$\tilde{D}_s = \tilde{D}_s^t + \tilde{D}_s^J \tag{3.6}$$

where $\tilde{D_s^t}$ and $\tilde{D_s^J}$ are the contributions to spin stiffness constant from kinetic energy and exchange energy respectively and are given by [132]:

$$\tilde{D_s^t} = \lim_{\phi \to 0} (\frac{1}{2}) \frac{\delta^2 T}{\delta \phi^2} \tag{3.7}$$

and

$$\tilde{D_s^J} = \lim_{\phi \to 0} (\frac{1}{2}) \frac{\delta^2 E_J^{sf}}{\delta \phi^2} \tag{3.8}$$

where ϕ is the magnetic twist corresponding to the staggered Peierl's phase ϕ_σ arising from the presence of the vector potential $\mathrm{A}(\overrightarrow{r})$, with the property [132]:

$$\phi_\downarrow = -\phi_\uparrow = \phi \tag{3.9}$$

with 'T' being the expectation value of the kinetic energy part of the Hamiltonian (3.1) and 'E_J^{sf}' is the spin flip contribution to the expectation value of exchange energy part of the Hamiltonian [132].

The hopping amplitude 't' gets modified to $\mathrm{t}_{ij} e^{i\phi_\sigma}$ with the inclusion of the Peierl's phase ϕ_σ, if $\mathrm{A}(\overrightarrow{r})$ has a component along the direction of hopping [132].

The energy expectation values are calculated in the Gutzwiller state, the proposed variational ground state, with the double occupancy exclusion condition on each site [133]:

$$|\psi_G\rangle = \prod_l (1 - \alpha \widehat{n}_{l\uparrow} \widehat{n}_{l\downarrow}) |FS\rangle \tag{3.10}$$

where $|FS\rangle$ is the non-interacting Fermi sea and the variational parameter α denotes the amplitude for the projection out of the doubly occupied sites corresponding to the strongly correlated systems. For very strongly correlated systems ie.,for infinitely

large value of onsite Coulomb repulsion U with respect to bandwidth, the detailed numerical results show that the variational parameter α very close to 1 in the half-filled to low doping regime for the 2D systems [172]. As an approximation, taken α=1 has been taken even for 1D model, implying complete projecting out of the doubly occupied sites [132].

Further, the Fermi sea in equation (3.10) can be expressed in terms of Fermion creation operators and thus equation (3.10) becomes:

$$|\psi_G\rangle = \prod_l (1 - \widehat{n}_{l\uparrow}\widehat{n}_{l\downarrow}) \prod_{k\sigma}^{k_F} \sum_{ij} C^{\dagger}_{i\sigma} C^{\dagger}_{j-\sigma} e^{i(\overrightarrow{r_i} - \overrightarrow{r_j}).\overrightarrow{k}} |vac\rangle \tag{3.11}$$

where $|vac\rangle$, i, j and l have the usual meaning as described earlier; k is the wave vector bounded by the Fermi wave vector k_F which is defined with respect to the non-interacting free carriers in the ideal Fermi sea after introduction of vacancies. It might be noted that k_F being the Fermi wave vector for the non-interacting carriers at T=0, all the k-states below k_F are completely filled, as are occurring in the above equation (3.11).

For 1-D systems, the Fermi wave vector is related to the number of occupied sites as:

$$k_F = n(\pi/2a) \tag{3.12}$$

where 'a' is the lattice constant and 'n' is the fraction of occupied sites in the system defined by:

$$n = N_l/N = (1 - \delta) \tag{3.13}$$

Here 'δ' is the doping concentration; 'N_l' and 'N' are the number of occupied lattice sites and the total number of lattice sites respectively.

Making use of equations (3.12) and (3.13):

$$k_F = (\pi/2a)(1-\delta) \tag{3.14}$$

Again combining equations (3.2) and (3.11), E_J^{sf} can be expressed as:

$$E_J^{sf} = (\frac{2t_{eff}^2 cos(2\phi)}{V_{eff}}) \frac{{}_{NDOC}\langle\psi_G|H'_J|\psi_G\rangle_{NDOC}}{{}_{NDOC}\langle\psi_G|\psi_G\rangle_{NDOC}} \tag{3.15}$$

where

$$H'_J = \overrightarrow{S_i}.\overrightarrow{S_j} - \frac{1}{4}n_i n_j \tag{3.16}$$

with ${}_{NDOC}\langle\psi_G|\psi_G\rangle_{NDOC}$ being the factor for the normalization of the Gutzwiller state; t_{eff} and V_{eff} are the effective nearest-neighbour hopping and on-site Coulomb barrier potential respectively in the $\delta \to 0$ limit [132]. In the case of one-dimensional systems, the initial J in the $\delta \to 0$ limit is modeled as t_{eff}^2/V_{eff}. Here it must be kept in mind that the investigation for the variation of effective exchange constant with doping concentration has been done by keeping the initial t_{eff} and V_{eff} constant i.e. bare 't' and 'J' as constants.

The detailed rigorous calculations have been carried out for determining the expectation value of exchange energy in the Gutwiller state. Then taking derivative twice in the $\phi \to 0$ limit, one can get the expression for $\tilde{D_s^J}$ for one-dimension as (for detailed scheme of application see Appendix A):

$$\tilde{D_s^J} = -4J \prod_{k,\sigma}^{k_F} 2(1-\delta)^2 \tag{3.17}$$

where 'J' is the bare exchange constant, as explained earlier. This equation (3.17) looks very similar to the one for $\tilde{D_s^J}$ as was obtained for 2D, but here k_F corresponds to the Fermi wave vector for 1-D as given in equation (3.12). It is also seen here that the magnitude of $\tilde{D_s^J}$ analytically goes to zero only for $\delta \rightarrow 1$ ie., for 100% doping concentration, which of course signifies non existence of carriers (holes) in the system! Similarly, the expression for $\tilde{D_s^t}$ is also derived (for derivational scheme see Appendix B):

$$\tilde{D_s^t} = (-t)[\prod_{k,\sigma}^{k_F} 4cos(ka)(1-\delta)^2 - N_l \prod_{k,\sigma}^{k_F} 4cos(ka)/N^2] \tag{3.18}$$

The second term in equation (3.18) appears due to complete projection of the doubly occupied sites and becomes negligible for very high values of δ, as the chances of double occupancy decrease with increase in vacancies in the system.

Then from equation (3.18) one sees that the quantity $\tilde{D_s^t}$ vanishes for $\delta \rightarrow 1$. Furthermore, $\tilde{D_s^t}$ also vanishes if at least one value of 'k' in the whole set of values of k in the range $0 \leq |k| \leq k_F$ is $\pi/2a$ [132]. This condition will be satisfied if the upper boundary of k is greater than or equal to $\pi/2$a, which can be ensured with $(k_F)_{threshold} = \pi/2$a [132].

Then from equation (3.14)

$$(\pi/2a)(1-\delta) = \pi/2a \tag{3.19}$$

This condition can only be satisfied for $\delta \rightarrow 0$ ie., in the undoped phase.

Hence, the spin stiffness constant at the $\delta \rightarrow 0$ limit is solely due to the contribution from the exchange energy part and the total $\tilde{D_s}$ vanishes theoretically only for 100% doping concentration.

As was explained in our earlier paper, $\tilde{D_s^J}$ and $\tilde{D_s^t}$ are further scaled down by ${}^{N_l}C_2$

which is the number of possible pairs of mobile holes in the system.
Thus,

$$D_s = \tilde{D}_s / {}^{N_l}C_2 \tag{3.20}$$

Further, we have defined the contribution to the generalized spin stiffness from the exchange energy, per pair (D_s^J) as:

$$D_s^J = \tilde{D}_s^J / {}^{N_l}C_2 \tag{3.21}$$

and the contribution to the generalized spin stiffness from the kinetic energy, per pair (D_s^t) as [**?**]:

$$D_s^t = \tilde{D}_s^t / {}^{N_l}C_2 \tag{3.22}$$

D_s^J and D_s^t are evaluated and plotted against δ for bare J/t=0.1 and for three different lattice lengths viz.(1900,1940,1960) which are presented in the next section. The comparison with other theoretical and experimental results on doped $YBa_2Cu_3O_{6+x}$ are also presented in the next section of this chapter. It is quite pertinent to mention that the results do not change with increasing lattice size and thus attain convergence and become free of finite size effects as much as possible.

3.3 Numerical Results and Comparison with Experimental and other Computational Results

A vast literature surver was done for finding relevant experimental results on quasi-1D strongly-correlated doped antiferromagnetic systems [173–179]. The very few avail-

able experimental results on the doped $SrCu_2O_3$, $Sr_2Cu_3O_5$, $CaCu_2O_3$ etc. could not be used for detailed comparison with our theoretical results on strongly correlated t-J model [173–179]. Hence, for a detailed and rigorous comparison, the neutron scattering results from doped $YBa_2Cu_3O_{6+x}$ have been considered, which has both Cu-O chains and planes and is a Mott-Hubbard insulator in the parental phase. Moreover, the doped phase can be very well described by the strongly correlated t-J model [180]. The doping in $YBa_2Cu_3O_{6+x}$ introduces the vacancies only in the chains upto a critical doping concentration viz. $x_c \sim 0.41$ and during this the valencies of copper and oxygen in the planes remain unchanged [159]. Here it is important to point out that the randomly doped oxygen atoms in the chains convert the neighbouring Cu^{+1} ions into Cu^{+2} [181]. The oxygen doping induces coupling between the spins situated on the chains, after a considerable amount of mobile holes have been generated [163]. The further doping introduces more number of mobile holes and reduces the antiferromagnetic coupling between the itinerant spin degrees of freedom. As a consequence, the chains play a very important role in determining the response of the system to any externally applied perturbation, in the under-doped regime.

The wave vector dependent static spin susceptibility of $YBa_2Cu_3O_{6+x}$ can be extracted from the constant q-scans of the available neutron scattering data [165]. The next step is to determine the effective spin exchange coupling J(q) for any stable magnetic state in an itinerant magnetic system. In general spin exchange constant can be shown to be directly related to the inverse of static wave-vector dependent spin susceptibility $\chi^{-1}(q)$ [142]. To elaborate slightly on this, the non-local static magnetic susceptibility ($\tilde{\chi}$) can be expressed as the variation in spin magnetization 'm' with respect to the external static magnetic field (H_{ext}) in the continuum case as follows [142]:

where $\{m_r\}$ denotes the magnetization at $\{\overrightarrow{r'}\}$, representing any thermodynami-

cally stable spin configuration and 'E' is the ground state energy assuming the system to be at zero temperature.

Therefore from equation (3.23), we can write $\tilde{\chi}$ as [142],

$$\tilde{\chi} = \tilde{\chi}\ \ \tilde{J}(\overrightarrow{r}, \overrightarrow{r\prime})\ \ \tilde{\chi} \tag{3.23}$$

where $\tilde{J}(\overrightarrow{r}, \overrightarrow{r\prime})$, the exchange coupling in real space connecting the spin magnetizations at $\overrightarrow{r}$ and $\overrightarrow{r\prime}$, is given by the usual definition [142],

$$\tilde{J}(\overrightarrow{r}\,\overrightarrow{r\prime}) = -\frac{\delta^2 E}{\delta m(\overrightarrow{r})\delta m(\overrightarrow{r\prime})}\bigg|_{\{m(\overrightarrow{r})\}=\{m_r\}} \tag{3.24}$$

The above equations are very general ones valid for any itinerant magnetic system. Now making use of equations (3.23) and (3.24) and for convenience calling $\tilde{J}(\overrightarrow{r}, \overrightarrow{r\prime})$ as $\tilde{J}_{eff}(\overrightarrow{r}, \overrightarrow{r\prime})$ and $\tilde{\chi}(\overrightarrow{r}, \overrightarrow{r\prime})$ as $\tilde{\chi}_{eff}(\overrightarrow{r}, \overrightarrow{r\prime})$, appropriate to a doped quantum antiferromagnet (a special type of strongly correlated itinerant magnet), one can arrive at the following relation,

$$\tilde{J}_{eff}(\overrightarrow{r}, \overrightarrow{r\prime}) = \tilde{\chi}^{-1}_{eff}(\overrightarrow{r}, \overrightarrow{r\prime}) \tag{3.25}$$

Here, transaltional invariance and isotropy ensure $\tilde{\chi}(\overrightarrow{r}, \overrightarrow{r\prime}) \equiv \tilde{\chi}(|\ \overrightarrow{r} - \overrightarrow{r\prime}\ |)$.

Now, taking the Fourier transform,

$$J_{eff}(q) = \chi^{-1}_{eff}(q) \tag{3.26}$$

It may be noted that the equation (3.26) is valid for all wave vectors, corresponding to any thermodynamically stable magnetic state, whether spontaneously magnetically ordered or not [142,182]. Hence, this equation is valid even for the exchange coupled paramagnetic state with short-range spin correlations and may be used for determin-

ing J_{eff}(q) with the procedure being called 'inverse susceptibility approach' [142,182]. Therefore, corresponding to the antiferromagnetic wave vector q=Q$\equiv \pi/a$,

$$J_{eff}(\pi/a) = \chi^{-1}_{eff}(\pi/a) \tag{3.27a}$$

and for ferromagnetic coupling,

$$J_{eff}(0) = \chi^{-1}_{eff}(0) \tag{3.27b}$$

Incidentally the above equations, valid even for a non-FL, look formally quite similar to the relation between the static spin susceptibility and the inverse of Landau parameter for a FL [183].

Using the minimization condition in equation(3.24), one can notice that all the above values of 'J_{eff}' are negative. Here, we will concentrate on the variation of the absolute magnitude of 'J_{eff}' with δ, since the sign of 'J' for ferromagnetic and antiferromagnetic coupling solely depends on the sign convention in writing the Hamiltonian (equation (3.2)).

Interestingly, the quantity D_s represents another form of this spin-spin coupling in an itinerant magnet and its equivalence with J_{eff} was established earlier. Here I present our results for the variation of D_s^J and D_s^t with δ for J/t=0.1, which is true for most of the cuprates [184].

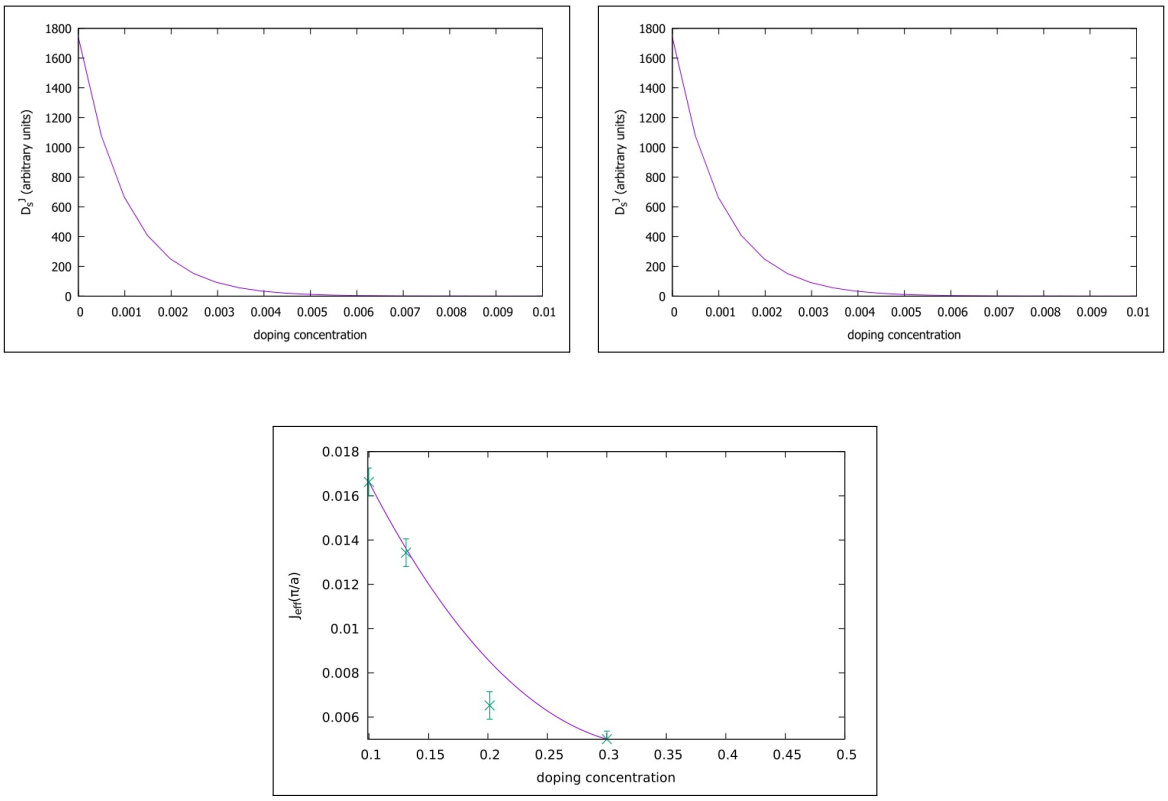

Figure 3.1: 'D_s^J' vs. doping concentration (δ) for: (a) lattice length=1900; (b) lattice length=1960; (c) $J_{eff}(\pi/a)$ vs. δ obtained from the neutron scattering results on $YBa_2Cu_3O_{6+x}$. (In Fig.(c): The line gives the best polynomial fit to the data) [168]

The plots in (Figs.(3.1a,b)) show that D_s^J falls drastically with increase in doping concentration and practically vanishes within $\delta \approx 0.005$. This δ is much lower than the critical doping concentration observed for the 2D lattices. The suppression of D_s^J corresponds to the fall in the "semi-localized part" of spin stiffness constant, further implying the destruction of original Heisenberg-like antiferromagnetic coupling in 1D with the introduction of very small amount of doping in the system.

Fig.(3.1c) shows the fall of $J_{eff}(\pi/a)$ as a function of δ, extracted from the constant q scans of neutron scattering data corresponding to q=Q$\equiv \pi/a$, which strongly resembles the behaviour our derived results of D_s^J against δ [168]. This rapid fall represents the loss in rigidity of the spins, as expected from the decay of semi-localized antiferromagnetism of the spins with Heisenberg-like character.

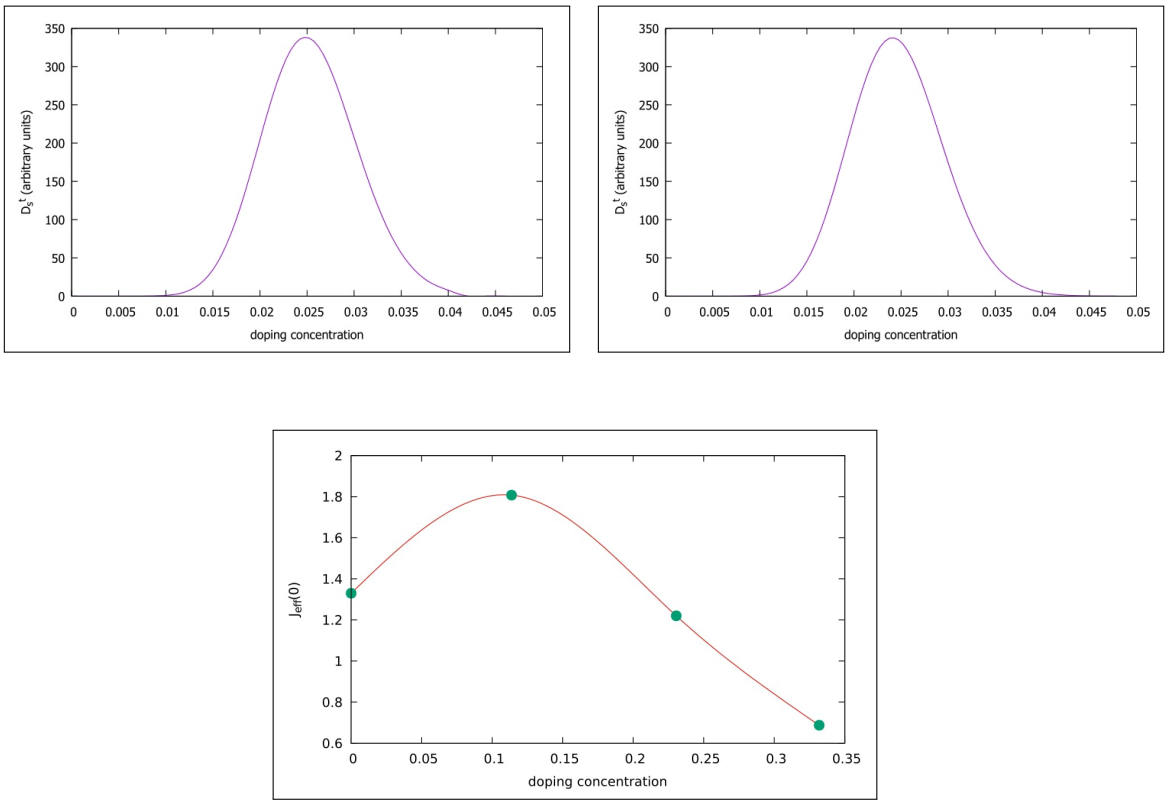

Figure 3.2: 'D_s^t' vs. doping concentration (δ) for: (a) lattice length=1900; (b) lattice length=1960; (c) $J_{eff}(0)$ vs. δ obtained from the dc susceptibilty measurements of $YBa_2Cu_3O_{6+x}$. (In Fig.(c): The line gives the best polynomial fit to the data) [165, 166]

Figs(3.2a,b) show that D_s^t vanishes at δ=0, in accordance to our analytical results in the previous section. Beyond $\delta \rightarrow 0$ limit, D_s^t increases with δ in the very low doping regime, followed by a subsequent fall throughout the rest of the doping region. This characteristic behaviour leads to the appearance of a maximum in the D_s^t vs. δ plot around 2%-3% doping concentration. The increase in the magnitude of D_s^t with δ and the appearance of the above peak signify the tendency of the itinerant spin degrees of freedom to develop another coupling, different from the original Heisenberg one.

The behaviour of experimentally extracted $J_{eff}(0)$ with increase in δ, in the low doping region, is shown in Fig.(3.2c) [165, 166]. $J_{eff}(0)$ initially increases with in-

creasing δ and again falls with further increase in doping concentration, giving rise to the appearance of a peak in the $J_{eff}(0)$ vs. δ plot (see Fig.(3.2c)]. A maximum is also seen in our calculated D_s^t vs. δ plot. Combining these experimental and theoretical results, we infer that there is a tendency of the itinerant spins in the system to develop a ferromagnetic-like coupling, corresponding to the wave vectors around q=0 [see Figs.(3.2a,b,c)). As δ is increased further, this coupling also gets greatly reduced and the spins become almost non-interacting to exhibit a behaviour analogous to Pauli-like in its magnetic response.

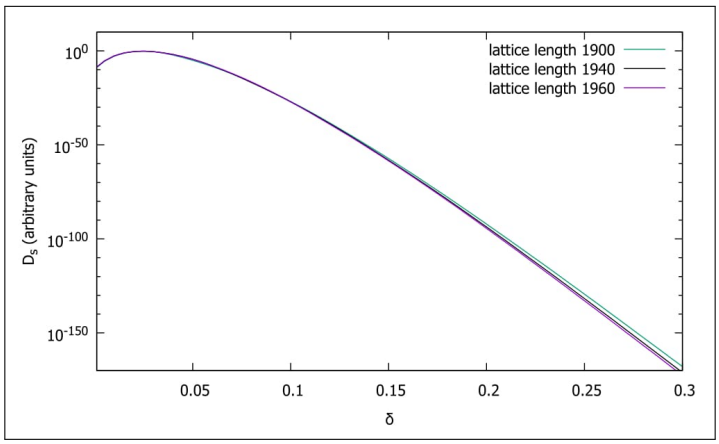

Figure 3.3: Scaled spin stiffness constant (D_s) vs. doping concentration (δ) for different lattice sizes in semi-logscale (Y-axis in log-scale)

The Fig.(3.3) shows the plot of D_s versus δ upto δ=0.3. There exists a very sharp peak situated very close to δ=0, corresponding to the original quasi-long range antiferromagnetic ordering of semi-localized nature. However, this peak occurring at the extremely small value of doping concentration could not be shown in this figure. The presence of the peak at finite δ shown in Fig.(3.3), does represent an itinerant magnetic coupling tendency and this reminds one of the Stoner-like behaviour of the spin susceptibility, although in a strongly correlated background here. Anyway,

it must be pointed out that this itinerant coupling tendency does not lead to any long-range order in the system, even at zero temperature. The above plot shows that the slope of the fall of D_s increases with increase in lattice size and the total spin stiffness practically vanishes much below 100% doping concentration. So it is worth mentioning that although analytical calculation proves the existence of rigidity of the spins upto 100% doping concentration, in reality the system becomes analogous to almost Pauli-paramagnetic-like at much lower value of doping concentration.

The comparison of our results with those from other theoretical approaches shows agreements and certain disgreements as well. This highlights the crucial importance of our formalism in describing the quasi-1D doped antiferromagnetic systems and also clearly brings out the shortcomings of a few of the other approaches. The singlet correlation between spins has been found previously using DMRG technique [156]. The calculated spin correlation falls with the increase in doping concentration [156]. As shown in Figs.(3.1-3.3), our derived D_s^J rapidly decreases with δ and practically vanishes within the range of very low doping concentration. Thus, this is in agreement with DMRG results in the low doping regime. Furthermore, the TMRG calculation shows an increase in static spin susceptibility ($\chi(0)$) with increase in δ [157]. The increase in static uniform susceptibility results in the fall of $J_{eff}(0)$ with δ, as discussed in detail in the previous section (see equation (3.27b)). So, this result is also in agreement with the behaviour of our calculated D_s^t as a function of δ, in the medium to over-doped regime.

Moreover, our analysis based on simple energetics consideration give an estimate of the size of a possible "Nagaoka strip" in a doped quantum antiferromagnet described by the t-J model in 1D, in analogy with the formation of a well-known "Nagaoka bubble" in 2D. The total energy of the Nagaoka strip with respect to the antiferro-

magnetically ordered state having no holes is given by [185]:

$$E = -2 + (2.40)^2/s^2 + 0.5Js \tag{3.28}$$

where 's' is the length of the possible Nagaoka strip in 1D, 0.5J is the energy cost of the creation of a ferromagnetic bond relative to an antiferromagnetic one [185]. Minimizing 'E' with respect to s gives:

$$s \approx 2.84J^{-1/3} \tag{3.29}$$

leading to,

$$E = -2 + 2.134J^{2/3} \tag{3.30}$$

Here 's' must be larger than one lattice spacing and also the system size must be much larger than 's' to avoid finite size effects [185]. The energetics consideration shows that there is a distinct possibility of formation of a Nagaoka strip, depending on the values of J , provided the above boundary conditions are satisfied.

3.4 Discussion

In the previous section, a detailed comparison of our calculational results with the relevant experimental and other theoretical ones are presented, which firmly established that the generalized spin stiffness constants can play the role of effective exchange constants for quasi-1D doped quantum antiferromagnets as well, like that in the case of quasi-2D approaches. Moreover, the results for 1D model are remarkably distinct from that of 2D and this striking contrast can have very different consequences for microscopic physics corresponding to various phenomena in quasi-1D and quasi-2D systems.

Our analytical and numerical results predicted the rapid decay of quasi-long-range ordered localized antiferromagnetic state, with increasing doping concentration (see Figs.(3.1a,b)). Most interestingly, our derived results in 1D, predicted the emergence of an unconventional itinerant paramagnetic phase with ferromagnetic spin-spin coupling, after the decay of quasi-long-ranged antiferromagnetically correlated one occurring at zero temperature (see Figs.(3.2a,b)). The comparison with experimentally extracted results from the chains of $YBa_2Cu_3O_{6+x}$ supports the emergence of this ferromagnetic-like coupling between the spin degrees of freedom, as described in the previous section [160, 163].

A few experimental studies had been carried out on the truly 1D Heisenberg chains like Sr_2CuO_3, where the intra-chain antiferromagnetic exchange constant (J=2200$\pm$200K) is much higher than the coupling between the chains [176, 183]. The susceptibility of Sr_2CuO_3 satisfies the Bonner Fisher behaviour throughout the entire temperature range [176, 186]. The doped Cu chains were also experimentally realized in $Ca_{2+x}Y_{2-x}Cu_5O_{10}$ [187]. The doping introduces static holes in the infinite chains of edge-linked CuO_4 plaquettes [187]. However, the prediction of ours is on the magnetic behaviour of purely 1D Cu-O chains doped with vacancies, which renders the holes to be itinerant. This should be taken up more seriously by computational physicists and experimentalists for further investigation.

The very novel prediction of ours regarding the tendency of spin-recoupling in 1D, is in sharp contrast to our former results in 2D, exhibiting a possibility of a quantum phase transition in the over-doped regime. The presence of a point of quantum phase transition in 2D possibly denotes the existence of a separated hole-rich and hole-deficient phase below the critical value of doping concentration, as was previously predicted by numerical calculations [149]. However, in 1D, the point of possible phase transition is not seen at any finite value of δ for our choice of J/t ratio. The

different phases of the 1-D t-J model was previously studied using the exact diagonalization results [154]. The presence of a phase separated state was confirmed by the divergence of thermodynamic compressibility around J_c/t=2.5-3.5 at various electron densities. At lower values of bare J/t, the phase separation is destroyed either in the limit of very low doping concentration ($\delta \sim 0$) or in the very high doping limit($\delta \sim 1$). This was denoted by a possible second order phase transition occurring at J/t=2 in the $\delta \sim 1$ limit [154].

The presence of a ferromagnetically ordered state in the two(three) dimensional t-J model was established by DMRG and classical Monte Carlo simulations [58, 188]. The motion of a single hole and a pair of holes in two dimension was studied using the exact diagonalization method [189]. The result shows that a single hole travels around a square to maintain the antiferromagnetic background intact, rather than travelling along a straight line [189]. Again, the motion of a single hole in the background of antiferromagnetically coupled spins were extensively studied in the atomic limit of the Hubbard model with U>>t. A single hole can form a ferromagnetic bubble (Nagaoka bubble) around itself to minimize the kinetic energy, provided J<<t [190]. The radius of the Nagaoka polaron increases with the decrease of J/t ratio [58, 188]. For finite values of J(J>0) and finite density of holes, the ground state is determined by the competing antiferromagnetic exchange interaction and Nagaoka ferromagnetism. This competition can lead to a phase separated state with a hole-rich ferromagnetic region and an antiferromagnetic region with localized spins [188]. For larger values of J/t, a different kind of spin arrangement is expected and there is a possibility that the introduced hole makes self-retracting excursions from the origin, leaving the antiferromagnetic background intact [191]. Interestingly, our calculations for the 1D t-J model with finite value of J/t($\sim$0.1) and finite number of holes, also show a tendency to develop a ferromagnetic coupling between the spins

in the lower doping region, which becomes more pronounced as J/t is decreased.

Recently, the phase diagram of the Hubbard model and frustrated Hubbard model has been studied using the density matrix embedding theory [192]. The strong coupling diagram technique revealed the influence of the long range spin and charge fluctuations in the long range antiferromagnetically ordered phase of the two-dimensional Fermionic Hubbard model, with large repulsions and at very low temperature [191]. The above technique showed the destruction of this antiferromagnetic ordering with the increase in doping concentration, similar to that of ours in the low doping regime [193]. In some other earlier works, the nature of the effective interaction between the static holes in doped $La_{2-x}Sr_xCuO_4$ was analytically studied in the very low doping region (x$\sim$0.05) [182]. The authors have shown that the addition of holes introduces ferromagnetic coupling between the Cu^{++} spins and the frustration leads to the emergence of a different type of a spin glass ordering in the under-doped regime [147, 150]. Later, a slightly different kind of model was derived from the two-band Emery model, which gets reduced to the Zhang-Rice proposed t-J model in the strong correlation limit [194]. For extermely large correlation the Zhange-Rice singlets are well formed, however, the singlets get deformed in the low energy limit and ferromagnetic bonds are formed between the neighbouring Cu atoms. The competing ferromagnetic and antiferromagnetic results in the spin-glass type of arrangement in general [194].

The strongly correlated 2D models often show a transition from a non-Fermi liquid (NFL) strange metal phase to weakly correlated Fermi liquid (FL) phase in the mid-δ regime with the same bare value of U [129, 158]. In contrast, the t-J model shows the possibility of 1D fermionic systems for small J behaving as Tomonaga-Luttinger liquids (TLL) with the power law scaling of the correlation functions [195]. Though, in this work, we did not analyze the behaviour of the k-dependent momentum dis-

tribution function near k_F, nevertheless, we could well specify the magnetic phases and the corresponding phase boundaries throughout the range.

Our overall calculation has been done considering the simplified t-J model on a 1D tight binding lattice under a semi-continuum approximation. The lattice sizes taken are also much below the thermodynamic limit (N$\rightarrow \infty$). However, the behaviour of the spin stiffness with δ remains unchanged with increase in lattice size and the size independence is reached with further increase in lattice size as the k-values are almost continuous for higher lattice sizes (see Figs(3.1a,b),(3.2a,b)). The applicability of the strongly correlated t-J model to the over-doped regime in real materials is questionable, as the on-site Coulomb correlation between the holes in the system weakens drastically with increase in δ in the higher doping regimes. Nevertheless, our non-perturbative calculations on the basis of the t-J model can correctly predict the magnetic behaviour of doped antiferromagnets keeping the 'no double occupancy condition' intact, at least in the under-doped regime.

I have already stated in the preceding sections that our results are all derived considering only the nearest neighbour hopping and interactions between the spin degrees of freedom (t-J model). Regardless of this, the detailed comparisons of our results with the available experimental results, clearly demonstrates the success of our approach and formalism for analysing the magnetic correlations present in the low-dimensional strongly correlated doped antiferromagnetic systems. However, for real materials, the higher neighbour terms for both hopping and interaction play a significant role in determining the magnetic properties and even the high temperature superconducting phase boundaries of the hole-doped cuprates [196]. Therefore, a deeper understanding of the magnetic phase boundaries of these materials requires the inclusion of higher neighbour hopping and interaction in the corresponding calculations. In this context, we have done some calculations, considering the t_1-t_2-t_3-J

model, which show that the point of possible quantum phase transition in 2D could be brought down to the mid-δ regime from the over-doped phase. This transition point incidentally may coincide with that of the cross-over from anomalous Mott-Hubbard conducting phase to normal Fermi liquid-like metallic phase in real materials [9, 197, 198]. Carrying out similar calculations for the 1D strongly correlated t_1-t_2-t_3-J model, we have found that the position of the peak in D_s occurring at a finite δ, gets shifted to lower values of δ and it reaches the $\delta \rightarrow 0$ limit beyond the critical values of t_2 and t_3. The calculations including the higher neighbour exchange interactions are also necessary to strengthen our approach in future, for detailed investigation of the magnetic correlations in the doped quantum antiferromagnets [110, 111, 113]. The calculations of charge couplings using a similar kind of prescription for the t_1-t_2-t_3-J model will be presented in detail in the next chapter

To summarize, our calculations for generalized spin stiffness constant, introduces a comprehensive way for determining the evolution of the effective exchange coupling for the 1D strongly correlated t-J model with doping. With this, it is also possible to determine the magnetic phases appearing in the strongly correlated long-range antiferromagnetic insulators upon hole doping, in both one and two dimensions. The effective spin-spin interactions in the short-ranged ordered conducting paramagnetic phases showing NFL behaviour, have been studied with much rigour and precision. Further, the study of the interactions between the charge degrees of freedom, in terms of generalized charge stiffness constant (spin symmetric quantity) are described in the next chapter.

Chapter 4

Investigation of charge coupling in low-dimensional hole-doped quantum antiferromagnets

4.1 Introduction

Most of the layered cuprate superconductors are known to exhibit many characterististic phases, supported by consistent experimental evidences [199–201]. As discussed in the last two chapters, the spin dynamics plays an important role in studying the magnetic behaviour of the phases, bearing the signatures of strong and weak correlations in the different doping regions. The phases include the long range ordered antiferromagnetic phase in low doping regime, anomalous non-Fermi liquid-like conducting phase and normal Fermi liquid-like conducting phase at higher doping regions. Interestingly, the optimally doped region shows high temperature superconductivity below the corresponding critical temperature [199–201]. However, the subsequent discussions about this unconventional superconductivity in cuprates are necessarily accompanied by the possibility of pair formation in these systems. The interaction between the charge degrees of freedom, in effect to the Coulomb

potential, are important in determining the pairing possibility in the strongly correlated doped phases [150]. Study of correlations between the spin and charge degrees of freedom in the itinerant phases of doped cuprates involves the Cu and the O bands [147, 150]. Later, the two band Hamiltonian was reduced to the well known single band t-J model in the low energy limit [119, 152, 153].

The magnetic interaction in 2D systems was studied using many theoretical approaches including Mori's projection technique based on two-time thermodynamic Green's function and Variational Monte Carlo simulations [123, 124, 127, 128, 205]. On the other hand, the 1D t-J model is exactly solvable using Bethe Ansatz at specific values of J/t [154, 203]. Density Matrix Renormalization Group (DMRG) and Transfer Matrix Renormalization Group (TMRG) techniques have been used very successfully in 1D to find the spin correlations away from the super-symmetric points [54, 156]. In 2D too, some attempts using DMRG have been done to find the spin and charge density orders in the doped Hubbard model [157]. In the previous chapters, we have discussed a non-perturbative quantum mechanical approach to determine the spin correlations in both 2D and 1D doped antiferromagnets, on the basis of generalized spin stiffness constant corresponding to the t-J model. Our results in 1D lead to a very interesting consequence regarding the formation of a new type of spin-spin coupling as doping increases, which is totally distinct from the original antiferromagnetic coupling seen in the insulating and under-doped phases. Our novel prediction was further supported by other experimental and theoretical results .

Beside the spin correlations, the attempts to determine the charge correlations include the determination of the inverse dielectric function, involving the standard many body formalism in a Fermi liquid [182]. The total free energy used in the calculation comprises of the Hartree-like term and the exchange correlation contributions.

It was found that the Coulomb interaction thus calculated from the inverse of dielectric function, can even change sign and turn attractive if the spin susceptibility is larger than a threshold value [182]. This can trigger the possibility of pairing in some of the doped antiferromagnetic systems. However, the above technique could not determine the charge coupling in strongly correlated phases of the systems, where the double fermionic occupancy on each site is disallowed.

The other approaches include the finding of the local charge stiffness tensor ($D_{\alpha\beta}$) as the response of the system to any change in boundary condition [204]. The component $D_{\alpha\alpha}$ was used to find the optical mass and was shown to be directly proprtional to the Drude weight [204]. But the magnitudes of charge stiffness constants, calculated by applying the Lanczos algorithm, were determined only at discrete values of hole concentrations [204, 205]. The Drude weight calculated by exact diagonalization technique in Hubbard cluster shows an increase in the lower doping regime, where the interacting holes are considered as the major carriers [164]. Furthermore, in the over-doped regime, the weakly interacting electrons take the role of the major carriers and the Drude weight falls in magnitude [206]. Moreover, the dynamical conductivity derived based on the memory function technique in terms of the Hubbard operators, was found to be proportional to doping concentration [119]. In contrast to the 2D case, both Hubbard and t-J models are exactly solvable in 1D, involving the Bethe ansatz [52, 79, 207, 208]. The transport properties for the 1D Hubbard model has been studied using the Bethe Ansatz solution combined with the global symmetry and the operator algebra for the Hubbard operators [209]. The charge stiffness constant calculated at finite temperature ($T>0$) corresponds to the response to a static field characterizing the weightage of the Drude peak [209]. However, these calculations were carried out only on the exactly half-filled Hubbard model i.e., zero doping limit. In order to have a more clearer, definite and detailed understanding of the

doping dependences of the charge stiffness, we embark upon an analytical approach.

In this chapter, I would describe a detailed formalism for determining the interaction and coupling between the charge degrees of freedom and to put forward a comparative study between the charge and the spin couplings. Similar to the case of spin degrees of freedom, here the doping dependence of charge-charge coupling is studied in terms of the evolution of generalized charge stiffness constant with doping concentration at T=0. In the strongly correlated under-doped regime, we have involved the nearest neighbour t-J model preventing the double occupancies. However, in the weakly correlated over-doped regime, we have used the t_1-t_2-t_3-J model with the Gutwiller variational parameter α very small or zero, which allows double occupancies in the system. The results of charge stiffness in the lower doping regions are compared with other theoretical and experimental results on layered cuprate systems [206, 211]. Based on the comparisons, we have shown a qualitative equivalence between Drude weight and our derived charge stiffness constant. The connection between charge stiffness and effective Coulomb interaction in the doped regimes is also established within the framework of random phase approximation (RPA). Finally, I have explored the consequences and various possibilities arising from our systematic studies as stated above.

4.2 Results

4.2.1 Calculational formalism and numerical results for charge stiffness

Strongly correlated and with nearest neighbour hopping

The nearest neighbour t-J model Hamiltonian for strongly correlated electronic systems is [146, 212]:

$$H_{t-J} = H_t + H_J \tag{4.1}$$

where H_t and H_J represents the hopping and exchange interactions involving nearest neighbour sites, respectively with restrictions on double occupancy at each site. The expression for the kinetic energy Hamiltonian is given as [146, 212]:

$$H_t = -\sum_{<i,j>,\sigma} t_{ij} X_i^{\sigma 0} X_j^{0\sigma} \tag{4.2}$$

Here t_{ij} represents the hopping amplitude from j^{th} to i^{th} site and for nearest neighbour t_{ij}=t and the X's are the Hubbard operators.

Again for the exchange energy part is represented as [146, 212]:

$$H_J = \sum_{<ij>} J_{ij}(\overrightarrow{S_i}.\overrightarrow{S_j} - \frac{1}{4} n_i n_j) \tag{4.3}$$

where S_i and S_j now represent the spin operators corresponding to the i^{th} and j^{th} sites respectively; J_{ij} is the exchange constant involving the i^{th} and the j^{th} site and for nearest neighbour pair $\langle ij \rangle$, J_{ij}=J; n_i and n_j are the occupation number operators for the i^{th} and j^{th} site respectively.

As was done earlier for generalized spin stiffness constant ($\tilde{D}_s$), a similar kind of equation also holds for the generalized charge stiffness ($\tilde{D}_c$)

$$\tilde{D}_c = \tilde{D}_c^t + \tilde{D}_c^J \tag{4.4}$$

where $\tilde{D}_c^t$ and $\tilde{D}_c^J$ are the contributions to charge stiffness constant from kinetic energy and exchange energy respectively and are given by [130, 132]:

$$\tilde{D}_c^t = \lim_{\phi \to 0} (\frac{1}{2}) \frac{\delta^2 T}{\delta \phi^2} \tag{4.5}$$

and

$$\tilde{D}_c^J = \lim_{\phi \to 0} (\frac{1}{2}) \frac{\delta^2 E_J}{\delta \phi^2} \tag{4.6}$$

where 'T' and 'E_J' are the kinetic energy expectation value and exchange energy expectation value of the t-J Hamiltonian. ϕ is the electric twist corresponding to the Peierl's phase ϕ_σ arising from the presence of the vector potential $A(\overrightarrow{r})$ as used in the definition of generalized stiffness constants [130, 132]. The quantity ϕ_σ has the following property for the spin symmetric case:

$$\phi_\downarrow = \phi_\uparrow = \phi \tag{4.7}$$

[This is unlike the spin asymmetric case, where we had used $\phi_\downarrow = -\phi_\uparrow = \phi$]

We have evaluated the expectation values in the Gutzwiller state.

$$|\psi_G\rangle = \prod_l (1 - \alpha \widehat{n}_{l\uparrow} \widehat{n}_{l\downarrow}) |FS\rangle \tag{4.8}$$

where α is the variational parameter deciding the amplitude for no-double occupancy of any site and |FS⟩ is the Fermi sea ground state. At first we take α=1 for completely projecting out the doubly occupied sites.

$$|\psi_G\rangle_{NDOC} = \prod_l (1 - \widehat{n}_{l\uparrow}\widehat{n}_{l\downarrow}) \prod_{k\sigma}^{k_F} \sum_{ij} C^\dagger_{i\sigma} C^\dagger_{j-\sigma} e^{i(\overrightarrow{r_i} - \overrightarrow{r_j}).\overrightarrow{k}} |vac\rangle \tag{4.9}$$

where $|vac\rangle$, i, j and l have the usual meaning.

The exchange energy for the spin symmetric case (see eq.(6)) can be written as:

$$E_J = (\frac{zt^2_{eff}}{V_{eff}}) \frac{{}_{NDOC}\langle\psi_G|H'_J|\psi_G\rangle_{NDOC}}{{}_{NDOC}\langle\psi_G|\psi_G\rangle_{NDOC}} \tag{4.10}$$

where 'z' is the co-ordination number i.e., z=4 for 2-D and 2 for 1-D and

$$H'_J = \overrightarrow{S_i}.\overrightarrow{S_j} - \frac{1}{4} n_i n_j \tag{4.11}$$

with ${}_{NDOC}\langle\psi_G|\psi_G\rangle_{NDOC}$ being the normalization factor for the Gutzwiller state $|\psi_G\rangle_{NDOC}$.

Since E_J is ϕ independent [see eq.(10)],

$$\tilde{D}^J_c = 0 \tag{4.12}$$

Thus $\tilde{D}_c = \tilde{D}^t_c$ always.

Hence the exchange energy contribution to charge stiffness vanishes in the entire doping region. This may be completely physical because the interchange of spins has no effect on the carriers in terms of their charge responses.

The total charge stiffness is given by the kinetic energy contribution to charge

stiffness ($\tilde{D}_c^t$). The kinetic energy is derived as:

In 2D,

$$T(\phi \neq 0) = (-t)[\prod_{k_x,\sigma}^{k_F} \sum_{\sigma} 4cos(k_x a)(1-\delta)^2 cos(\phi_\sigma) - N_l \prod_{k_x,\sigma}^{k_F} \sum_{\sigma} 4cos(k_x a)cos(\phi_\sigma)/N^2] \tag{4.13}$$

Now taking the second order derivative, one can get:

$$\tilde{D}_c = (t)[\prod_{k_x,\sigma}^{k_F} 4cos(k_x a)(1-\delta)^2 - N_l \prod_{k_x,\sigma}^{k_F} 4cos(k_x a)/N^2] \tag{4.14}$$

(while the vector potential is applied in x-direction)

Similarly, for 1D,

$$\tilde{D}_c = (t)[\prod_{k,\sigma}^{k_F} 4cos(ka)(1-\delta)^2 - N_l \prod_{k,\sigma}^{k_F} 4cos(ka)/N^2] \tag{4.15}$$

where N_l=N(1-δ), N is the total number of sites and 'δ' is the doping concentration and the Fermi momentum k_F in 2-D has the form in the quasi-continuum approximation [132]:

$$k_F = \frac{\sqrt{2\pi(1-\delta)}}{a} \tag{4.16}$$

and in 1-D:

$$k_F = (\pi/2a)(1-\delta) \tag{4.17}$$

Here it can be noted that the form of $\tilde{D}_c^t$ is similar to that of $\tilde{D}_s^t$ in both one and two dimensions. Hence following the same arguments described in our two previous

papers, $\tilde{D}_c$ vanishes if at least one value of k_x in 2D (k in 1D) satisfies:
For 2D,

$$k_x a = \pi/2 \tag{4.18}$$

and for 1D

$$ka = \pi/2 \tag{4.19}$$

This condition can be satisfied only when $k_F a = \pi/2$. Using the expressions for k_F (see eqs. (4.16,4.17)), one can get the vanishing conditions are $\delta \to 1$ and $\delta \leqslant 0.61$ for 2D model and at $\delta \to 1$ and $\delta \to 0$ for 1D. For the vector potential applied in the x-direction, we get the value of $\delta = \delta_c \approx 0.61$, below which the charge stiffness remains zero in 2D.

The total charge stiffness constants derived for the strongly correlated $\alpha = 1$ case in 2D and 1D are plotted against δ (see Figs.(4.1,4.2)). In the plots, the total charge stiffness has been scaled down by the number of pairs of mobile holes in the system, to extract an equivalent stiffness corresponding to a pair of mobile charge carriers:

$$D_c = \tilde{D}_c / {}^{N_l}C_2 \tag{4.20}$$

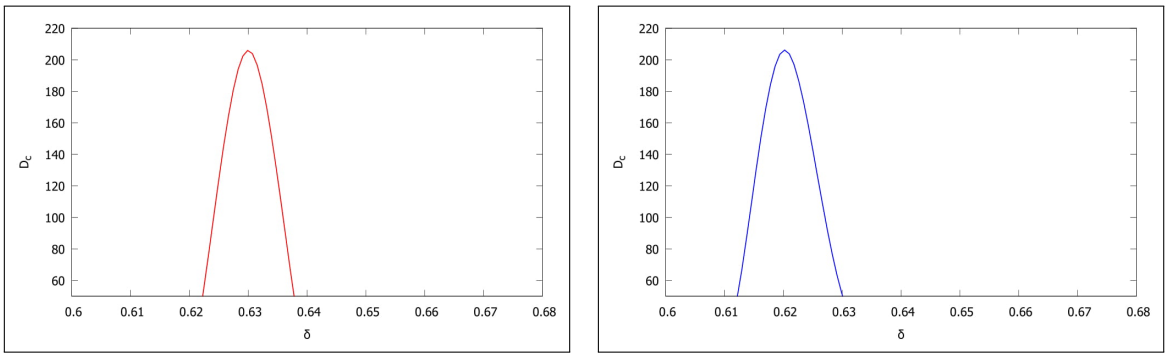

Figure 4.1: D_c vs. δ in 2D: (a) lattice size=700x700; (b) lattice size=800x800

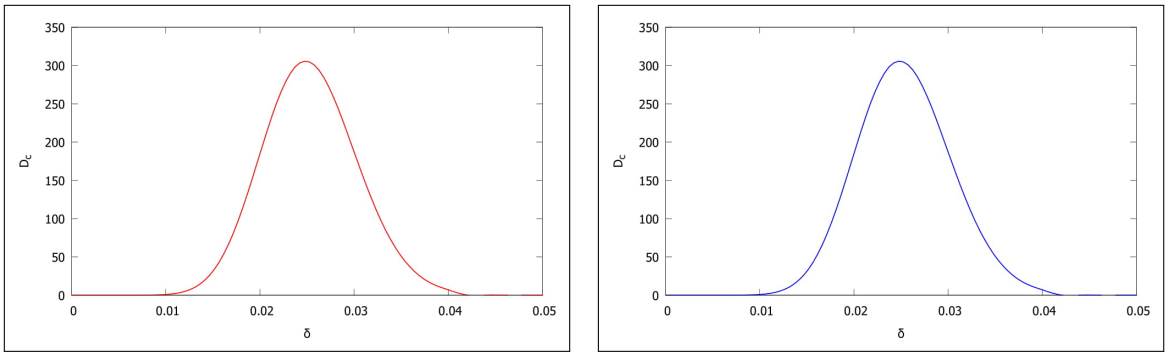

Figure 4.2: D_c vs. δ in 1D: (a) lattice length=1800; (b) lattice length=1900

In 2D, the scaled charged stiffness constant vanishes upto the critical doping concentration δ_c, followed by a sharp rise in D_c. The D_c again falls drastically with further increase in doping concentration, giving rise to the appearance of a very sharp cusp-like peak in the over-doped region as shown in Figs.(4.1a,b). For the 1D model, D_c shows a maximum in the low doping region, and zero elsewhere (see Fig.(4.2a,b)). Nevertheless, the calculation in the over-doped regime is not justified only with the nearest neighbour t-J model. The inclusion of higher neighbour hopping terms are necessary for correctly predicting the behaviour of the higher doping regions.

Weakly correlated with higher neighbour hoppings

In the previous sub-section, the charge stiffness in the strongly correlated regime is derived, considering only the nearest neighbour interaction. Now, in this sub-section I will consider the stiffness constants for any general value of α. As stated earler, the value of α controls the amount of double occupancies in the system and the smaller values of α allow higher number of doubly occupied sites. Here, for a comparative study, we consider the the limiting case of the highly over-doped regime, which mimics the ideal Fermi sea with α=0 i.e, allowing double occupancies in the system. Moreover, in the over-doped regime, the higher neighbour hoppings are also significant, so two higher neighbour terms are incorporated in the t-J model.
The t_1-t_2-t_3-J model is given as [213]:

$$H = -t_1 \sum_{<i,j>,\sigma} C^{\dagger}_{i\sigma} C_{j\sigma} - t_2 \sum_{<<i,j>>,\sigma} C^{\dagger}_{i\sigma} C_{j\sigma} - t_3 \sum_{<<<i,j>>>,\sigma} C^{\dagger}_{i\sigma} C_{j\sigma} + J \sum_{<i,j>,\sigma} S_i.S_j \tag{4.21}$$

where t_1, t_2 and t_3 represent the first, second and third neighbour hopping amplitudes respectively.

With the vector potential applied along the x-direction as before, we get, in 2D,

$$\begin{aligned} \tilde{D}_c = [\prod_{k_x,\sigma}^{k_F} 4\{(t_1)cos(k_x a) + (t_2)cos(2k_x a) + (t_3)cos(3k_x a)\}(1-\delta)^2 - \\ \alpha N_l \prod_{k_x,\sigma}^{k_F} 4\{(t_1)cos(k_x a) + (t_2)cos(2k_x a) + (t_3)cos(3k_x a)\}/N^2] \end{aligned} \tag{4.22}$$

and in 1D,

$$\tilde{D}_c = [\prod_{k,\sigma}^{k_F} 4\{(t_1)cos(ka) + (t_2)cos(2ka) + (t_3)cos(3ka)\}(1-\delta)^2 - \alpha N_l \prod_{k,\sigma}^{k_F} 4\{(t_1)cos(ka) + (t_2)cos(2ka) + (t_3)cos(3ka)\}/N^2] \quad (4.23)$$

Now, I consider the limiting case with α=0 i.e, the double occupancy is totally allowed on the sites and then the Gutzwiller state reduces to that of an ideal Fermi system:

$$|FS\rangle = \prod_{k\sigma}^{k_F} \sum_{ij} C^{\dagger}_{i\sigma} C^{\dagger}_{j-\sigma} e^{i(\overrightarrow{r_i} - \overrightarrow{r_j}).\overrightarrow{k}} |vac\rangle \quad (4.24)$$

Calculating the kinetic energy in this case (α=0) for 2D,

$$\tilde{D}_c = \prod_{k_x,\sigma}^{k_F} 4\{(t_1)cos(k_x a) + (t_2)cos(2k_x a) + (t_3)cos(3k_x a)\}(1-\delta)^2 \quad (4.25)$$

and for 1D,

$$\tilde{D}_c = \prod_{k,\sigma}^{k_F} 4\{(t_1)cos(ka) + (t_2)cos(2ka) + (t_3)cos(3ka)\}(1-\delta)^2 \quad (4.26)$$

From eqs.(4.22-4.26), one can see that the vanishing conditions for $\tilde{D}_c$ corresponding to α=0 in 2D are $\delta \to 1$ and $\delta \leqslant \delta_c$, where δ_c depends on the relative magnitudes of t_1, t_2 and t_3. For t_2=t_3=0, the value of δ_c goes to 0.61, which is exactly the same as the corresponding value of δ_c obtained for the nearest neighbour t-J model. For 1D t_1-t_2-t_3-J model, D_c vanishes only at $\delta \to 1$, however, the vanishing conditions for pure t-J model are retained for t_2=t_3=0. In this case, the point, where the stiffness exhibits a jump (δ_c) appears in the optimal doping region which is much lower than

that was obtained from the nearest neighbour t-J model. The charge stiffness again falls with further increase in doping concentration, due to the the presence of large number of vacancies in the system. The recent experimental observations from some of the doped correlated systems seem to have a link with this result of ours [214].

The plots of D_c for weakly correlated t_1-t_2-t_3-J model in two dimension, are presented in Fig.(4.3). The corresponding plots for 1D are given in Fig.(4.4). The values of t_2/t_1 and t_3/t_1 were determined by fitting the tight binding Fermi surfaces to the experimental results on $La_{2-x}Sr_xCuO_4$ and Bi2212 [215, 216]. The second neighbour hopping amplitude was found to be of opposite sign with respect to the first neighbour hopping. Here, we have done the calculations for a range of feasible values of t_2 and t_3 and presented a result for a few sets of t_2/t_1 and t_3/t_1.

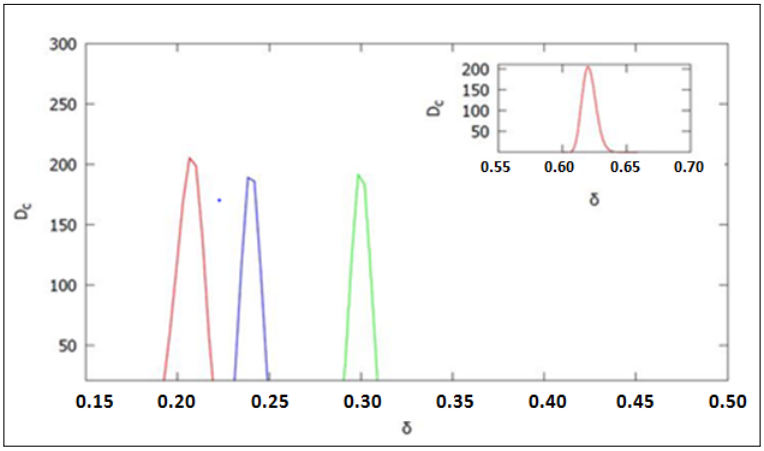

Figure 4.3: D_c vs. δ for 2D t_1-t_2-t_3-J model, with α=0; (a)peak at δ ∼0.29 (t_2=-0.53t_1,t_3=0.24t_1) [green line]; (b)peak at δ ∼0.23 (t_2=-0.52t_1,t_3=0.45t_1) [blue line]; (c)peak at δ ∼0.19 (t_2=-0.6t_1,t_3=0.56t_1) [red line] [in the inset is shown D_c vs. δ for t_2=t_3=0; the peak is seen at δ ∼0.61]

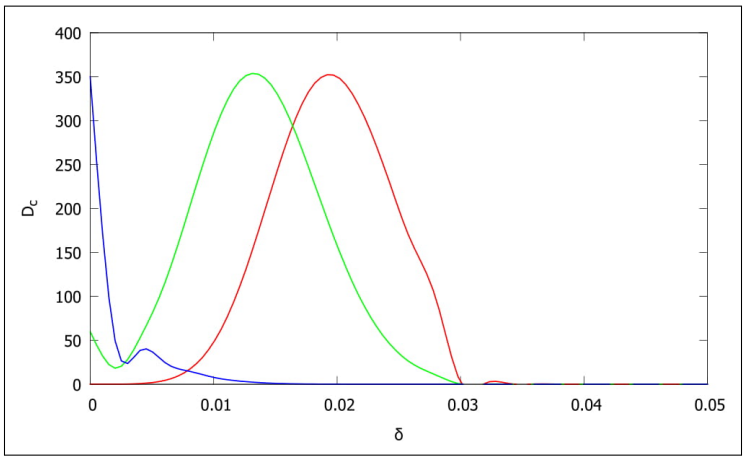

Figure 4.4: D_c vs. δ for 1D t_1-t_2-t_3-J model, with α=0; (a)peak at δ ∼0.02 (t_2=-0.01t_1,t_3=0.005t_1) [red line]; (b)peak at δ ∼0.013 (t_2=-0.02t_1,t_3=0.01t_1) [green line]; (c)peak at δ →0 limit (t_2=-0.04t_1,t_3=0.02t_1) [blue line]

The Fig.(4.3) shows that the maximum in D_c shifts to the optimal doping region for range of values of t_2/t_1 and t_3/t_1. Again, the peak gradually shifts to further lower doping concentration for relatively higher magnitudes of second and third neigbour hopping amplitudes (| t_2 | and | t_3 |)(see Fig.(4.3)). Here one might notice that the magnitude of the scaled charge stiffness is greatly reduced with increase in doping, however, in the previous section it is shown from the analytical calculations, that it quantitatively goes to zero only at 100% doping concentration, denoting the absence of any carrier in the system.

Similarly in 1D too, the peak in D_c shifts to very low doping regime as | t_2 | and | t_3 | are enhanced and the position of the peak reaches δ →0 limit at t_2 ≈-0.04t_1 and t_3 ≈0.02t_1 (see (Fig.(4.4)).

4.2.2 Comparison with other theoretical and experimental results

The imaginary conductivity for the electric field applied in the x-direction can be expressed using the Linear Response Theory as [131, 210]:

$$\sigma''_{xx}(\omega) = \frac{2e^2}{L^d \hbar^2 \omega}[\frac{1}{2d}\langle -T\rangle - \mathcal{P}\sum_{\nu\neq 0}\frac{|\ \langle 0\mid j_x \mid \nu\rangle\ |^2\ (E_\nu - E_0)}{(E_\nu - E_0)^2 - \hbar^2\omega^2}] \tag{4.27}$$

where 'L' is the lattice length in any direction of the 'd'-dimensional lattice. $\langle T\rangle$ is the kinetic energy expectation value of the operator T_x=-2t$\sum$cos $k_x C_k^\dagger C_k$ and the paramagnetic current density in x-direction is defined by j_x=2t$\sum$sin $k_x C_k^\dagger C_k$ [131]. 'E_ν' and 'E_0' are the energy eigen values of the ν^{th} state ($\mid \nu\rangle$) and the ground state ($\mid 0\rangle$) respectively [131]. In the very low frequency limit, the imaginary conductivity is related to the charge stiffness (D_c) by [131, 210]:

$$lim_{\omega\to 0}\omega\sigma''_{xx}(\omega) = (2e^2/\hbar^2)D_c \tag{4.28}$$

Using the Kramer's Kronig transformation, the real conductivity in the low frequency limit is derived as [131, 210]:

$$\sigma'_{xx}(\omega) = \frac{2\pi e^2}{\hbar}[D\delta(\hbar\omega) + \frac{1}{L^d}\sum_{\nu\neq 0}|\ \langle 0\mid j_x \mid \nu\rangle\ |^2\ \delta((E_\nu - E_0)^2 - \hbar^2\omega^2)] \tag{4.29}$$

'D' is the Drude weight implying the free acceleration of the electrons or dc conductivity. In the low ω limit, the Drude weight corresponds to the charge stiffness constant (D_c) (see eqs.(4.27)-(4.28)) [131].

The Drude weight calculated using exact diagonalization for Hubbard model on 4x4 site cluster is shown in Fig.(4.5) [206].

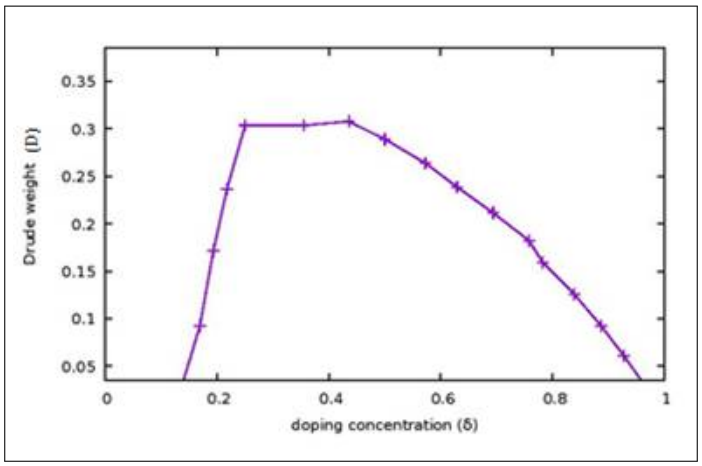

Figure 4.5: Drude weight vs. doping on 4x4 cluster for U/t=4 using exact diagonalization technique [reproduced from ref.([206])

From Fig.(4.5), it can be seen that in the very low doping region, the Drude weight is zero as a result of insulating behaviour of the antiferromagnets. As doping is increased, dc conductivity increases and again falls with further increase in doping. This fall is believed to be due to change in the nature of major carriers from 'vacancies' to 'holes' [206]. The result is very much qualitatively similar in nature to that of ours (see Fig.(4.3)), which shows that the charge stiffness also shows a peak around the optimal doping region and a sharp decrease as δ is increased further.
In the present sub-section, I have also presented the comparison between our results of charge stiffness and effective Coulomb interaction for doped systems. In this context, it must be pointed out that no direct experimental results are available for effective Coulomb interaction (V_{eff}) of layered cuprate systems. So, one can extract V_{eff} from results of optical experiments, using the constitutive equations as given below. V_{eff} in the long wavelength limit of the antiferromagnetic wave vector (Q=q-π=0) is related to the imaginary conductivity by the standard constitutive equations

in the continuum limit [34]:

$$\epsilon'(\omega) = 1 - \frac{4\pi\sigma''}{\omega} \tag{4.30}$$

Thus, the effective Coulomb interaction.

$$V_{eff}(\omega) = \frac{V_0}{\epsilon'(\omega)} \tag{4.31}$$

leading to

$$V_{eff}(\omega) = \frac{V_0}{1 - \frac{4\pi\sigma''}{\omega}} \tag{4.32}$$

and using eq.(4.28) in the very low frequency limit,

$$V_{eff}(\omega) = \frac{V_0}{1 - \frac{4\pi D_c}{\omega^2}} \tag{4.33}$$

with V_0 being the bare Coulomb interaction.

ϵ' is the real part of the dynamic dielectric function and σ'' represents the imaginary part of the dynamic conductivity, which can be extracted experimentally.

The most of the experiments carried out on the planes of lightly and optimally doped $La_{2-x}Sr_xCuO_4$ are at high frequency and at much higher temperatures (>>0K), which are not suitable for comparison with our results. However, here, a transmitted THz time-domain spectroscopy (THz-TDS) on $La_{2-x}Sr_xCuO_4$has been considered [211]. The effective Coulomb interaction is derived from the experimentally extracted imaginary conductivity using eq.(4.32). It is found that the effective Coulomb interaction is small and remains almost constant throughout the lower doping region (in the calculation, we have used the bare onsite Coulomb interaction V_0=3.5eV in

the undoped phase [211]). This result is similar to that of our derived charge stiffness constant as a function of doping in the under-doped region. Moreover, the eq.(4.33) shows the possibility of $V_{eff}(\omega)$ turning attractive for $\omega \to 0$; assuming $D_c \propto D$ in the RPA-like treatment of correlated phase, even with the values of D_c, as allowed by stability criterion. Thereafter, we are awaiting our theoretical prediction of effective Coulomb repulsion to be directly tested by experiments in near future.

4.3 Discussion

The generalized charge stiffness constants for 2D and 1D t-J-like models in strong and weak correlation limits are calculated. A weak dimensional dependence is seen for coupling between the mobile charge degrees of freedom. Furthermore, our calculations bring out several important features and conclusions covering various aspects of correlated fermionic systems in low dimensions. These are discussed below in detail:

4.3.1 Equivalence of generalized charge stiffness constant with Drude weight and effective Coulomb interaction

The D_c in 2D remains zero upto $\delta=\delta_c=0.61$ and then exhibits a sharp rise in value. δ_c shifts to optimal doping region when t_2 and t_3 are included. The effective Drude weight (D) also shows a similar kind of behaviour as shown in the previous section (see Fig.(4.5)) [206]. In the low doping region, the Drude weight remains zero, signifying the insulating behaviour of the antiferromagnets. Further, the rise in the magnitude of 'D' with doping indicates the rise in the number of vacancies as major carriers and if the doping is still increased, one can observe a fall in 'D'. As we have already mentioned that, this behaviour owes it's origin to the change of the

nature of major carriers from vacancies to mobile holes in the medium doping region and as the doping is increased further, D falls due to sharp decrease in the number ofmobile holes [206].

Moreover, in this chapter, I have also tried to establish a connection between our derived D_c and effective Coulomb interaction in doped antiferromagnetic systems, within the RPA. The V_{eff} extracted from experimental data shows that the effective Coulomb interaction remains almost constant in the lower doping region, which is very similar to the behaviour of our derived charge stiffness in the entire under-doped regime (see Fig.(4.3)) [211]. The characteristic behaviour of the coupling between the charge degrees of freedom in the low doping regime is quite physical. In the under-doped regime, the correlation is very strong with α=1, preventing two carriers from coming close to each other and thus largely suppressing the itinerant behaviour of the charges. As a result, the Drude weight is very small and the charges remain far apart to feel the mutual repulsion. This gives a zero value to charge stiffness, which remains constant throughout the lower doping region. When the doping concentration is gradually increased, the charge degrees of freedom become mobile and they can now feel the repulsive interaction as long as the δ does not become very high so as to screen the Coulomb repulsion between the mobile carriers.

4.3.2 Effective Coulomb interaction for high density electron gas

In the medium and the over-doped regime, where the correlation weakens and the charges become mobile, one can take the continuum approximation and observe a point of discontinuity in the Lindhard function at $q=2k_F$ ('q' is the charge ordering wave vector). Then, using different values of the ordering wave vector 'q', it can be shown that the discontinuity appears at some value of δ in the optimal doping region

(Fermi momentum being related to δ by eq.(4.16)) [217, 218]. This discontinuity in the Lindard function also manifests itself in the calculation of dielectric function and as a result V_{eff} shows a jump at the corresponding value of doping concentration [217, 218] (see Appendix C). This characterisctic behaviour is very similar to our result of derived charge stiffness constant (see Fig.4.1), which possibly signifies the tendency of the formation of charge ordering or charge density waves as the idea put forward by Overhauser [219]. Hence, the similarity in the behaviour of D_c and V_{eff} proves the qualitative equivalence between the two, even in the over-doped regime of these doped itinerant systems. Considering the equivalence, we have drawn a phase diagram of the doped antiferromagnets in 2D, based on their charge responses from the t_1-t_2-t_3-J model (see Fig.(4.6)). In the phase diagram, the values of critical doping concentration (δ_c) for different values of t_3/t_1 ratio are shown, taking t_2/t_1 as parameter. One can also notice that for a particular value of t_3/t_1, the transition between the two regions of different charge couplings, takes place at a lower value of doping concentration for higher values of $|t_2/t_1|$.

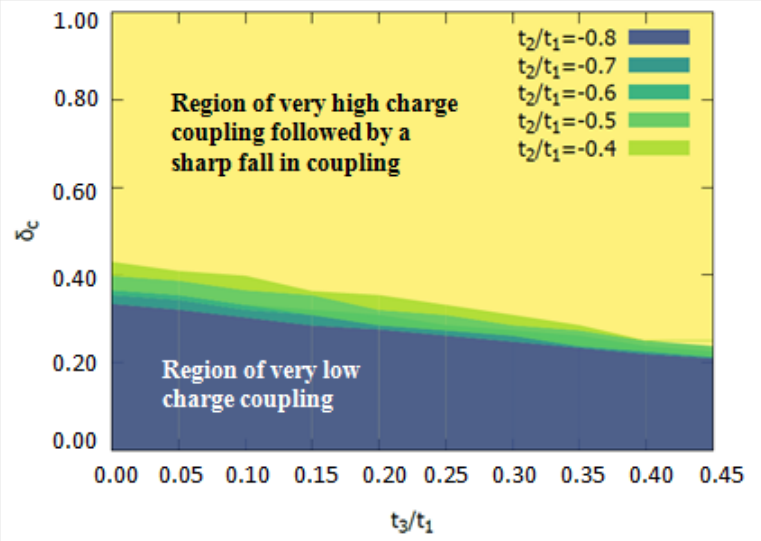

Figure 4.6: Phase diagram showing the critical doping concentration (δ_c), separating the regions of charge couplings, as a function of t_3/t_1 (with t_2/t_1 ratio as the parameter). The regions of doping concentration below δ_c represent the regime very low charge coupling and above δ_c, the interaction shows a very high value, followed by a sharp fall. The different colours are used for different ratios of t_2/t_1 [α=1 has been taken].

4.3.3 Comparison between behaviours of D_c and D_s in 2D

The exchange energy contribution to D_c vanishes in the entire doping region (see eq.(4.12)), resulting in the distinct behaviour of spin and charge stiffness constants. It has been shown that D_c for two-dimensional lattice with pure t-J model remains zero throughout the lower doping region and exhibits a sharp rise at δ=δ_c=0.61. After this point, D_c immediately falls as doping is increased further (see Fig.(4.1)). The parameter δ_c shifts to the optimal doping region when two higher neighbour hoppings are included (see Fig.(4.3)).

The region of enhanced Coulomb interaction around δ_c may imply a tendency towards the formation of a charge density wave, as described in the previous subsection [218, 219]. Some of the previous theoretical results also confirms the presence of charge density wave states in the context of single-band t-J-U model [220]. Inter-

estingly, the spin stiffness constant (D_s) also shows a point of inflection (indicative of a possible phase transition) at the same δ, where D_c exhibits the sharp rise. Furthermore, D_c and D_s show almost identical behaviour for $\delta > \delta_c$, i.e. in the over-doped regime, which is an expected behaviour of Fermi liquid-like phases. In the under-doped regime however, the behaviour of the two stiffness constants are very different. Thus it can be concluded that we get the two regions of distinctly different behaviours. The regions are very likely to characterize (i) an anomalous conducting phase and (ii) a Fermi liquid-like metallic phase.

4.3.4 Comparison between behaviours of D_c and D_s in 1D

For t-J model, the quantity D_c in 1D vanishes at δ=0 and $\delta \rightarrow$0 and exhibits a maximum in the lower doping region. The peak shifts to further lower doping as the higher neighbour hopping amplitudes are increased and reaches the $\delta \rightarrow$0 limit at critical values of t_2 and t_3(see Figs.(4.2),(4.4)). In the previous chapter, I have shown that in one dimension, D_s displays a high value at $\delta \rightarrow$0 limit and falls rapidly with increase in doping concentration. The drastic fall is immediately followed by the formation of a peak in the under-doped regime. Hence, we see that D_s and D_c show completely distinct behaviour only in the very low doping region, whereas they show a similar trend as doping is slightly increased.

Furthermore, it is also seen that the tendency towards the formation of charge density wave occurs at much lower doping concentration in 1D than in 2D. Thus the dimensional dependence of charge stiffness in low dimensional systems is also established, similar to the spin stiffness case.

4.3.5 Possibility of pair formation

In some of the recent works, real space pairing has been studied in the framework of the t-J-like models mostly in the under-doped phase [129,221–223]. In our calculation we do not get any region of negative charge stiffness, as is expected from the stability criteria (see eqs.(4.2)-(4.5)). However, eq.(4.33) shows that the effective Coulomb interaction can be attractive in a range of doping concentration, where charge stiffness constant has a large non-zero value. This signifies the possibility of superconducting pair formation in a region where D_c shows a peak, i.e., the region of optimal opting concentration (see Fig(4.3)).

Chapter 5

Conclusion

In this final chapter, I am giving brief summary and concluding remarks regarding all the works described in the previous chapters.

A quantum mechanical, non-perturbative approach has been put forward for deriving the generalized spin stiffness constant based on the t-J-like models. Involving this approach, one can very well derive the effective coupling strengths between the spin degrees of freedom in the strongly correlated doped itinerant phases of the antiferromagnets, which had been a challenge to the theoreticians so far. The results described in the previous chapters bring forward many interesting features and characteristics of the doped phases and also strongly highlight the dimensional dependence of spin correlations, even in the low dimensional systems.

In the second chapter, I have discussed the detailed formalism for the calculation of spin-spin coupling in terms of generalized spin stiffness constant (D_s) using the Gutzwiller projected out state. The results are compared with the effective exchange constant (J_{eff}) extracted from experimental and theoretical results on the layers of $L_{2-x}Sr_xCuO_4$ [105, 136]. Based on this comparison the equivalence between D_s and J_{eff} is established for doped quantum antiferromagnets. Moreover, the rapid fall in

J_{eff} with increase in doping concentration (δ) denotes the weakening of the antiferromagnetic interaction and the destruction of the quasi-long range ordering in the very low δ regime (see Fig.(2.2)). However, the short range correlations persist in the system upto 100% doping concentration. Furthermore, the plots of D_s against δ exhibit a shoulder-like structure or a point of inflection at $\delta \sim 0.61$, which possibly represents a point of quantum phase transition (see Fig.2.4). The point of possible phase transition can denote the transition from a separated hole rich and hole deficient phase, as was obtained by Emery et al [149].

The next chapter deals with the calculation of generalized spin stiffness for one dimensional t-J model. The results in 1D are compared with the experimental results on $YBa_2Cu_3O_{6+x}$ upto 41% doping concentration [165, 166, 168]. This comparison is valid in this doping region, since the holes doped in $YBa_2Cu_3O_{6+x}$ enters into the chains of compound keeping the valences of the planes unchanged [159–162]. Similar to the 2D case, the comparison establishes the equivalence of generalized spin stiffness and effective exchange constant of one dimensional doped antiferromagnets too. More interestingly, in 1D, a novel prediction is given regarding the tendency of the itinerant spins to form a ferromagnetic-like coupling, after the destruction of original antiferromagnetic ordering in parental phase. This result also gets good support from experimental results on YBCO [165, 166].

In the fourth chapter, following a parallel approach, we have derived the generalized charge stiffness constant D_c(spin symmetric) corresponding to the doped itinerant phases. Here, we have separately considered the strongly correlated under-doped regime and weakly correlated over-doped region. The strongly correlated region is described with the help of nearest neighbour t-J model with the variational parameter α=1 and over-doped regime is studied with the help of t_1-t_2-t_3-J model. The results are compared with the Drude weights (D) for different doping concentrations,

obtained from other theoretical results [206]. As described in the previous chapter, the Drude weight remains zero in the lower doping region, due to suppression of the motion of carriers as a result of very high Coulomb repulsion. Now, when the doping is increased, 'D' increases and falls again with further increase in δ, as the mobile holes assume the role of major carriers replacing the vacancies. This nature is similar to the behaviour of derived D_c shown in Figs.(4.1-4.3).

The results in the under-doped regime are also compared with the results of optical experiments on the layers of $La_{2-x}Sr_xCuO_4$ [211]. In the under-doped region, the carriers are immobile and the Coulomb repulsion remains almost constant, because the carriers remain far apart to feel the effective interaction due to one another. As δ is increased, the carriers gain mobility and they can approach the vicinity of other charges and the effective repulsion becomes high as long as the carriers are not drastically decreased due to very high doping. Moreover, in a certain range of doping, one can get attractive Coulomb interaction, even with positive D_c as can be seen from eq.(4.33). This can be a possible scenario for pair formation in the doped antiferromagnetic systems.

In the later part, the comparison with the high density electron gas involving the interacting Lindhard function has lead to the prediction of the tendency of charge density wave instability in the region where the charge stiffness as well as the Coulomb repulsion exhibits a sudden rise in magnitude. This charge density wave instability is similar to the one put forward by Overhauser [219].

Appendix A

$$H'_J = S_i.S_j - (\frac{1}{4})n_i n_j \tag{A.1}$$

In terms of fermion operators,

$$H'_J = \sum_{\sigma} C^{\dagger}_{i-\sigma} C_{i\sigma} C^{\dagger}_{j\sigma} C_{j-\sigma} \tag{A.2}$$

Thus making use of equation (2.10),

$$H'_J|\psi_G\rangle_{NDOC} = \sum_{\sigma} C^{\dagger}_{i-\sigma} C_{i\sigma} C^{\dagger}_{j\sigma} C_{j-\sigma} \prod_{l} (1 - \widehat{n}_{l\uparrow}\widehat{n}_{l\downarrow}) \prod_{k}^{k_F} \sum_{i',j'} e^{i(r_{i'} - r_{j'}).k} |i'\sigma, j' - \sigma\rangle \tag{A.3}$$

where 'i$'\sigma$' and 'j$' - \sigma$' denotes fermions at sites 'i'' and 'j'' with spins 'σ' and '$-\sigma$' respectively.

$$H'_J|\psi_G\rangle_{NDOC} = \prod_{l} (1 - \widehat{n}_{l\uparrow}\widehat{n}_{l\downarrow}) \prod_{k}^{k_F} \sum_{i',j'} \delta_{ii'}\delta_{jj'} e^{i(r_{i'} - r_{j'}).k} |i' - \sigma, j'\sigma\rangle \tag{A.4}$$

$$_{NDOC}\langle\psi_G|H'_J|\psi_G\rangle_{NDOC} =_{NDOC} \langle\psi_G| \prod_{k}^{k_F} e^{i(r_i - r_j).k} |i - \sigma, j\sigma\rangle \tag{A.5}$$

Here '$\widehat{n}_{l\uparrow}\widehat{n}_{l\downarrow}$' does not contribute since exchange is not possible between up and down spins on the same site and i and j are the nearest neighbour occupied sites.

Further,

$$ {}_{NDOC}\langle\psi_G|\psi_G\rangle_{NDOC} = \langle vac| \prod_{k'} \sum_{i',j',\sigma} e^{-i(r_{i'}-r_{j'}).k'} C_{j',-\sigma} C_{i,\sigma} (1-\widehat{n}_{l\downarrow}\widehat{n}_{l\uparrow}-....)(1-\widehat{n}_{l\uparrow}\widehat{n}_{l\downarrow}-....) $$

$$ \prod_{k'} \sum_{i',j',\sigma} e^{i(r_i-r_j).k} |i\sigma, j-\sigma\rangle \quad \text{(A.6)} $$

Simplifying equations (2.35) and (2.36),

$$ \frac{{}_{NDOC}\langle\psi_G|H'_J|\psi_G\rangle_{NDOC}}{{}_{NDOC}\langle\psi_G|\psi_G\rangle_{NDOC}} = \prod_{k}^{k_F} 2(1-\delta)^2 \quad \text{(A.7)} $$

Appendix B

$$ H_t = \sum_{<m,n>,\sigma} (t_{m,n} e^{i\phi_\sigma} C^\dagger_{m\sigma} C_{n\sigma} + t_{n,m} e^{-i\phi_\sigma} C^\dagger_{n\sigma} C_{m\sigma} \quad \text{(B.1)} $$

Therefore

$$ H_t|\psi_G\rangle_{NDOC} = \sum_{<m,n>,\sigma} (t_{m,n} e^{i\phi_\sigma} C^\dagger_{m\sigma} C_{n\sigma} + t_{n,m} e^{-i\phi_\sigma} C^\dagger_{n\sigma} C_{m\sigma} \times (1-\widehat{n}_{1\uparrow}\widehat{n}_{1\downarrow}-\widehat{n}_{1\uparrow}\widehat{n}_{1\downarrow}-....) $$

$$ \prod_{k}^{k_F} \sum_{i,j} e^{i(r_i-r_j).k} |i\sigma, j-\sigma\rangle \quad \text{(B.2)} $$

$$= (t)\prod_{k}^{k_F}\sum_{i,j,\sigma}[e^{i\phi_\sigma}\{\delta_{i+1,m}\delta_{i,n}|((i+1)\sigma, j-\sigma\rangle + \delta_{j+1,m}\delta_{j,n}|i\sigma,(j+1)-\sigma\rangle\}+$$

$$e^{-i\phi_\sigma}\{.....\}]e^{i(r_i-r_j).k} - \sum_{l}\prod_{k}^{k_F}[e^{i\phi_\sigma}\{\delta_{l+1,m}\delta_{l,n}|(l+1),\sigma,l\sigma\rangle + \delta_{l+1,m}\delta_{l,n}|l\sigma,(l+1)-\sigma\rangle$$

$$+ e^{-i\phi_\sigma}\{.....\}]] \quad \text{(B.3)}$$

where the sum over l is carried out involving all the occupied sites N_l.

Simplifying Eqs. (2.40) and using (2.36) we get,

$$T(\phi \neq 0) = (t)[\prod_{k,\sigma}^{k_F}\sum_{\sigma} 4cos(ka)(1-\delta)^2 cos(\phi_\sigma) - N_l\prod_{k,\sigma}^{k_F}\sum_{\sigma} 4cos(ka)cos(\phi_\sigma)/N^2] \quad \text{(B.4)}$$

Appendix C

The longitudinal electronic dynamic dielectric function for a weakly correlated Fermi liquid-like phase for band electrons can be expressed as [132, 217, 218]:

$$\epsilon^{-1}(\overline{q}+\overline{G},\overline{q}+\overline{G'},\omega) = 1 + V_0(\overline{q}+\overline{G})\chi(\overline{q}+\overline{G},\overline{q}+\overline{G'},\omega) \quad \text{(C.1)}$$

where $\overline{G}$ and $\overline{G'}$ are Umklapp vectors corresponding to the lattice background and in 2D [217]

$$V_0(\overline{q}+\overline{G}) = \frac{2\pi e^2}{|\overline{q}+\overline{G}|} \tag{C.2}$$

is the bare Coulomb interaction between the electrons, projected in a 2D layer.

At the conventional RPA level χ, the screened dynamic charge susceptibility neglecting the exchange-correlation effects, is given by [217, 218]:

$$\chi(\overline{q}+\overline{G},\overline{q}+\overline{G'},\omega) = \frac{\chi_0(\overline{q}+\overline{G},\overline{q}+\overline{G'},\omega)}{1-V_0\chi_0(\overline{q}+\overline{G},\overline{q}+\overline{G'},\omega)} \tag{C.3}$$

where, $\chi_0(\overline{q}+\overline{G}, \overline{q}+\overline{G'},\omega)$ is the free charge dynamic susceptibility given by the Lindhard function [218].

Hence, the effective static Coulomb interaction obeys the equation:

$$\frac{1}{V_{eff}(\overline{q}+\overline{G'},0)} = -\chi_0(\overline{q}+\overline{G},\overline{q}+\overline{G'},0) + \frac{1}{V_0(\overline{q}+\overline{G})} \tag{C.4}$$

Bibliography

[1] K.Andres, J.E.Graebner, H.R.Ott, Phys.Rev.Lett 35, 1779 (1975)

[2] F.Steglich, J.Aarts, C.D.Bredl, W.Liecke, D.Meschede, W.Franz, H.Schäfer, Phys.Rev.Lett. 43, 1892 (1979).

[3] N.F.Mott, "Metal-Insulator Transition", Taylor and Francis, London, Second edition (1990)

[4] J.Hubbard, Proc.R.Soc.London A 276, 238 (1963)

[5] M.L. Néel, Ann.Phys. 11, 232 (1936)

[6] E.J.W. Verwey, P.W.Haayman, Physica 8, 979 (1941)

[7] W.Heitler, F.London, Z.Phys. 44, 455 (1927)

[8] (a) D.C.Johnston, Advances in Physics 59, 803 (2010);
(b) F.Peng, Y.Sun, C.J.Pickard, R.J.Needs, Q.Wu, Y.Ma, Phy.Rev.Lett. 119, 107001 (2017)

[9] (a) B.Keimer, S.A.Kivelson, M.R.Norman, S.Uchida, J.Zaanen, Nature 518, 179 (2015);
(b)K. Jin, N. P. Butch, K. Kirshenbaum, J. Paglione, R. L. Greene, Nature 476, 73 (2011)

[10] (a) J. Bardeen, L. N. Cooper, J. R. Schrieffer, Phy Rev. 106, 162 (1957);
(b) J.Bardeen, L.N.Cooper, J.R.Schrieffer, Phy.Rev. 108, 1175 (1957)

[11] M.R.Schafroth, J.M.Blatt, S.T.Bluttler, Helv.Phys.Acta. 30, 93 (1957)

[12] N.N. Bogoliubov, Izv. Akad. Nauk SSSR 11, 77 (1947); J.Phys. (Moscow) 11, 23 (1947)

[13] J.R.Schrieffer, "Theory of Superconductivity", Westview Press, Revised Edition (1983)

[14] T.Matsubara, J.M.Blatt, Progr.Theoret.Phys. (Kyoto) 23, 451 (1960)

[15] J.M.Blatt, Progr.Theoret.Phys. (Kyoto) 27, 1137 (1962)

[16] B.T.Matthias, Science 144, 373 (1964)

[17] O.V.Lounasmaa, E.Kojo, Ann. Acad. Sci. Fennicae Ser. A VI 36 (1959)

[18] R.J.Donnelly, C.F.Barenghy, J.Phy.Chem.Ref.Data 27, 1217 (1998)

[19] W.H.Keesom, J.A.Kok, Leiden Commun. 221e, 743 (1932)

[20] L.Pitaevskii, "Phenomenology and Microscopic Theory: Theoretical Foundations", edited by K.H. Bennemann and John.B.Ketterson: "Superconductivity", Springer, Berlin, Heidelberg (2008)

[21] G.A.C.Ummarino, "Eliashberg Theory", edited by E.Pavarini, E.Koch, and U.Schollwöck: "Emergent Phenomena in Correlated Matter Modeling and Simulation", Vol-3, Verlag des Forschungszentrum Jülich (2013)

[22] (a) G.M.Éliashberg, Sov.Phys. JETP 11, 696 (1960);
(b) G.M.Éliashberg Sov.Phys. JETP 12, 1000 (1961)

[23] (a) C.Proust, E.Boaknin, R.W.Hill, L.Taillefer, A.P.Mackenzie, Phy.Rev.Lett. 89, 147003 (2002);
(b) C.Stock, C.Broholm, J.Hudis, H.J.Kang, C.Petrovic, Phy.Rev.Lett. 100, 087001 (2008)

[24] A.F.Kemper, D.G.S.P.Doluweera, T.A.Maier, M.Jarrell, P.J.Hirschfeld, H.P.Cheng, Phy.Rev. B 79, 104502 (2009)

[25] P.A.Lee, Phys.Rev.Lett. 71, 1887 (1993)

[26] (a) D.R.Harshman, L.F.Schneemeyer, J.V.Waszczak, G.Aeppli, R.J.Cava, B.Batlogg, L.W.Rupp, E.J.Ansaldo, D.L.Williams, Phy.Rev. B 39, 851 (1989);
(b) L.Elbaum, R.L.Greene, F.Holtzberg, A.P.Malozemoff, Y.Yeshurun, Phys.Rev.Lett. 62, 217 (1989)

[27] J.Zaanen, G.A.Sawatzky, J.W.Allen Phys.Rev.Lett. 55, 418 (1985)

[28] N.F.Mott, Philos.Mag. 6, 62 (1961)

[29] J.Zaanen, G.A.Sawatzky, J.W.Allen, J.Mag. and Mag.Mat. 54-57, 607 (1986)

[30] M.Tinkham, "Introduction to Superconductivity", McGraw-Hill, Inc., New York, Second edition (1996)

[31] H.Frölich, Proc.R.Soc.Lond. A 215, 291 (1952)

[32] J.Bardeen, D.Pines, Phy.Rev.99, 1140 (1955)

[33] D.Pines, Phy.Rev. 109, 280 (1958)

[34] N.W.Ashcroft, N.D.Mermin, "Solid State Physics", Harcourt College Publishers (1976), Preprint (2015)

[35] J.G.Bednorz, K.A.Müller, Z.Phys.B 64, 189 (1986)

[36] M.K.Wu, J.R.Ashburn, C.J.Torng, P.H.Hor, R. L.Meng, L.Gao, Z.J.Huang, Y.Q.Wang, C.W.Chu, Phy.Rev.Lett. 58, 908 (1987)

[37] Report by the Commitee On Opportunities in High Magnetic Field Science, "Opportunities in High Magnetic Field Science", The National Academic Press, Washington D.C. (2005)

[38] (a) R.M.Hazen, C.T.Prewitt, R.J.Angel, N.L.Ross, L.W.Finger, C.G.Hadidiacos , D.R.Veblen , P.J. Heaney, P.H.Hor, R.L.Meng , Y.Y.Sun, W.Q.Wang, Y.Y. Xue , Z.J.Huang, L.Gao, J. Bechtold, C.W.Chu, Phys.Rev.Lett. 60, 1174 (1988); (b) R.M.Hazen, L.W.Finger, R.J.Angel, C.T.Prewitt, N.L. Ross, H.K.Mao, C.G.Hadidiacos, P.H.Hor, R.L.Meng, C.W.Chu, Phys.Rev. B 35, 7238(R) (1988)

[39] W.Jin, S.Hao, H.Zhang, New J.Phys. 11, 113036 (2009)

[40] R.Wesche, "Physical Properties of High-Temperature Superconductors", Wiley Series in Materials for Electronics and Optoelectronic Applications, U.K. (2015)

[41] G.Rietveld, M.Glastra, D.van de Marel, Physics C 241, 257 (1995)

[42] M.Decroux, A.Junod, A.Bezinge, D.Cattani, J.Cors, J.L.Jorda, A.Stettler, M.Francois, K.Yvon, ϕ.Fischer, J.Muller, Europhys.Lett. 3, 1035 (1987)

[43] H.H.Wu, M.Buchholz, C.Trabant, C.F.Chang, A.C.Komarek, F.Heigl, M.Zimmermann, M.Cwik, F.Nakamura, M.Braden, C.Schüβler-Langeheine, Nat.Comm. 3, 1023 (2012)

[44] R.M.Hazen, "Physical Properties of High Temperature Superconductors II", D.M.Ginsberg (ed.), World Scientific, Singapore, 1990

[45] R.J.Cava, B.Batlogg, R.B.van Dover, D.W.Murphy, S.Sunshine, T.Siegrist, J.P.Remeika, E.A.Rietman, S.Zahurak, G.P.Espinosa, Phy.Rev.Lett. 58, 1676 (1987)

[46] R.Beyers, G.Lim, E.M.Engler, R.J.Savoy, T.M.Shaw, T.R.Dinger, W.J.Gallagher, R.L.Sandstrom, Appl.Phys.Lett. 50, 1918 (1987)

[47] M.A.Beno, L.Soderholm, D.W.Capone, D.G.Hinks, J.D.Jorgensen, J.D.Grace, I.K.Schuller, C.U.Segre, K.Zhang, Appl.Phys.Lett. 51, 57 (1987)

[48] E.Stilp, A.Suter, T.Prokscha, Z.Salman, E.Morenzoni, H.Keller, P.Pahlke, R.Huhne, C.Bernhard, R.Liang, W.N.Hardy, D.A.Bonn, J.C.Baglo, R.F.Kiefl, Scientific Reports 4, 6250 (2014)

[49] P.Fazekas, "Lecture Notes on Electron Correlation and Magnetism", World Scientific, Singapore, Reprint 2003

[50] (a) P.W.Anderson, Phy.Rev. 79, 350 (1950);
(b) P.W.Anderson, Phy.Rev. 115, 2 (1959)

[51] H.Bethe, Z.Phys. 71, 205 (1931)

[52] E.H.Lieb, F.Y.Wu, Phys.Rev.Lett. 20, 1445 (1968)

[53] (a)M.Takahasi, Prog.Theor.Phys. 47, 69 (1972);
(b) M.Takahasi, Prog.Theor.Phys. 52, 103 (1974)

[54] N.Kawakami, T.Usuki, A.Okiji, Phys.Lett. A 137, 287 (1989)

[55] T.Usuki, N.Kawakami, A.Okiji, J.Phys.Soc. Japan 59, 1357 (1990)

[56] J.E.Hirsch, Phy.Rev. B 31, 4403 (1985)

[57] C.J.Halboth, W.Metzner, Phy.Rev.Lett. 85, 5162 (2000)

[58] S.R.White,D.J.Scalapino, R.L.Sugar, E.Y.Loh, J.E.Gubernatis, R.T.Scalettar, Phy.Rev. B 40, 506 (1989)

[59] (a) T.A.Maier, M.Jarrell, T.C.Schulthess, P.R.C.Kent, J.B.White, Phy.Rev.Lett. 95, 237001 (2005);
(b) N.S.Vidyadhiraja, A.Macridin, C.Sen, M.Jarrell, M.Ma, Phy.Rev.Lett. 102, 206407 (2009)

[60] R.T.Scalettar, E.Y.Loh, J.E.Gubernatis, A.Moreo, S.R.White,D.J.Scalapino, R.L.Sugar, E.Dagotto, Phy.Rev.Lett. 62, 1407 (1989)

[61] M.Kato, K.Machida, H.Nakanishi, M.Fujita, J.Phys.Soc.Japan 59, 1047 (1990)

[62] M.C.Gutzwiller, Phy.Rev.Lett. 10, 159 (1963)

[63] J. Kanamori, Prog.Theor.Phys. 30, 275 (1963)

[64] (a) J.Hubbard, Proc.R.Soc.London A 277, 237 (1964);
(b) J.Hubbard, Proc.R.Soc.London A 281, 401 (1965);
(c) J.Hubbard, Proc.R.Soc.London A 542, 196 (1965)

[65] edited by D.Baeriswyl, D.K.Camobell, J.M.P.Carmelo, F.Guinea, E.Louis, "The Hubbard Model: Its Physics and Mathematical Physics", Springer Sience + Business Media, New York (1995)

[66] U.Wolff, Nucl.Phys. 8225 [FS9], 391 (1983)

[67] A.E.Ruckenstein, P.J.Hirschfeld, J.Appel, Phys.Rev.B 36, 857 (1987)

[68] J.E.Hirsch, Phys.Rev.Lett. 53, 2327 (1984)

[69] P.G.J.van Dongen, Phy.Rev.Lett. 67, 757 (1991)

[70] J.W.Cannon, E.Fradkin, Phys.Rev.B 41, 9435 (1990)

[71] J.Voit, Phys.Rev.B 45, 4027 (1992)

[72] F.Mila, X.Zotos, Euro.Phys.Lett. 24, 133 (1993)

[73] M.Tsuchiizu, A.Furusaki, Phys.Rev.Lett. 88, 056402 (2002)

[74] E.Jeckelmann, Phys.Rev.Lett. 89, 236401 (2002)

[75] K.Penc, F.Mila, Phys.Rev.B 49, 9670 (1994)

[76] S.J.Gu, S.S.Deng, Y.Q.Li, H.Q.Lin, Phys.Rev.Lett. 93, 086402 (2004)

[77] P.A.Lee, N.Nagaosa, X.Wen, Rev.Mod.Phys. 78, 17 (2006)

[78] Y.A.Izyumov, Physics-/uspekhi 40, 445 (1997)

[79] S.Sarkar, "Exactly Solvable Models of Strongly Correlated Electrons", World Scientific (2004)

[80] A.B.Harris, R.V.Lange, Phys.Rev. 157, 295 (1967)

[81] K.A.Chao, J.Spalek, A.M.Oles, J.Phys. C 10, L271 (1977)

[82] C.Gros, R.Joynt, T.M.Rice, Phys.Rev. B 36, 381 (1987)

[83] S.G.Ovchinnikov, V.V.Val'kov, "Hubbard Operators in the Theory of Strongly Correlated Electrons", Imperial College Press, London (2004)

[84] F.C.Zhang, T.M.Rice, Phy.Rev. B 37, 3759 (1988)

[85] W.Stephan, P.Horsch, Phy.Rev.Lett. 66, 2258 (1991)

[86] (a) M.Boninsegni, E.Manousakis, Phy.Rev. B 46, 560 (1992);
(b) H.Yokoyama, M.Ogata, J.Phys.Soc.Jpn 65, 3615 (1996)

[87] P.Corboz, S.R.White, G.Vidal, M.Troyer, Phy.Rev. B 84, 041108 (2011)

[88] T.Tohyama, Phy.Rev. B 70, 174517 (2004)

[89] T.Tanamoto, H.Kohno, H.Fukuyama, J.Phys.Soc.Jpn 62, 717 (1993)

[90] P.Benard, L.Chen, A.M.S.Tremblay, Phy.Rev. B 47, 15217 (1993)

[91] Q.Si, Y.Zha, K.Levin, J.P.Lu, Phy.Rev. B 47, 9055 (1993)

[92] N.P.Armitage, F.Ronning, D.H.Lu, C.Kim, A.Damascelli, K.M.Shen, D.L.Feng, H.Eisaki, Z.X.Shen, P.K.Mang, N.Kaneko, M.Greven, Y.Onose, Y.Taguchi, Y.Tokura, Phy.Rev.Lett. 88, 257001 (2002)

[93] A.Damascelli, Z.Hussain, Z.X.Shen, Rev.Mod.Phys. 75, 473 (2003)

[94] T.Tohyama, S.Maekawa, Phys.Rev. B 49, 3596 (1994)

[95] P.A.Lee, Phys.Rev.Lett. 63, 680 (1989)

[96] Q.Yuan, Y.Chen, T.K.Lee, C.S.Ting, Phys.Rev. B 69, 214523 (2004)

[97] G.Kotliar, A.E.Ruckenstein, Phys. Rev. Lett. 57, 1362 (1986)

[98] M.Deeg, H.Fehske, H.Buttner, Europhys. Lett. 26, 109 (1994)

[99] (a) A.Himeda, M.Ogata, Phys.Rev. B 60, R9935 (1999);
(b) M.Ogata, A.Himeda, arXiv:Cond-mat/0003465 v1 (unpublished) (2000);
(c) A.Himeda, M.Ogata, Phys.Rev.Lett. 85, 4345 (2000)

[100] F.C.Zhang, C.Gros, T.M.Rice, H.Shiba, Supercond.Sci.Technol. 1, 1 (1988)

[101] D.Vollhardt, Rev.Mod.Phys. 56, 1 (1984)

[102] H.Yokoyama, M.Ogata, J.Phys.Soc.Jpn. 65, 11 (1996)

[103] T.Ogawa, K.Kanda, T.Matsubara, Prog.Theor.Phys. 53, 614 (1975)

[104] (a) P.W.Anderson, Phys.Rev.Lett. 96, 017001 (2006);
(b) T.Tohyama, S.Maekawa, Phys.Rev. B 67, 092509 (2003);
(c) M.B. Maple, Preprint arXiv:Cond-mat/9802202 (unpublished) (1998).

[105] T.R.Thurston, R.J.Birgeneau, M.A.Kastner, N.W.Preyer, G.Shirane, Y.Fujii, K.Yamada, Y.Endoh, K.Kakurai, M.Matsuda, Y.Hidaka, T.Murakami, Phys.Rev. B 40, 4585 (1989)

[106] N.S.Mondal, N.K.Ghosh, Pramana 74, 115 (2010).

[107] J.Jedrak, J.Spalek, Phys.Rev. B 83, 104512 (2011).

[108] P.Corboz, T.M.Rice, M.Troyer, Phys.Rev.Lett. 113, 046402 (2014).

[109] P.Corboz, S.R.White, G.Vidal, M.Troyer, Phys.Rev. B 84, 041108 (2011).

[110] (a) A.V.Chubukov, Phys.Rev. B 44, 392 (1991);
(b) A.V.Chubukov, S.Sachdev, T.Senthil, Nucl.Phys. B 426, 601 (1994).

[111] (a)P.Sindzingre, N.Shannon, T.Momoi, J.Phys:Conference Series 200, 022058 (2010);
(b) M.Mambrini, A.Läuchli, D.Poilblanc, F.Mila, Phys.Rev. B 74, 14422 (2006).

[112] Y.Z.You, F.Yang, S.P.Kou, Z.Y.Weng, Phys.Rev. B 84, 054527 (2011).

[113] R.Yu, J.X.Zhu, Q.Si, Phys.Rev. B 89, 024509 (2014).

[114] M.A.Kastner, R.J.Birgeneau, T.R.Thurston, P.J.Picone, H.P.Jenssen, D.R. Gabbe, M.Sato, K.Fukuda, S.Shamoto, Y.Endoh, K.Yamada, Phys.Rev. B 38, 6636 (1988).

[115] O.P.Vajk, M.Greven, P.K.Mang, J.W.Lynn, Solid State Commun. 126, 93 (2003).

[116] A.Sherman, M.Schreiber, Eur. Phys.J. B 32, 203 (2003).

[117] A.Sherman, Phys.Rev. B 70, 184512 (2004).

[118] T.C.Ribeiro, A.Seidel, J.H. Han, D.H.Lee, Europhys.Lett. 76, 891 (2006).

[119] N.M. Plakida, Z. Phys. B 103, 383 (1997).

[120] G.Jackeli, N.M.Plakida, Theor.Math.Phys. 114, 335 (1998).

[121] A.A.Vladimirov, D.Ihle, N.M.Plakida, Phys.Rev. B 85, 224536 (2012).

[122] N.M.Plakida, V.S.Oudovenko, Phys.Rev. B 59, 11949 (1999).

[123] J.Kaczmarczyk, J.Spalek, T.Schickling, J.Bünemann, Phy.Rev.B 88, 115127 (2013)

[124] D.J.Scalapino, "Handbook of High- Temperature Superconductivity" edited by J.R. Schrieffer and J.S. Brooks (Eds), Springer, New York, Chap.-13, (2007).

[125] A.A.Vladimirov, D.Ihle, N.M.Plakida, Theor.Math.Phys. 145, 1576 (2005).

[126] A.A.Vladimirov, D.Ihle, N.M.Plakida, Theor.Math.Phys. 152, 1331 (2007).

[127] A.A.Vladimirov, D.Ihle, N.M.Plakida, Phys.Rev. B 80, 104425 (2009).

[128] A.A.Vladimirov, D.Ihle, N.M.Plakida, Phys.Rev. B 83, 024411 (2011).

[129] (a) J.Spalek, M.Zegrodnik, J.Kaczmarczyk, Phy.Rev.B 95, 024506 (2017);
(b) J.Spalek, Cond.Mat.Phys. 11, 455-462 (2008)

[130] (a) W.Kohn, Phys.Rev. A 133, 171 (1964);
(b) D.J.Thouless, Phys.Rep. 13, 94 (1974)

[131] B.S. Shastry, B.Sutherland, Phys.Rev.Lett. 65, 243 (1990).

[132] R.Chaudhury, J.Phys.: Condens. Matter 19, 496203 (2007).

[133] (a) C.Panagopoulos, J.L.Tallon, B.D.Rainford, J.R.Cooper, C.A.Scott, T.Xiang, Solid State Commun. 126, 47 (2003).
(b) S.Uchida, Solid State Commun. 126, 57 (2003).

[134] S.Chakravarty, B.I.Halperin, D.R.Nelson, Phys.Rev. B 39, 2344 (1989).

[135] P.Hasenfratz, F.Niedermayer, Phys.Lett. B 268, 231 (1991).

[136] E.Manousakis, Phys.Rev. B 45, 7570 (1992).

[137] N.Bulut, D.Hone, D.J.Scalapino, E.Y.Loh, Phys.Rev.Lett. 62, 2192 (1989).

[138] A.I.Liechtenstein, V.I.Anisimov, J.Zaanen, Phys.Rev. B 52, 5467 (1995).

[139] V.P.Antropov, M.A.Katsnelson, A.I.Liechtenstein, Physica B 237–238, 336 (1997).

[140] E.Ruiz, S.Alvarez, J.Cano, V.Polo, J.Chem.Phys. 123, 164110 (2005).

[141] S.H.Liu, Phys.Rev. B 15, 4281 (1977).

[142] V.P.Antropov, J.Mag.Magn.Mater. 262, 192 (2003).

[143] V.P.Antropov, M.V.Schilfgaarde, S.Brink, J.L.Xu, J.Appl.Phys. 99, 08F507 (2006).

[144] D.R.Nelson, J.M.Kosterlitz, Phys.Rev.Lett. 39, 1201 (1977).

[145] A.W.Sandik, R.G.Melko, Ann.Phys. 321, 1651 (2006).

[146] R.Chaudhury, Theor.Math.Phys. 136, 1022 (2003).

[147] R.J.Birgeneau, M.A.Kastner, A.Aharony, Z.Phys. B 71, 57 (1988).

[148] H.Q.Ding, M.Makivic, Phys.Rev. B 43, 2662 (1991).

[149] V.J.Emery, S.A.Kivelson, H.Q.Lin, Phys.Rev.Lett. 64, 3562 (1990).

[150] A. Aharony, R. J. Birgeneau, A. Coniglio, M.A. Kastner, H.E.Stanley Phy.Rev.Lett. 60, 1330 (1988)

[151] V.J.Emery, Phys.Rev.Lett 58, 2794 (1987)

[152] F.C.Zhang, T.M.Rice, Phys.Rev.B 41, 7243 (1990)

[153] N.M.Plakida, R.Hayn, J.L.Richard, Phys.Rev.B 51, 16599 (1995)

[154] M.Ogata, M.U.Luchini, S.Sorella, F.F.Assaad, Phys.Rev.Lett. 66, 2388 (1991)

[155] N.Kawakami, S.K. Yang, Phys.Rev.Lett. 65, 2309 (1990)

[156] B.Sciolla, A.Tokuno, S.Uchino, P.Barmettler, T.Giamarchi, C.Kollath, Phys.Rev.A 88, 063629 (2013)

[157] J.Sirker, A.Klümper, Phys.Rev.B 66, 245102 (2002)

[158] (a) S.Tomonaga, Prog.Theo.Phys.5, 544 (1950)
(b) J.M.Luttinger, J.Math.Phys. 4, 1154 (1963)

[159] N.M.Plakida, "High-Temperature Superconductivity", Pages-82-83, Chapter-III, Springer-Verlag, Germany (2010)

[160] I.K.Schuller, D.G.Hinks, M.A.Beno, D.W.Capone II, L.Soderholm, J.P.Locquet, Y.Bruynseraede, C.U.Segre, K.Zhang, Solid State Comm. 63, 385 (1987)

[161] A.A. Aligia, Eur.Phys.Lett. 26, 153 (1994)

[162] A.J.Achkar, R.Sutarto, X.Mao, F.He, A.Frano, S.B.Canosa, M.L.Tacon, G.Ghiringhelli, L.Braicovich, M.Minola, M M.Sala, C.Mazzoli, R.Liang, D.A.Bonn, W.N.Hardy, B.Keimer, G.A.Sawatzky, D.G.Hawthorn, Phys.Rev.Lett. 109, 167001 (2012)

[163] H.A. Mook, P. Dai, S.M.Hayden, A.Hiess, J.W.Lynn, S.H.Lee, F. Doğan, Phy. Rev. B 66, 144513 (2002)

[164] E.Blackburn, J.Chang, M. Hücker, A.T.Holmes, N.B.Christensen, R. Liang, D.A.Bonn, W.N.Hardy, U.Rütt, O.Gutowski, M.V.Zimmermann, E.M.Forgan, S.M.Hayden, Phy. Rev. Lett. 110, 137004 (2013)

[165] J.M.Tranquada, A.H.Moudden, A.I.Goldman, P.Zolliker, D.E.Cox, G.Shirane, S.K.Sinha, D.Vaknin, D.C.Johnston, M.S.Alvarez, A.J.Jacobson, J.T.Lewandowski, J.M.Newsam, Phys.Rev.B 38, 2477 (1988)

[166] D.C.Johnston, S.K.Sinha, A.J.Jacobson, J.M.Newsam, Physica C 153, 572 (1988)

[167] G.D.Mahan, "Many-Particle Physics", Pages-358-361, Chapter-V, Kluwer Academic/Plenum Publishers, New York (2000)

[168] (a) P. Dai, H.A. Mook, R. D. Hunt, F. Doğan, Phy. Rev. B 63, 054525 (2001); (b) D.Haug, V.Hinkov, Y.Sidis, P.Bourges, N.B. Christensen, A.Ivanov, T.Keller, C.T.Lin, B.Keimer, New J.Phys. 12, 105006 (2010)

[169] V.P. Antropov, B.N. Harmon, A.N. Smirnov, J.Mag.Magn.Mater. 200, 148 (1999)

[170] J.C.Bonner, M.E.Fisher, Phys.Rev.A 135, 640 (1964)

[171] (a) S.O.Diallo, V.P.Antropov, T.G.Perring, C.Broholm, J.J.Pulikkotil, N.Ni, S.L.Bud′ko, P.C.Canfield, A.Kreyssig, A.I.Goldman, R.J.McQueeney, Phys.Rev.Lett. 102, 187206 (2009);
(b) A.Solontsov, V.P.Antropov, Phys.Rev.B 81, 104403 (2010)

[172] (a)T.M.Rice, K.Ueda, Phys.Rev.Lett. 55, 995 (1985)
(b)W.Metzner, D.Vollhardt, Phys.Rev.Lett. 59, 121 (1987)

[173] M.Azzouz, K.Shahin, G.Y.Chitov, Phys.Rev.B 76, 132410 (2007)

[174] Y.J. Xu, H.Zhao, Y.G.Chen, Y.H. Yan, Eur.Phys.J. B 85, 393 (2012)

[175] (a)E.Bordas, C.D.Graaf, r.Caballol, C.J.Calzado, Phys.Rev.B 71, 045108 (2005);
(b)F.B.Ramos, J.C.Xavier, Phys.Rev.B 89, 094424 (2014)

[176] H.Alloul, J.Bobroff, M.Gabay, P.J.Hirschfeld, Rev.Mod.Phys. 81, 45 (2009)

[177] C.D.Graaf, F.Illas, Phys.Rev.B 63, 014404 (2000)

[178] T.Valla, T.E.Kidd, P.D.Johnson, K.W.Kim, C.C.Homes, G.D.Gu, Phys.Rev.B 77, 054503 (2008)

[179] M.Takigawa, Y.Heights, N.Motoyama, H.Eisaki, S.Uchida, Phys.Rev.B 55, 14129 (1997)

[180] F.Onufrieva, J.R.Mignod, Phys.Rev.B 52, 7572 (1995)

[181] B.W.Veal, A.P.Paulikas, Physica C 184, 321 (1991)

[182] (a) R.Chaudhury, S.S.Jha, Pramana 22, 431 (1984);
(b) Y.A.Uspenskii, Soy.Phys.JETP 49, 822 (1979);
(c) V.L.Ginzburg, D.A.Kirzhnits, Phy.Rep. C4, 344 (1972)

[183] T.Moriya, "Spin Fluctuations in Itinerant Electron Magnetism", edited by P.Fulde, Chapter-III, Springer-Verlag, Germany (1985)

[184] C.L.Kane, P.A. Lee, N.Read, Phys.Rev.B 39, 6880 (1988)

[185] S.R.White, I.Affleck, Phy.Rev. B 64, 024411 (2001)

[186] (a)A.Keren, L.P.Le, G.M.Luke, B.Sternlieb, W.D.Wu, Y.J.Uemura, S.Tajima, S.Uchida, Phys.Rev.B 48, 12926 (1993);
(b)T.Ami, M.K.Crawford, R.L.Harlow, Z.R.Wang, D.C.Johnston, Q.Huang, R.W.Erwin, Phys.Rev.B 51, 5994 (1995);
(c)N.Motoyama, H.Eisaki, S.Uchida, Phy.Rev.Lett. 76, 3212 (1996);
(d)K.R.Thurber, A.W.Hunt, T.Imai, F.C.Chou, Phy.Rev.Lett. 87, 247202 (2001)

[187] (a)A.Hayashi, B.Batlogg, R.J.Cava, Phys.Rev.B 58, 2678 (1998);
(b)H.F.Fong, B.Keimer, J.W.Lynn, A. Hayashi, R. J. Cava, Phys.Rev.B 59, 6873 (1999)

[188] M.M.Maśka, M.Mierzejewski, E.A.Kochetov, L.Vidmar, J. Bonča, O.P.Sushkov, Phys.Rev.B 85, 245113 (2012)

[189] Y.Nagaoka, Phys.Rev. 147, 392 (1966)

[190] W.F.Brinkman, T.M.Rice, Phys.Rev.B 2, 1324 (1970)

[191] S.A.Trugman, Phys.Rev.B 37, 1597 (1987)

[192] B.X.Zheng, G.K.L.Chan, Phys.Rev.B 90, 035126 (2016)

[193] (a)A.Sherman, arXiv: Cond-mat/1708.05818 (unpublished) (2017);
(b)A. Sherman, Eur.Phys.J. B 90, 120 (2017);
(c)A. Sherman, J.Magn.Magn. Mater. 440, 97 (2017)

[194] H.Y.Deng, J.Phys.:Condens.Matter 21, 075702 (2009)

[195] (a)K.Sconhammer, arXiv: Cond-mat/0305035v2 (unpublished) (2003);
(b)A.J.Schofield, Contemporary Physics 40, 95 (1999)

[196] (a)Tiago C. Ribeiro, Xiao-Gang Wen, Phys.Rev.Lett. 95, 057001 (2005);
(b)A.J.Millis, A.Zimmers, R.P.S.M.Lobo, N.Bontemps, C.C.Homes, Phys.Rev.Lett. 72, 224517 (2005)

[197] (a)A.M.Goldman, Annu.Rev.Mater.Res. 44, 45 (2014)
(b)E.G.Akpojotor, Int.J.Theo.Math.Phys. 4(3), 103 (2014)

[198] (a)P.Phillips, Nature Physics 6, 931 (2010);
(b)A.A.Kordyuk, Low Temp.Phys. 41, 319 (2015)

[199] D.Rybicki, M.Jurkutat, S.Reichardt, C.Kapusta, J.Haase, Nature Communications 7, 11413 (2016)

[200] D.Chakraborty, C.Morice, C.Pépin, Phy.Rev.B 97, 214501 (2018)

[201] K.V.Mitsen, O.M.Ivanenko, Physics-Uspekhi 60, 402 (2017)

[202] M.Vojta, S.Sachdev, Phy.Rev.Lett. 83, 3916 (1999)

[203] H.C.Jiang, T.P.Devereaux, Science 365, 1424 (2019)

[204] D.Poilblanc, Phy.Rev.B 44, 9562 (1991)

[205] J.Jaklič, P,Prelovšek, Phy. Rev. B 52, 6903 (1995)

[206] E.Dagotto, A.Moreo, F.Ortolani, D.Poilblanc, J.Riera, Phy.Rev.B 45, 10741 (1992)

[207] M.Takahashi, Progr.Theoret.Phys. 47, 69 (1972)

[208] M.J.Martins, P.B.Ramos, Nuclear Phys. B 522, 413 (1998)

[209] J.M.P.Carmelo, S.J.Gu, P.D.Sacramento, Annals of Physics 399, 484 (2013)

[210] D.Pines, P.Nozieres, "Theory of Quantum Liquids", Benjamin, New York (1966); R.Bari, D.Adler, R.V.Lang, Phys.Rev.B 2, 2898 (1970); I.Sadakata, E.Hanamura, J.Phys.Soc.Jpn. 34, 882 (1973); P.F.Maldague, Phys.Rev.B 16, 2437 (1977)

[211] D.Nakamura, Y.Imai, A.Maeda, I.Tsukada, J.Phys.Soc.Jpn. 81, 044709 (2012)

[212] D.Volhardt, Rev.Mod.Phys. 56, 99 (1984); F.C.Zhang, T.M.Rice, Phys.Rev. B 37, 3759 (1988)

[213] V.N.Kotov, O.P.Sushkov, Phy.Rev. B 70, 195105 (2004)

[214] J.Leshen, M.Kavai, I.Giannakis, Y.Kaneko, Y.Tokura, S.Mukherjee, W.C.Lee, P.Ayanjian, Communication Physics 2, 36 (2019)

[215] T.Tohyama, Susumu Nagai, Yasumasa Shibata, Sadamichi Maekawa, J.Low Temp. Phys. 117, 211 (1999)

[216] T.Tohyama, S.Nagai, Y.Shibata, S.Maekawa, Phys.Rev.B 82, 4910 (1999)

[217] V.L.Ginzburg, D.A.Kirzhnits, "High-Temperature Superconductivity", by chapter-III, New York: Consultants Bureau (1982)

[218] G.F.Giuliani,G.Vignale, "Quantum Theory of the Electron liquid", chapter-IV,V, Cambridge University Press (2005) (2007)

[219] A.W.Overhauser, Phy.Rev. 128, 1437 (1962)

[220] M.Zegrodnik, J.Spalek, Phy.Rev.B 98, 155144 (2018)

[221] V.Y.Yushankhai, N.M.Plakida, P.Kalinay, Physica C 174, 401 (1991)

[222] Kazuhiko Sakakibara, Ikuo Ichinose, Tetsuo Matsui, Phys.Rev.B 46, 14779 (1992)

[223] N.M.Plakida, V.S. Oudovenko, P.Horsch, and A.I.Liechtenstein, Phy.Rev.B 55, R11997(R) (1997)